Università degli Studi di Pisa

DIPARTIMENTO DI INGEGNERIA INDUSTRIALE
Corso di Laurea Magistrale in Ingegneria Aerospaziale

Tesi di laurea magistrale

Design of the Mu2e calorimeter cooling system

Candidato:
Francesco Neri
Matricola 516308

Relatori:
Prof. Luca d'Agostino
Prof. Simone Donati
Dott. Ing. Fabrizio Raffaelli

Anno Accademico 2018–2019

Ai miei genitori

Ringraziamenti

Sento il dovere di ringraziare svariate persone al termine della stesura di questa tesi. Il primo grande ringraziamento va al Professor Simone Donati, grazie a lui ho vissuto una delle esperienze più importanti e formative della mia vita al Fermilab. Ha inoltre corretto più e più volte la forma grammaticale del testo, e per questo gli sono immensamente grato.

Un altro ringraziamento va all'Ingegner Fabrizio Raffaelli, sempre disponibile ad aiutarmi nei momenti di dubbio. Molte delle idee intelligenti presenti nell'impianto sono merito suo.

Ringrazio il Professor Luca d'Agostino, sempre disponibile per chiarimenti e discussioni di qualsiasi natura. Durante questi ultimi due anni di università mi ha trasmesso una profonda passione per i suoi corsi di studio, spero in futuro di lavorare in tali campi.

Devo ringraziare anche l'Ingegner Daniele Pasciuto, che mi ha praticamente fatto da supervisore durante il periodo negli Stati Uniti. Molte soluzioni tecniche sono frutto di conversazioni nate con lui.

Passando ai ringraziamenti più informali non potrei non citare Matteo, Micol e Francesca. Sono le tre persone con cui ho condiviso maggiormente "la vacanza" in America, e nonostante il poco tempo a disposizione è nata una profonda amicizia. Grazie a loro ho dei bellissimi ricordi, non dimenticherò mai le nostre numerose cene insieme.

Un grazie va ovviamente anche a tutti i miei amici più stretti, quelli di ogni giorno e quelli che mi hanno accompagnato durante il periodo universitario. I ricordi più belli sono legati a loro.

Per finire non potrei non ringraziare la mia famiglia. Nonostante le numerose discussioni è solamente merito loro il raggiungimento di questo traguardo, spero siano orgogliosi di me.

Abstract

The goal of the Mu2e experiment at Fermi National Accelerator Laboratory (Fermilab) is the search for the neutrino-less coherent conversion of the muon into an electron, in the field of an aluminum nucleus. The observation of this physics process would unambiguously demonstrate the existence of physics beyond the Standard Model. Although in the past there has been an intense experimental research activity in this direction, all the previous searches have given null results. The experimental technique employed by Mu2e experiment has been designed to improve the sensitivity by four orders of magnitude with respect to similar previous experiments.

Mu2e is a complex experimental apparatus composed of a high intensity pulsed muon beam line and several complementary particle detectors including a straw-tracker and a crystal-based electromagnetic calorimeter. The calorimeter has been designed and will be built by the international collaboration among the Italian National Institute of Nuclear Physics (INFN), the California Institute of Technology (Caltech) and the Fermilab. The calorimeter measures electrons energy, time and position of impact, which is all fundamental information to aid the straw-tracker in reconstructing the electrons trajectories and kinematic parameters. This has to be done with the energy and time resolution necessary to identify the conversion electrons from the electrons produced by the muons decay in flight and in the muons nuclear capture, which are much more frequent physics processes. The calorimeter is a challenging detector, since it operates in a hostile environment of 1 T magnetic field, a harsh radiation level and 10^{-7} Atm vacuum. The detector will be installed inside an evacuated cryostat and will be accessible for maintenance only for an extremely limited number of weeks per year.

Operation in vacuum has an important impact on the detector design: all the selected components have to be vacuum-compatible and a dedicated cooling system is necessary to maintain electronic parts within a temperature range compatible with a safe long-term operation. The design of the cooling system has been complicated by the high radiation level expected in the experimental area during operation, since this has required the adoption of special radiation-hard electronic components which typically have a larger power dissipation than standard components.

A preliminary conceptual design of the cooling system was already available when I started working on my Thesis [23], [17], [28], [26], [18], [4], [24]. The goal of my work has been finalising the conceptual design and developing the executive project to a sufficient level of maturity to select the components (chiller, pumps, valves, etc. . .) available on the market.

Starting from the analysis of the several heat sources present in the calorimeter, which include 1400 Silicon PhotoMultipliers (SiPM), the associated front-end electronic boards which provide power and readout, and 180 data acquisition boards which acquire and transmit the calorimeter data to the Mu2e global data acquisition system, I estimated the total and the distribution of the dissipated power in the detector. Given the constraints on the temperature ranges in which each component can safely operate, I have selected the most adequate cooling fluid and designed the hydraulic circuit. To perform this task, I employed standard mathematical models and computer simulations (using commercial software packages to perform finite element analysis) which were verified in the INFN laboratories through experimental tests. Finally, I have selected the commercial components adequate for the designed system. The data sheets of suggested components are reported in Appendix B.

Contents

List of Figures

List of Tables

Chapter 1

The Mu2e experiment

This Chapter reports the physics motivations and experimental techniques employed by the muon to electron conversion experiment (Mu2e), in place at *Fermi National Accelerator Laboratory* (Fermilab). I also reported an overview of the Fermilab accelerator complex which provides the high intensity muon beam line, along with the necessary particle detectors. The Italian National Institute of Nuclear Physics (INFN), in collaboration with the California Institute of Technology (Caltech) and Fermilab, is responsible for the design and construction of the detector named *electromagnetic calorimeter*. At the moment of writing this Thesis, the calorimeter has been almost completely designed. Detector construction will begin in the year 2020 and will be completed within 2021, just in time to begin the Mu2e data taking, planned for the year 2022.

1.1 The Standard Model

The theory named Standard Model of particle physics provides a satisfactory physical model to explain the phenomenology of three among the four known fundamental forces[1]. The model provides a satisfactory description of the interactions among elementary particles, and how they are mediated by a "relative exchange" of particles (fig. 1.1). Attempts to include the gravitational force in the Standard Model have not provided satisfactory results yet[2].

Although the Standard Model predictions have been experimentally verified with high precision, we know this theory is incomplete and needs an extension to incorporate phenomena such as *neutrino oscillations*[3] and the existence of *dark matter*[4] which have both been observed experimentally but have not yet found a

[1]The four fundamental forces are: the electromagnetic, the weak, the strong and the gravitational force. The gravitational is the only one not covered by the standard model

[2]The theory able to link together general relativity and quantum mechanics would be the so called "Theory of everything", that would fully explains and links together all the physical aspects of the universe

[3]Neutrino oscillation is a quantum mechanical phenomenon whereby a neutrino created with a specific lepton family number (lepton flavor: electron, muon, or tau) can later be measured having a different lepton family number.

[4]Dark matter is a form of matter thought to account for approximately 85% of the matter in the universe, and about a quarter of its total energy density. Its presence is implied in a

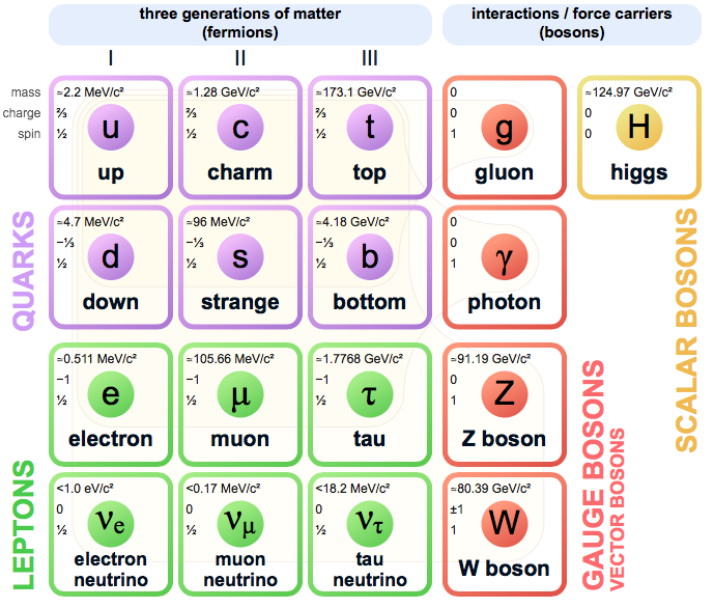

Figure 1.1: Summary table of the elementary constituents of matter, quarks, leptons and gauge bosons. (*Image courtesy of Fehling Dave*)

fully satisfactory theoretical interpretation.

All the elementary constituents of matter can be classified according to two categories: *fermions*, i.e. quarks and leptons, the 1/2 spin[5] elementary constituents of matter, and *bosons*, the integer spin mediators of the fundamental forces. Fermions are classified according their interactions (or equivalently, by what charges they carry). There are six quarks (up, down, charm, strange, top, bottom), and six leptons (electron, electron neutrino, muon, muon neutrino, tau, tau neutrino). Quarks carry color charge and interact via the strong interaction. A phenomenon called color confinement results in quarks being very strongly bound to each other, forming color-neutral composite particles (hadrons) containing either a quark and an antiquark (mesons) or three quarks (baryons). The familiar proton and neutron are the two baryons with the smallest masses. Quarks also carry electric charge and weak isospin. Hence they interact with other fermions both electromagnetically and via the weak interaction. The remaining six fermions are called leptons and do not carry color charge. The three neutrinos do not carry electric charge either, so their interactions are limited to the weak force, which makes them notoriously difficult to detect. However, by virtue of carrying an electric charge, the electron, muon, and tau all interact electromagnetically and weakly. The six quarks and leptons are grouped into three families.

The the first generation of quarks includes:

- The quark up
- The quark down

variety of astrophysical observations, including gravitational effects which cannot be explained by accepted theories of gravity unless more matter is present than the visible one.

[5]In quantum mechanics the spin is an intrinsic form of angular momentum carried by elementary particles, composite particles (hadrons), and atomic nuclei.

The second one contains:

- The quark strange
- The quark charm

And finally the third one contains

- The quark top
- The quark bottom

The the first generation of leptons includes:

- The electron e
- The electron neutrino ν_e

The second one contains the muonic leptons:

- The muon μ
- The muon neutrino ν_μ

And finally the third one, containing the tauonic leptons:

- The tau τ
- The tau neutrino ν_τ

Each member of a generation has greater mass than particles belonging to lower generations. Ordinary matter (i.e. atoms, neutrons, and protons) is made of particles belonging to the first generation. Specifically, all atoms consist of electrons orbiting around atomic nuclei, ultimately constituted of up and down quarks. The second and third generation charged particles, on the other hand, decay with very short half-lives and are observed only in very high-energy environments. Neutrinos of all generations also do not decay, the pervade the universe and rarely interact with other particles.

In the Standard Model, bosons are defined as force carriers that mediate the strong, weak, and electromagnetic fundamental interactions. The interactions in physics are the ways in which the particles influence other particles. The Standard Model explains such forces as resulting from elementary particles exchanging other particles, generally referred to as force mediating particles (i.e. the bosons), as listed below:

- The photons γ, that mediate the electromagnetic force between charged particles. They are massless;
- The W^+,W^- and Z bosons mediate the weak interactions between particles of different flavors. They are massive;

- The eigth *gluons* mediate the strong interactions between color charged particles (the quarks). They are massless and with an effective color charge, hence they can also interact among themselves;

- The *Higgs particle* is a massive scalar elementary particle theorized by Peter Higgs in 1964. It plays a unique role in the Standard Model, explaining why the other elementary particles, except the photon and gluon, are massive. In particular, the Higgs boson explains why the photon has no mass, while the W and Z bosons are very heavy. Higgs discovery of CERN Large Hadron Collider has been a recent triumph of the Standard Model.

1.1.1 Charged lepton flavor violation (CLFV)

The muon and tau are unstable particles, while the electron is stable. The muon decays with a probability of approximately 100% to a muon neutrino ν_μ, an electron e, and an electron antineutrino $\bar{\nu_e}$[6]. In symbols the previous physics process can be indicated as $\mu \rightarrow \nu_\mu e \bar{\nu_e}$.

In a small fraction of cases, also other particles with a net charge equal to zero may be produced in the muon decay (e.g. a photon, or an electron-positron[7] pair). In all these processes the lepton flavour is conserved separately for every lepton family. In other words, the final state includes a muon neutrino, which belongs to the same family and has the same lepton number as the parent muon, and also an electron and an electron antineutrino, which have zero lepton number in total, since particles and antiparticles are conventionally assigned opposite lepton numbers.

Searches for Charged Lepton Flavor Violating processes, such as the muon to electron conversion ($\mu \rightarrow e\gamma$)[8], with no muon neutrino, nor electron antineutrino in the final state, have so far yielded null results. CLFV processes are expected within the Standard Model with a probability $<10^{-54}$. With the current level of experimental precision, such effects are obviously beyond the experimental reach. Although the Standard Model has been accurately tested, we know it is an incomplete theory. Several extensions of the model include CLFV processes and allow the decay $\mu \rightarrow e\gamma$, and also the *coherent neutrino-less muon conversion to an electron in the field of a nucleus* ($\mu N \rightarrow eN$), with probability rates sufficient to be measured in the next generation experiments, including Mu2e.

Mu2e has been designed and is currently being constructed at Fermilab to search for the neutrino-less muon conversion to an electron in the field of an aluminum nucleus. The current experimental limit on the branching factor of this process has been set at the level of 10^{-12} by the SINDRUM II experiment, performed at the Paul Scherrer Institut at Zurich. The Mu2e sensitivity will allow to observe muon conversion events if this process has a probability of the order of 10^{-17}. However, in case no conversion event is observed, Mu2e will set an upper

[6] In particle physics, every type of particle has an associated antiparticle with the same mass but with opposite physical charges (such as electric charge).

[7] the positron is the antiparticle of electron

[8] γ is the symbol representing the photon.

Figure 1.2: Aerial view of the Fermilab site. The Mu2e facility is close to the center. Many other experiments are hosted in the site (TEVATRON etc ...)

limit to the probability of the process and will improve the current experimental limit from SINDRUM II of four orders of magnitude.

The international Mu2e collaboration is completing the design of the various detector components and will begin to build the experiment in the year 2020. The construction is expected to be completed within the year 2021. The beginning of data taking is planned for the year 2022, and will continue for about three years. Future upgrades of the experimental apparatus planned for the years 2025 and beyond will further improve the experimental Mu2e sensitivity by a factor of 10.

1.2 The Fermilab accelerator complex

Fermilab is located in Batavia, about 50 km west of Chicago, Illinois (USA). It is a US Department of Energy Laboratory, operated by the Universities Research Association (URA) since its founding in 1967 to 2006. Since 2007 it has been operated by the partnership between the University of Chicago and the University Research Association, named Fermilab Research Alliance (FRA). The name Fermilab was given to the laboratory in 1974 to honour the memory of the Italian Nobel prize Enrico Fermi.

Fig. 1.2 shows an aerial view of the laboratory, which has played a major role in the field of high energy physics for the last forty years. Among its scientific achievements, it is worth mentioning the discovery of three among the four particles of the model's third generation: the bottom quark (May-June 1977), the top quark (February 1995) and the tau neutrino (July 2000).

1.2.1 The accelerators chain

The accelerator complex is composed of several stages:

- The first stage is a *Cockcroft-Walton generator*, which turns hydrogen gas into H^- ions by flowing it into a container lined with molybdenum electrodes

(a matchbox sized, oval shaped cathode and a surrounding anode, separated by 1 mm and held in place by glass ceramic insulators). A magnetron[9] is used to generate a plasma to form H^- ions close to the metal surface. A 750 keV electrostatic field is applied by the Cockcroft-Walton generator, and the ions are accelerated out of the container;

- The second stage is a Linear Accelerator (or *Linac*), which accelerates the ions to the energy of 400 MeV (approximately 70% of the speed of light). Just before entering the next accelerator, the ions pass through a carbon foil, where they lose the electrons producing a H^+ ion beam (called proton beam);

- The third section is the *Booster Ring*. The Booster ring is a 468 m circular accelerator that uses magnets to bend the proton beam in a circular path. The protons coming from the Linac travel around the Booster about 20000 times in 33 ms, in order to multiply the accelerating electric field. Each revolution gives the protons more energy, until the beam leaves the ring at approximately 8 GeV;

- Finally the protons are injected into the *Recycler Ring*, where they circulate while getting rebounded by a 2.5 MHz frequency system. The reformatted bunches are transported to the delivery ring, where they are slowly extracted from the Mu2e detector through a new external beamline (figure 1.3);

1.3 The Mu2e experimental facility

The Mu2e experimental apparatus is extensively described in the conceptual *Design and Technical Report* [2]. The layout of the muon beam line and the detector system are also shown in Figure 1.4.

1.3.1 Production solenoid

The Mu2e magnet system consists of three large superconducting solenoids. The first component in the chain of magnets is the Production Solenoid (PS), whose role is to collect and focus pions[10] and muons generated in the collision of an 8-GeV proton beam with a tilted high-Z target, by supplying a peak axial field between 4.6 T and 5.0 T and an axial field gradient of about 1 T/m, within a 1.5 m warm bore.

The PS is a challenging magnet because of the relatively high intensity magnetic field and the harsh radiation environment that require state-of-the-art conductors

[9] A high powered vacuum tube that generates microwaves using the interaction of electrons streams with a magnetic field, while moving past a series of open metal cavities (cavity resonators).

[10] In particle physics, a pion is any of the three subatomic particles: π^+, π^-, π^0 (depending of their net charge). Pions consist of a quark and antiquark, and are the lightest among the mesons. Charged pions most often decay into muons and muon neutrinos, while neutral pions generally decay into gamma rays.

Figure 1.3: Layout of the Mu2e facility (lower right) relative to the accelerator complex that provides the proton beam to the detector. Protons are transported from the Booster through the MI-8 beamline to the Recycler Ring, where they circulate while being rebounded by a 2.5 MHz RF system. The reformatted bunches are kicked into the P1 line and transported to the Delivery Ring, where they are slowly extracted for the Mu2e detectors

in terms of the current-carrying capacity and structural strength. The PS coil is protected by a massive Heat and Radiation Shield (HRS).

1.3.2 Transport solenoid

The role of the S-shaped Transport Solenoid (TS) is to filter and transport the muon beam (around 1011 muons per second) to the Detector Solenoid. It is composed of 14 superconducting units (solenoids and toroids) and is divided in five sections:

- a 1 m long straight section;
- a 90 degree elbow, with 3 m radius of curvature;
- a second 2 m long straight section;
- a second 90 degree elbow, similar to the first, that turns the beam line in a direction parallel to the first one;
- a final 1 m long straight section.

The resulting length of the Transport Solenoid is 13 m. To improve the purity of the muon beam, the Transport Solenoid has an absorber placed in its central part that stops charged particles (mainly antiprotons). A state-of-the-art collimator system is placed in the same zone to select only low energy muons with momentum below 0.08 GeV/c. Moreover, the S-shape of the solenoid removes

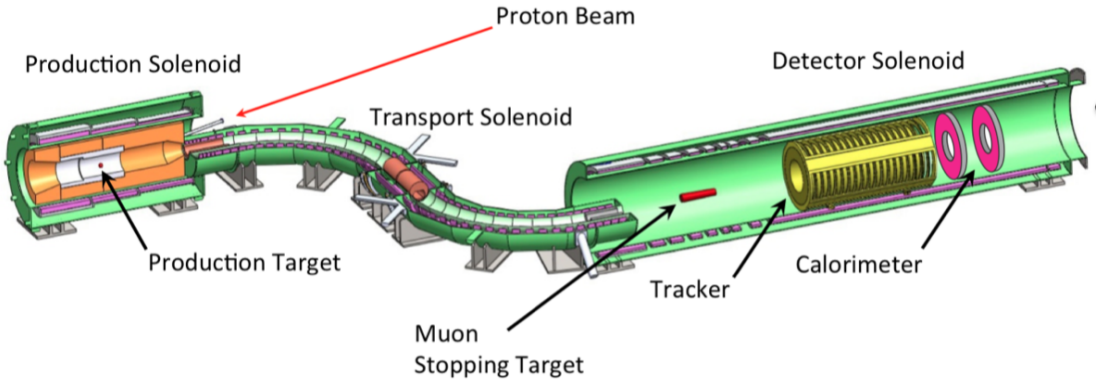

Figure 1.4: Mu2e apparatus: the proton beam enters from the right at the junction between the Production Solenoid and the Transport Solenoid, and strikes the production target. The cosmic ray veto system, which surrounds the Detector Solenoid, and the muon stopping monitor are not shown in this scheme (source: Mu2e experiment data center).

neutral particles, that in absence of an electromagnetic interaction travel in a straight direction.

1.3.3 Detector solenoid

The Detector Solenoid (DS) is 11 m long and provides a decreasing magnetic field in the first sector (from 2 T to 1 T). It hosts the muon stopping target, schematically represented in fig. 1.5.

Muons impacting the disks come to rest and replace the electrons lying in the $1s$ orbit of the aluminum atoms. The lifetime of the muon in the muonic atom is 864 ns. The non-uniformity of magnetic field plays an important role in reducing the background coming from high energy electrons transported to the Detector Solenoid. The magnetic field gradient is generated by introducing spacers to change the winding density of the superconducting cable, which is made out of aluminum-stabilized $NiTi$.

The second sector of the Detector Solenoid houses the detectors: the *tracker* and the *calorimeter*, which are described in more detail in section 1.3.4. In this sector the magnetic field is relatively uniform and has the average intensity of 1 T.

1.3.4 The tracker and the electromagnetic calorimeter

The Mu2e tracker and electromagnetic calorimeter are placed inside the Detector Solenoid. The Mu2e collaboration decided to use a tracker design similar to the one developed by the MECO collaboration (fig. 1.6).

The tracker resides in a uniform 1 T solenoidal magnetic field and in the environmental pressure of approximately $1.33 \cdot 10^{-2}$ Pa to reduce multiple scattering[11] to a negligible level. It reconstructs particle trajectories with high efficiency, and measures the parameters of the helical trajectories with extreme accuracy.

[11] Scattering produced with lower energy level particles

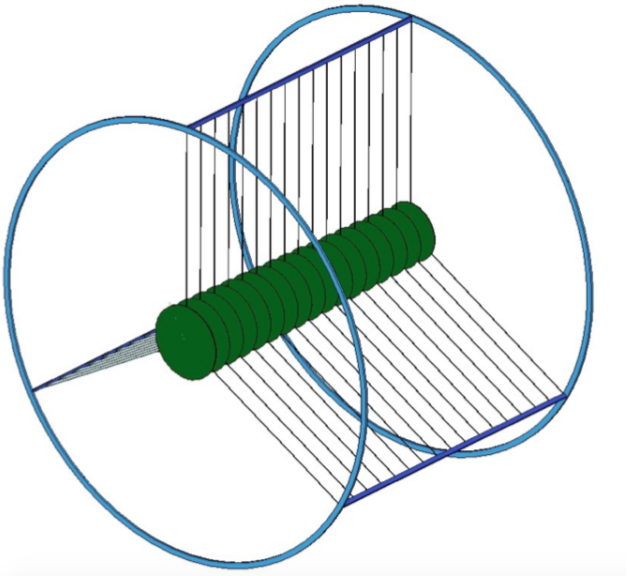

Figure 1.5: The Mu2e stopping target is made of 17 aluminum disks, 0.2 mm thick, spaced 5.0 cm apart along the Detector Solenoid axis. The disks radii decrease from 8.3 cm at the upstream end to 6.53 cm at the downstream end (source: Mu2e experiment data center).

Given that multiple scattering in the tracker dominates the resolution on the measurement of the helix parameters, the mechanical structure of the detector has been made extremely light. The tracker is made of *straw drift* tubes; and is called T-tracker because the straws are transverse to the axis of the Detector Solenoid. The basic detector element is made of a 20 μm sense wire inside a straw tube filled with gas. The straws are 5 mm diameter tubes, made of 15 μm thick metallic Mylar. The tracker is made of approximately 2000 straws arranged along 18 stations across the 3 m tracker length. One tracker plane consists of two layers of straws to improve the reconstruction efficiency and help to overcome the classic left-right ambiguity. A 1 mm gap between straws allows for manufacturing tolerance and expansion due to the internal pressure. A larger radius ring outside the active detector region supports the straws and the electronics boards. Each straw has one preamplifier and one time-to-digital converter (TDC) placed on each tip to measure the signal arrival time on both sides. It uses also analog to digital converters (ADC) to measure the total integrated charge, providing useful information for particle identification. The tracker has been designed to observe only electrons with energy greater than 53 MeV. Electrons below this threshold travel undetected in the central un-instrumented volume of the tracker. They are approximately the 3% of the total electron flux coming from muon decays. Since momentum resolution is a crucial factor to suppress critical backgrounds, the tracker is required to have a momentum resolution better than 180 keV for 100 MeV electrons.

The Mu2e calorimeter provides additional energy, position, and timing information to improve particle trajectory reconstruction performed by the tracker. The two detectors use complementary physical and technological processes to perform their measurements, to rely on uncorrelated error sources. This helps to reduce backgrounds and provides a cross check to verify the quality of signal events. The

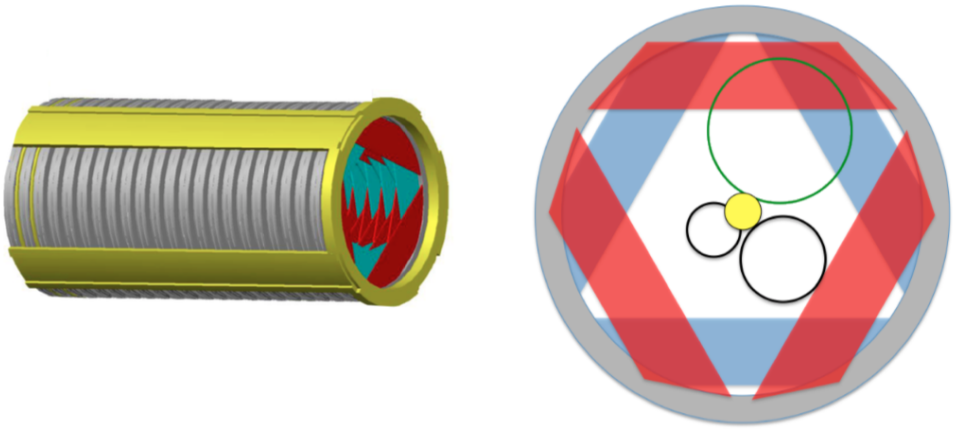

(a) The Mu2e *Tracker*; some of the 18 station of the tracking system are visible on the right.

(b) Cross-sectional wiew of the Mu2e *Tracker*.

Figure 1.6: The Mu2e tracker is composed of 18 tracking system stations. Thanks to the design only electrons with energy above 53 MeV are reconstructed. Lower energy electrons pass through the central un-instrumented part of the device and leave no track. This effect is due to the spiral motion of electrical charges in a uniform magnetic field (source: Mu2e experiment data center)

calorimeter operates in the same solenoidal magnetic field and vacuum level of the tracker. It handles a large flux of particles, mostly a low energy background of protons, neutrons and gamma rays produced by muon captures in the stopping target. It also handles the large flux of electrons coming from muons decays in the aluminum stopping target, and other produced particles during the beam injection. A more detailed description of the calorimeter is reported in chapter 2.

1.3.5 Cosmic ray veto

Cosmic ray muons can initiate background processes and generate particles that interact with the detectors and produce undesired noise. Simulation shows that approximately one background event generated by cosmic ray muons may be erroneously reconstructed as a conversion electron signal per day. This source of background should and can be reduced to a negligible level introducing passive and active shielding. The *Cosmic Ray Veto* (CRV) surrounds the entire volume occupied by the Detector Solenoid and the downstream part of the Transport Solenoid. It consists of four layers of extruded scintillator strips with silicon photosensors and aluminum absorbers.

The cosmic-ray induced background rate will be monitored between beam spills and when the beam is turned off. This allows to perform a direct measurement of the background levels. The study of the background rate will be initiated as soon as the Detector Solenoid and the cosmic ray veto are in place.

1.3.6 Trigger and data acquisition system

The Trigger and Data Acquisition (TDAQ) systems provide hardware and software tools to record the digitized data read from the detectors. The TDAQ synchronizes and controls the data-streams received from the detectors. We have estimated that the online detector bandwidth requirement for the DAQ is around 100 GB/s in streaming mode.

The TDAQ also combines information from all the detector data sources and applies filters (triggers) to reduce this rate by a factor of several thousands, before the data get delivered to the offline permanent storage. Essentially, this is obtained by applying standard cross checks to validate the consistency of data coming from the detectors and performing an event reconstruction as accurate as possible within the timing constraints.

Chapter 2

The Mu2e electromagnetic calorimeter

The Mu2e detectors have been designed to reject backgrounds to a level consistent with a single event sensitivity for the $\mu N \to eN$ coherent conversion in the order of 10^{-17}. The electromagnetic calorimeter is a vital link in the chain of background defenses. Since the quality of track reconstruction is fundamental for background rejection, a particular concern is due to false tracks arising from pattern recognition errors caused by the high rate of hits in the detector. These errors frequently derive from accidental noise and lower energy electron hits which may generate segments of tracks erroneously recombined into trajectories compatible with higher energy electrons which mimic the real muon conversion signal. The calorimeter provides precise time windows where the tracker hits have to be located. This greatly reduces the amount of hits processed to perform pattern recognition and simplifies the computational problem and improves tracking quality.

2.1 Conceptual detector design

The electrons produced in the decay of the muons at rest in the Aluminium target have a maximum energy of approximately 100 MeV. They follow helical trajectories in the solenoidal magnetic field and traverse the straw tracker planes before hitting the front faces of the calorimeter crystals. In this energy range, the Mu2e energy and time resolution requirements can be well satisfied by a total absorption calorimeter employing a homogeneous continuous medium. The sensitive material could either be a liquid, such as xenon (Xe), or a scintillating crystal[1]. The Mu2e collaboration has chosen the scintillating crystals technology. Several crystals have been considered, including barium fluoride (BaF2) and cesium iodide (CsI). The final choice has been a matrix of relatively cheap undoped CsI crystals, arranged in two annular disks (fig. 2.1 and 2.2).

The scintillation light generated by the electrons which hit and traverse each CsI crystal is read out by two large-area solid-state photodetectors (SiPMs)[2],

[1] A scintillator is a material that exhibits scintillation (the property of luminescence) when excited by ionizing radiation.

[2] SiPMs stand for: *Silicon Photomultiplier*. It is a sensor that addresses the challenge

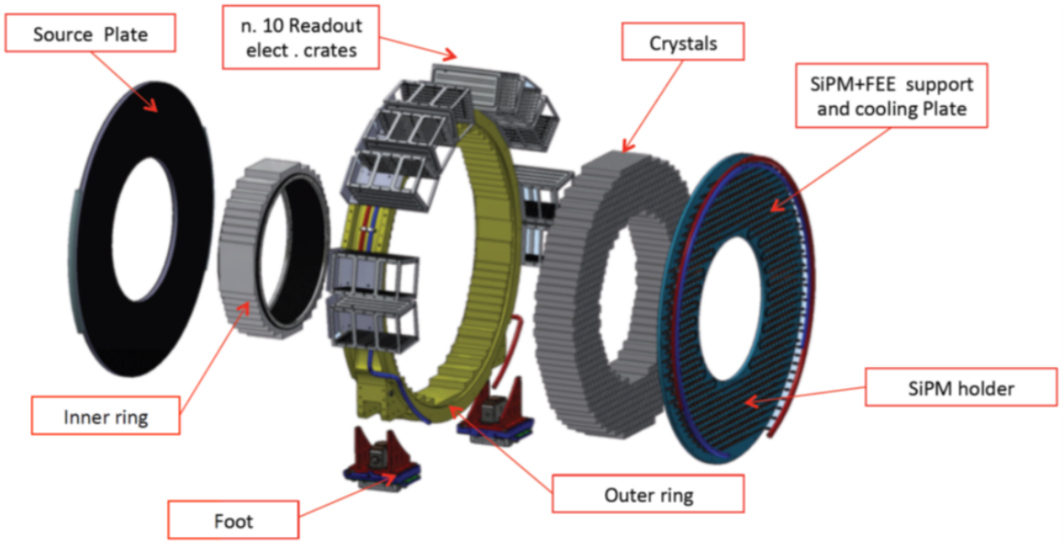

Figure 2.1: Exploded CAD view of one calorimeter disk. All the main components are indicated. (*Source: Mu2e experiment data center*)

preferred to standard photomultipliers because of the high magnetic field involved.

While the front end electronics (FEE) servicing the SiPM (shown in fig. 2.3) is mounted on the rear side of every disk, the voltage distribution, slow control and data acquisition boards are hosted in 10 crates mounted on the external lateral surface of the disk (fig. 2.4).

A laser flasher system provides light to each crystal through a network of optical fibres to perform relative calibrations and for monitoring purposes.

A circulating radioactive liquid source system is housed in the front plate of the disks to provide absolute calibration and determine the absolute energy scale.

The crystals are supported by a structure composed of two concentrical rings: the *Inner Ring* and the *Outer ring*, that can slide along the beam line thanks to horizontal rails.

2.2 Technical specifications

The primary function of the electromagnetic calorimeter is to measure the electrons energy, position of impact and timing to complement the straw-tracker information in the offline reconstruction of electron trajectories. Moreover, the calorimeter provides fast information to the trigger for the online data selection. The detector has been designed taking into account the following technical specifications [25]:

- provide energy resolution of 5% at 100 MeV to confirm the electron momentum measurement performed by the tracker;
- provide timing resolution better than 0.5 ns to ensure that energy deposits in the calorimeter are in time with the hits reconstructed in the tracker;

of sensing, timing and quantifying low-light signals, coming from the crystals, down to the single-photon level (the sensitivity needed for this type of experiment)

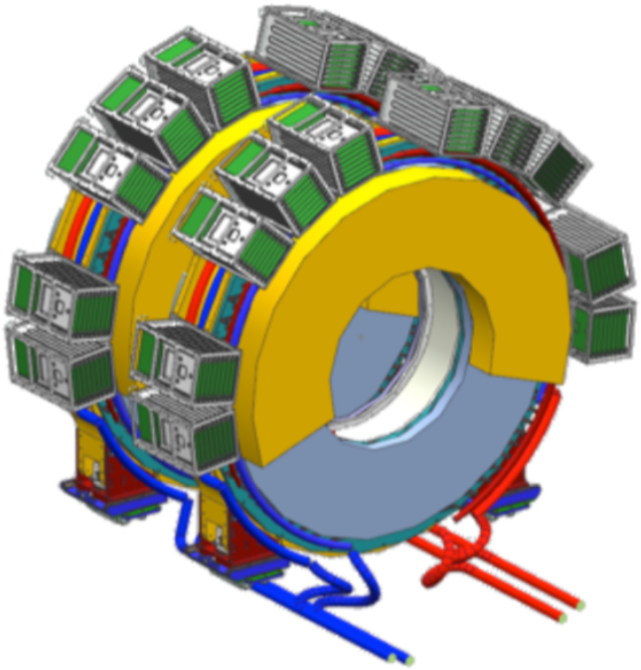

Figure 2.2: CAD model of the Mu2e electromagnetic calorimeter. The 20 custom crates host the boards for voltage distribution, slow control and data acquisition, are colored in grey and green. The calorimeter can slide along the beam line direction thanks to horizontal rails. (*Source: Mu2e experiment data center*)

- provide position resolution better than 1 cm to allow a comparison between the energy deposits position measured by the detector, and the extrapolated trajectories of the reconstructed tracks;
- provide additional information useful for particle identification that can be combined with the tracker information, improving the muon-electron separation;
- provide a trigger, either in hardware, or in software, or in firmware, that can be used to identify and select events with significant energy deposits;
- operate in the hostile, high-rate, Mu2e environment with intact functionality for radiation exposures up to 20 Gy/yr per crystal, and for a neutron equivalent flux up to $10^{11}\ MeV n_{eq}/cm^2 yr$.

2.3 Calorimeter mechanics

The calorimeter is located inside the Mu2e cryostat (part of the detector solenoid). It is composed of two identical disks (fig. 2.2). The inner cylinder is made of carbon fibre to minimise the amount of passive material in the region where spiralling electrons are mostly concentrated. The outer cylinder is made of aluminum and can be as robust as required to support the crystals load (mainly the weight). The disks have an inner radius of 374 mm, outer radius 660 mm, and are made

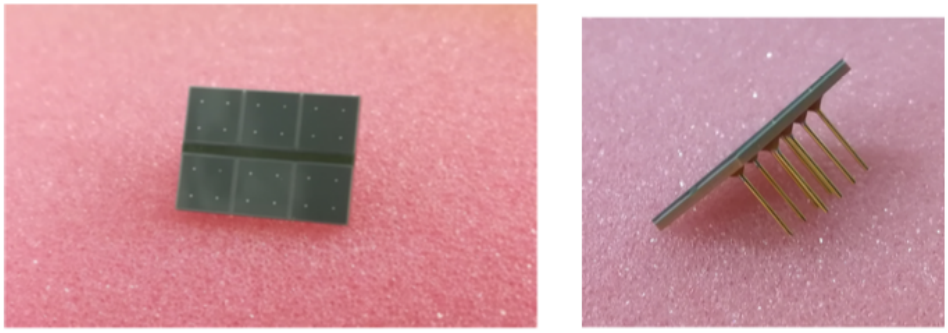

Figure 2.3: Overview of the SiPMs. The 8 pins connect the sensors to the front end electronic boards.

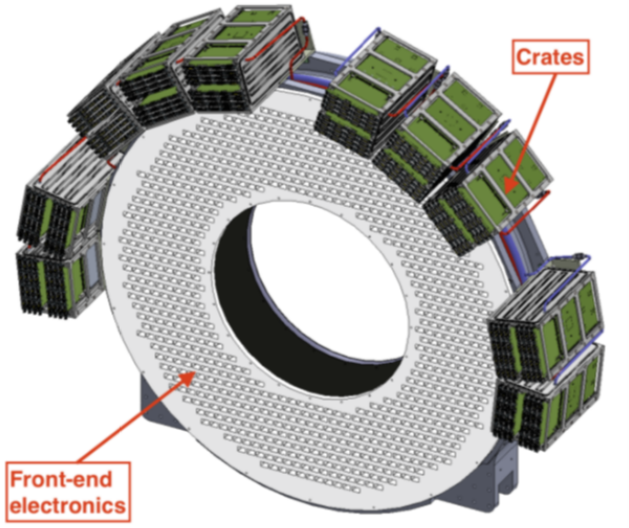

Figure 2.4: Backplate of one calorimeter disk. The front end electronics (FEE) is mounted on the holed backplate, while the crates are externally fastened to the disk.

out of 674 staggered trapezoidal crystals. The crystals are 220 mm long with a square base and a side length of 34 mm. Each crystal is wrapped with 8 layers of 25 μm thick Tyvek reflective film to maximise light transport within the crystal and minimise cross-talk among crystals.

The mechanical structure of each disk is made of two coaxial cylinders (inner and outer ring in fig. 2.1) which support the weight of the crystals, and two plates which connect the rings. The front plate facing the beam is made out of low radiation length material to minimise the electron energy deposit and preserve the electron energy measurement. It is designed to accommodate the calibration source circuit where a radioactive fluid flows. The back plate supports the photosensors, the front-end electronics, the cooling pipes and is made out of the polymer named PEEK (the acronym for *PolyEther Ether Ketone*). This material has the following important characteristics:

- it has an extremely limited outgassing rate, which is crucial for operation in vacuum;

- it has a low thermal conductivity (0.25 W/Km). This important feature will be explained later;
- it has a good mechanical strength and stiffness, so that the plate will have extremely limited deformations;
- it can be easily machined;
- it can be used in a high magnetic field environment.

Other important components of the calorimeter are the front-end and data-acquisition electronic boards. There are several type of different boards, each one with its function. Some of them provide the power to the front-end electronics (that act only as preamplifiers of the SiPM signals) and to the SiPM. They also perform the digitalization of the signals and are hosted in 20 DAQ (Digital Acquisition) crates, (fig. 2.4), positioned on the outer surface of the disks (10 for each disk), in order to gain as much space as possible. Every crate hosts 9 boards, 8 of them provide power to the photosensors and perform signal digitisation, one provides clock distribution.

A crucial function of the mechanical structure is to integrate a dedicated cooling system to provide the cooling to the electronic components. Heat dissipation is mainly due to the SiPM front-end and read-out electronics. The cooling system is a critical part, since the calorimeter operates in vacuum and there is no outer environment that allows to extract heat by convection.

The radiative heat transfer between two surfaces depends on the difference between the fourth power of the temperature of the two surfaces (*Stefan-Boltzmann law*). Unfortunately, in our case this effect is negligible and the only available heat transfer method is the convection-conduction.

We have designed a cooling system consisting of little pipes running through all the components. The cooling fluid circulates through the pipes and extracts heat via convection through the pipe walls. The pipe walls, now pretty cold, extract heat via conduction from the components of interest (in the vicinity of SiPM and FEE board). In this way the cooling fluid raises its temperature and needs to be run through a chiller[3] in order to repeat the cooling circuit. As a necessary by-product, refrigeration in the chiller creates waste heat that must be exhausted. This is accomplished by running through the chiller a water flow coming from the Mu2e building to dispose the heat. The maximum available flow rate is of 10 gal/min (37.9 l/min), with a max temperature raising of 47 $^\circ F$ (26 $^\circ C$). This results in a maximum disposable power of:

$$P = \dot{m} c_p \Delta T \simeq 82\ kW$$

which is well above the maximum estimated value of the dissipated power for nominal calorimeter operations.

[3]A chiller is a machine that removes heat from a liquid via a vapour-compression or absorption refrigeration cycle. The liquid can then be circulated through a heat exchanger to cool equipment, or another process stream (such as air or process water)

To improve the cooling system performance the thermal contact between the pipes and the electronic components has been optimised. The cooling station composed of a chiller, a set of pumps, a reservoir, and all the related services is placed outside the cryostat in a *mechanical alcove*. I sketched the configuration for the mechanical room, represented in fig. 2.5. The pipes connecting the mechanical alcove to the cryostat are called *routing pipes* (shown in fig. 2.6).

2.4 Calorimeter electronics

The entire calorimeter electronics can be divided in two subsystems with different functions and locations:

- **the front-end electronics (FEE)**: is composed by the SiPM and the front-end boards. It is mounted on the backplate, facing the rear side of the crystals. The FEE system converts the light emitted by the SiPM into an electric signal that is then transmitted to the DAQ system;
- **the digital acquisition electronics (DAQ)**: is composed by the data acquisition boards that perform the digitization of the analog signals received from the front-end boards and provide it to the data storage system of the calorimeter. They also provide power and monitor the front end electronics status.

The FEE system is composed of the SiPM and the front-end boards. It is mounted on the backplate and faces the rear side of the crystals.

The DAQ system is composed of the data acquisition boards which digitise the analog signals received from the front end boards and transmit it to the data storage system of the experiment. They also provide power and monitor the front end electronics status.

2.4.1 The front-end electronics

A single front-end electronic unit of the calorimeter is composed by the following parts (shown in fig. 2.7):

- one **CsI crystal**: the electrons impinging on the crystal's frontal surface penetrate the material and generate an electromagnetic shower. The photons produced by scintillation diffuse through the crystal volume and get transported to the rear side of the crystal where the SiPM is faced;
- two **SiPM**: they face the rear side of the crystal and convert the light produced by the scintillation into an electric signal;
- two **front end boards**: electrically connected to both the SiPM. They provide power to the SiPM and amplify their signals. The amplification has to be performed in the immediate proximity of the weak signal source, otherwise would be lost in electric noise;

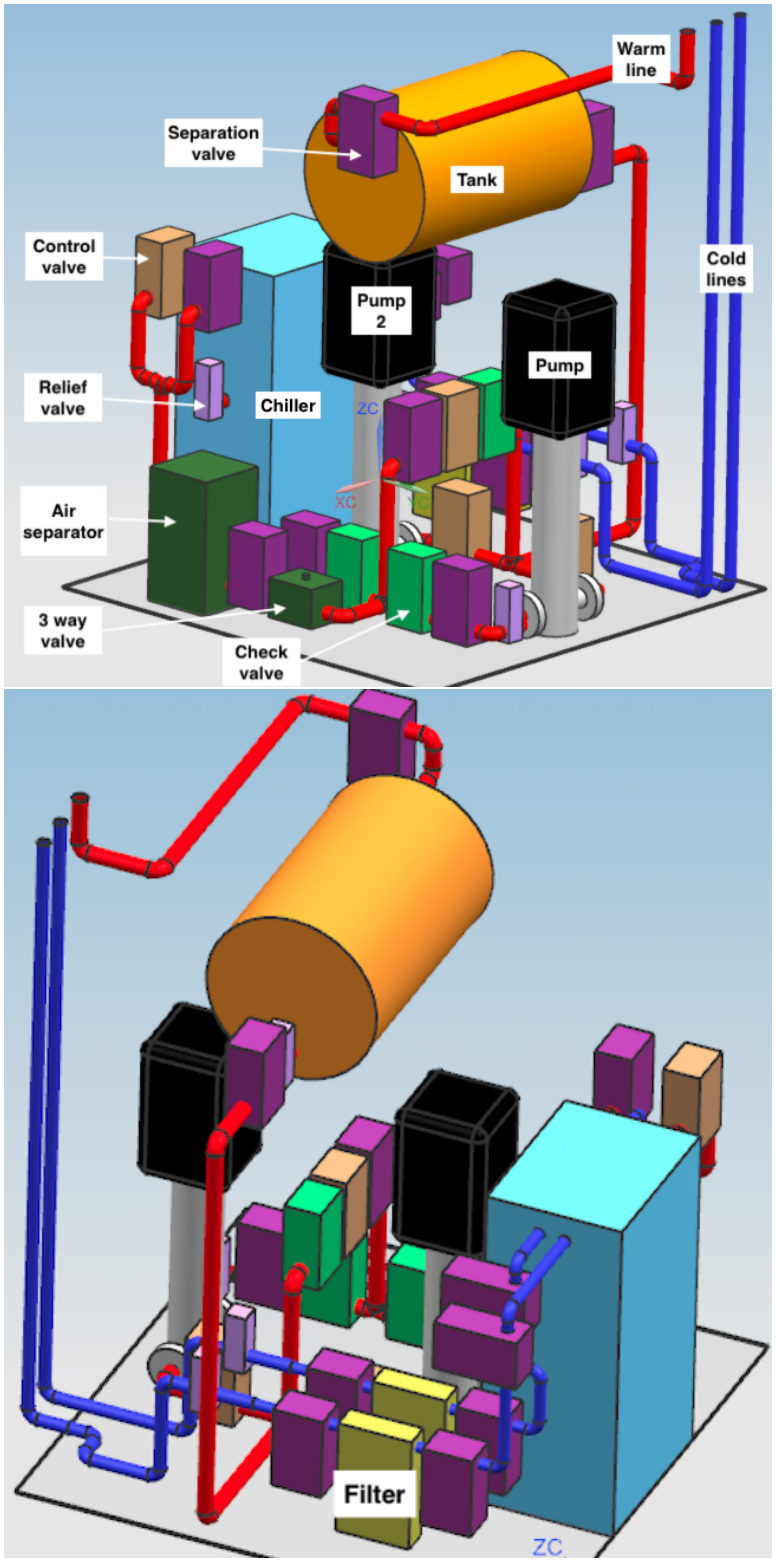

Figure 2.5: CAD model of the mechanical alcove. The drawing does not provide a final configuration for the room, but it helps in circuit calculations and further analysis. Nonetheless the final layout could be similar to this. The circuit process diagram and components will be explained in the following chapters.

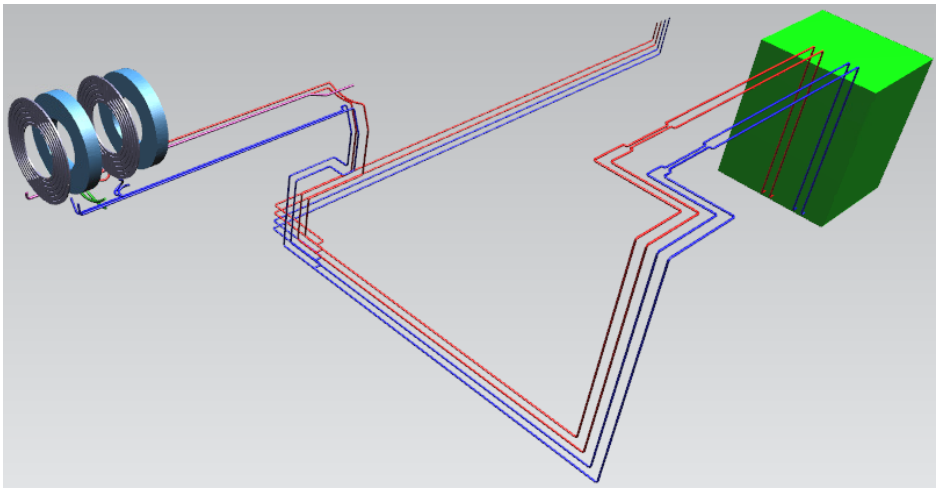

Figure 2.6: CAD model of the routing pipes. The green box represents the mechanical alcove, while the endless terminations are connected to the testing group. (*Source: Mu2e database*)

Table 2.1: Summary of the components of the FEE electronics.

Component	Number per disk	Total (2 disks)
CsI crystals	674	1348
SiPM	1348	2696
Mech supports	674	1348
FEE boards	1348	2696

- one mechanical support: made of copper to support the SiPM and the FEE boards. It works as a "thermal bridge" for heat transfer from the sources (electronic boards and SiPM) to the sink (cooling fluid).

There are two SiPM per crystal electrically connected to two front-end boards. The reason for having two of them is to provide a more robust measurement and don't lose data if one photo sensor fails during data taking. The total resulting number of photo sensors is 1348 per disk (2692 in total).

A summary for the components number of the FEE electronics is reported in table 2.1.

The front-end electronics for the calorimeter readout consists of two discrete and independent chips (Amp-HV) placed on one unique front end board electrically connected to the back of the photo-sensor pins. The chips provide both the amplification and the local linear regulation to the photo-sensor bias voltage. Groups of 16 Amp-HV chips are controlled by one dedicated ARM controller placed on one interface board located in the DAQ crate. This board distributes low voltage and high voltage reference values, sets and reads back the locally regulated voltages. The Amp-HV is a multilayer double-sided discrete component board that performs out the two tasks of amplifying the signal and providing a locally regulated bias voltage, significantly reducing the noise loop-area.

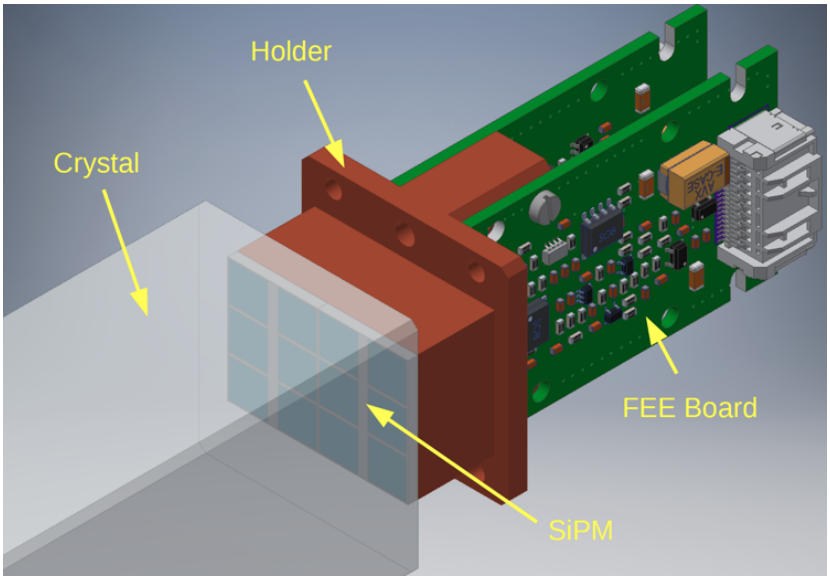

Figure 2.7: CAD model of one front-end unit. The brown structure is the copper mechanical support of the two SiPM and front-end boards. It is the component connected directly to the backplate.

Table 2.2: Summary of crate components number.

Component	Number per disk	Total (2 disks)
Crates	10	20
DIRAC+Interface boards	80	160
Clock boards	10	20

2.4.2 DAQ electronics

The analog signals produced by the front end electronics are transmitted to the data acquisition boards, hosted in the DAQ crates. Since the main function of the data acquisition boards is to digitize and transmit the analog signals to the global Mu2e data acquisition, these boards are named *waveform digitizers* or *DIRAC* (Digitizer ReAdout Controller). Additional boards are necessary to provide and distribute power to the front end boards, monitor the photosensors and front-end electronics performance. These boards are called *interface boards*.

In the current design, there are 10 crates per disk, and each crate hosts 8 DIRAC and 8 interface boards (fastened together to form 8 single boards). Every crate also has one further board to provide clock distribution to the system (fig. 2.8).

In table 2.2 is reported a summary of the crate components number.

The DIRAC board is characterized by the following components (fig. 2.9):

- **1 Field Programmable Gate Array (FPGA)**: is an integrated circuit designed to be configured by a customer. It contains an array of programmable logic blocks, and a hierarchy of reconfigurable interconnects, that allow the blocks to be "wired together". Logic blocks can be configured to perform complex combinational functions, or merely simple logic gates like

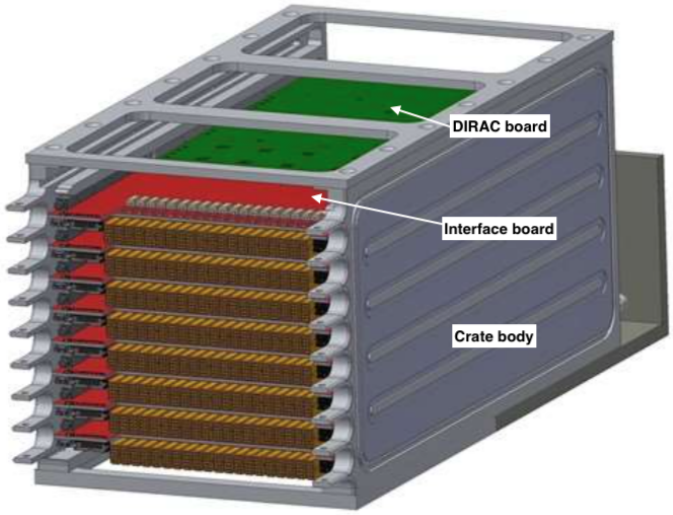

Figure 2.8: CAD view of a crate in which the 8 DAQ boards are mounted. [26]

AND and XOR. It is the most complex component of the board; processes the data received from the SiPM previously digitized by the Analog to Digital Converters (ADC);

- **4 DC-DC converters**: they transform the voltage received from the external power supply to the values required;
- **10 Analog to Digital Converter (ADC)**: they convert analog signals received from the front end boards into digital signals to be further processed by the FPGA and then transmitted to the DAQ system;
- **6 low dropout Linear Regulator**: they provide low voltage and high current outputs with a minimum of external components. It offers high precision and ultra-low dropout of 500 mV in the worst case conditions;
- **1 Jitter Cleaner:** it cleans the clock signal and distributes it to the ADCs and FPGA mainly.

The interface board (also called *mezzanine board*) is mechanically attached to the DIRAC board, and is contains these components:

- **1 voltage regulator**: transforms the 28 V received from the power supplies (placed outside the cryostat) to the 8 V used by the front end electronics board;
- **1 ARM Controller and I2C drivers** to monitor the performance of the front-end electronics.

Every electronic component dissipates heat towards the environment during operation due to the *Joule effect*. The vacuum inside the cryostat (where all these components lie) does not allow to cool the calorimeter using the standard forced

Figure 2.9: Components on a working prototype of the DIRAC board (Courtesy of INFN).

air cooling system. This problem requires a dedicated cooling system. This is the main purpose of this Thesis (and of all the previous ones [17], [28], [23], [26], [4]).

In the following Chapters all the requirements requested to the cooling system will be assessed, and after that two simple systems will be designed and verified.

Chapter 3

The calorimeter cooling system

The calorimeter will be installed inside an evacuated cryostat maintained at the average pressure of $1.3 \cdot 10^{-7} Atm$ during data taking. The consequence of operating in vacuum is that a dedicated cooling system is necessary to remove the power dissipated by the electronic components. In this respect, the most sensitive components are the SiPM since their operational temperature is limited below $0\ ^{\circ}C$ depending on the dose of absorbed radiation. We plan to keep the calorimeter SiPM at the temperature of $0\ ^{\circ}C$ until the radiation absorbed during operation degrades their performance and forces to reduce their operational temperature to approximately -10 degree C. The thermal constraints for the electronic components employed in the DAQ boards are looser since in this case operational temperatures of the order of $60\ ^{\circ}C$ are perfectly safe. We have designed a cooling system based on the principle of a low temperature fluid flowing in a hydraulic circuit in thermal contact with the electronic components through a network of pipes. Electronic power is thus removed through a combination of forced convection (fluid-pipe) and conduction (pipe-target component). The cooling system inside the cryostat is fed by an external hydraulic circuit which includes a cooling station and all the necessary services. The cooling circuits of the front end units and DAQ crates, which are located in different zones of the detector, are branches of the same circuit. In other words, they share the same cooling and pumping stations outside the cryostat but have independent branches to cool down the different zones. A simplified scheme of the cooling system is reported in figure 3.1.

Before showing the characteristics of the thermal loads, we have analysed the technical requirements of the cooling system in terms of heat absorption. Section (3.1) summarises all the technical requirements.

3.1 Technical requirements

3.1.1 Thermal requirements

Table 3.1 reports the constraints in terms of maximum allowed operational temperatures of the electronic components employed in the calorimeter. Some of these values may still change since the choice of the electronic components has not been completely finalized yet. but we do not expect significant changes. I have quoted

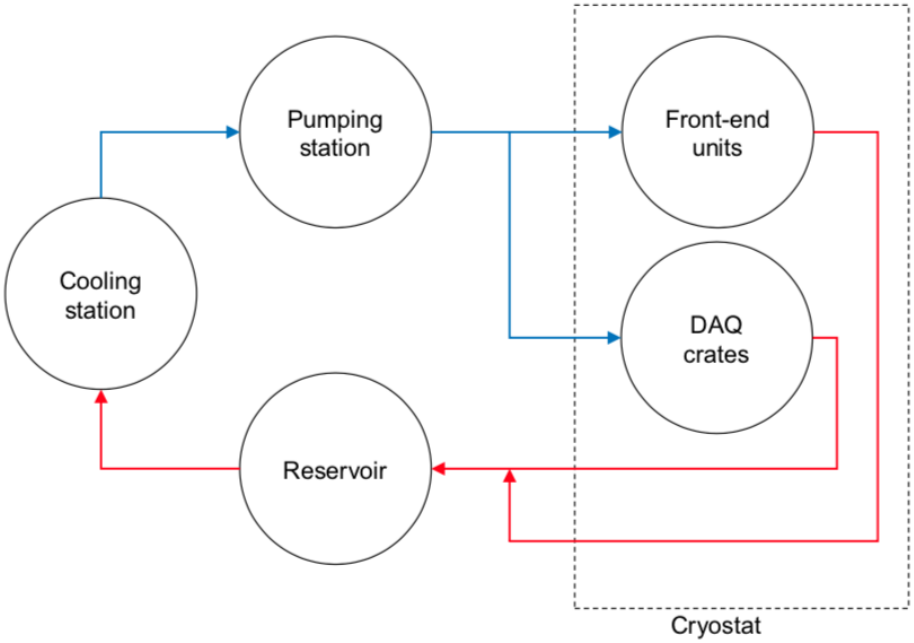

Figure 3.1: Schematic idea of the cooling system.

Table 3.1: Maximum allowable temperatures for the electronic components.

Component	**Critical** T $[°C]$	**Max requested** T $[°C]$	**Location**
SiPM	-10	-10	FEE
FEE boards	125	125	FEE
ADC	125	60	DAQ
FPGA	100	60	DAQ
DC-DC	100	60	DAQ
Linear Regulator	125	60	DAQ
Jitter Cleaner	125	60	DAQ

the operational temperature of -10 $°C$ irradiated SiPM.

According to the data-sheets, all the electronic components can safely operate at temperatures above 100 $°C$. For safety reasons we have decided to keep the maximum operational temperature in the range of half the critical temperature and the cooling system has been designed to easily provide this condition.

3.1.2 Electric power requirements

The cooling system includes several machines:

- Pump: the machine that pushes the fluid along the circuit against the head loss. This machine needs an electric motor;

Table 3.2: Electric power budget summary for the mechanical room. (Source: Mu2e building)

Component	**Percentage of total**	**Electric budget** $[kW]$
Chiller	50%	12.5
Pumping group	20%	5
Control cabinet	10%	2.5
Miscellaneous	5%	1.25
Margin	15%	3.75
Total	100%	25

- Chiller: the machine that constantly cools the fluid. It has an internal compressor driven by an electric motor;
- Control system: all the equipment needed for the circuit regulation (control valves, sensors etc..).

All these components absorb electric power. This means that the mechanical alcove must deliver a certain amount of electric power to the equipment. Table 3.2 reports the electric power budget.

3.1.3 Mechanical alcove requirements

All the equipment needed by the cooling system must be contained in the mechanical alcove. This room is a cube of dimensions 2 X 2 X 2.5 m, with the longest side along the height direction. The room is at ambient temperature and is located in the same building of the Mu2e experiment.

The connections between the mechanical alcove and the cryostat, where the Mu2e experiment is contained, are implemented by means of the routing system (fig. 2.6). Obviously the routing connections should not interfere with other components present in the building.

3.2 Thermal load of the system

All the electronic components have an intrinsic power dissipation in form of heat production (due to the Joule effect). This heat, if not well disposed of, will rapidly increase the temperature of the components until a new thermal equilibrium is reached. In an insulated system like the calorimeter, in which the only form of available heat exchange is the radiation with the cryostat walls, the equilibrium temperature would be quite high in absence of a cooling system. The components of the calorimeter would reach a temperature at which their exchange of thermal power with the cryostat walls would be exactly equal to the incoming thermal power of the electronics. This of course would imply a calorimeter at higher temperature than the cryostat walls (25 $^{\circ}C$). This temperature would not be acceptable for the electronics (in particular the SiPM, having requirements

Table 3.3: Thermal powers dissipated from the calorimeter electronics.

Component	**Unit power** $[W]$	**Total number**	**Total power** $[W]$
Outer SiPM	0.16	2128	342
Inner SiPM	0.48	568	274
FEE boards	0.36	2696	957
DAQ crates	296	20	5920
Total			**7492**

$< 0\ ^{\circ}C$). This is the reason for having a dedicated cooling system to keep the temperature of the electronic components at acceptable values.

First of all we have estimated the power dissipated by each component and to be disposed of through the cooling system. We have performed several tests and simulations ([26], [17]). Table 3.3 reports our estimates.

The thermal load due to the electronics is not the only information necessary to properly design the cooling system. Since that some components need to be colder than the cryostat temperature ($\simeq 25\ ^{\circ}C$), the cooling fluid has to be flown at lower temperatures as well. This forces environmental heat to get into the cooling system. This happens because in the routing system and in the mechanical alcove all the pipes are directly in contact with the external air and provide natural convection. This term of external heat flowing into the cooling system will be minimised by insulating the pipes with proper material (mainly *polyurethane*).

Another contribution to the incoming thermal power is due to different sources of mechanical dissipation: pumps, valves, tanks etc...

All these terms cannot be calculated before having the complete final design. We can only make a conservative estimate at design level and verify with a direct measurement once the system is assembled. After some iterations the selected value for these terms has been 3300 W. The resulting final thermal load is approximately

$$P_{th} \simeq 10.8\ \ kW$$

This thermal power must be extracted with the cooling system to keep the system at thermal equilibrium.

The cooling system has a fluid flowing through the pipes and absorbing electronics heat and contemporaneously increasing its temperature. After passing through the chiller[1] its temperature is decreased and the fluid begins a new cycle. The value of 10.8 kW is the most important parameter for the choice of the cooling station.

[1] A chiller is a machine that removes heat from a liquid via a thermodynamics cycle. This liquid can then be circulated through a heat exchanger to cool equipment, or another process stream (such as our cooling fluid for the calorimeter). As a necessary by-product, refrigeration creates waste heat that must be exhausted to ambience. The types of refrigeration systems of chillers are the air cooling condenser, and the water cooled condenser.

3.3 The electronics cooling geometry

Once the thermal power to be removed has been estimated, it is necessary to design the geometry of the heat exchangers. The zones in which heat has to be transmitted are:

- **FEE**: in this zone the fluid absorbs heat from the front end boards and SiPM;
- **DAQ**: in this zone the fluid absorbs heat from the electronic boards inside the DAQ crates.

In the following pages the geometry of the cooling channels close to the electronic components will be defined. The final design has been completed after several iterations, carried out during earlier Theses by former students involved in this project [17], [28], [26], [15], [7], [4].

3.3.1 FEE cooling geometry

The cooling system for the FEE zone consists of a network of 38 copper pipes connected with the inlet and outlet manifold to the routing system. There are 18 straight and 20 curved pipes with 180 degrees elbows for each calorimeter disk. The pipes have an internal diameter of 3 mm and an external diameter of 4 mm.

Because of the small dimensions involved in this pipe network, it is important to have a pure and dirt-free fluid. This will be achieved by means of suitable filters located along the circuit.

This design (fig. 3.2 and 3.3) has the following advantages:

- relatively low cost ;
- most pipes are in thermal contact with approximately the same number of front end units and approximately remove the same amount of power;
- simple to build;
- it allows to have short pipes without many turns that would increase the head loss

The pipe network runs between the back plate and the front-end units, removing heat via convection and conduction (figure 3.4).

The back plate performs the function of mechanical support for the FEE boards and for the cooling system itself, as shown in fig. 3.4a. Each unit is joint to two pipe cases with four screws, and the pipe cases are fastened to the back plate with several screws as well. The pipe cases are made of copper just alike the pipes to reduce the thermal resistance of the path[2].

Each pipe is connected to the inlet and outlet manifold by means of *Swagelok VCR* connectors (fig. 3.3), which are brazed with an extremely careful procedure to make sure there is a high quality thermal connection.

[2]Copper is one of the economically affordable materials with the highest thermal conductivity

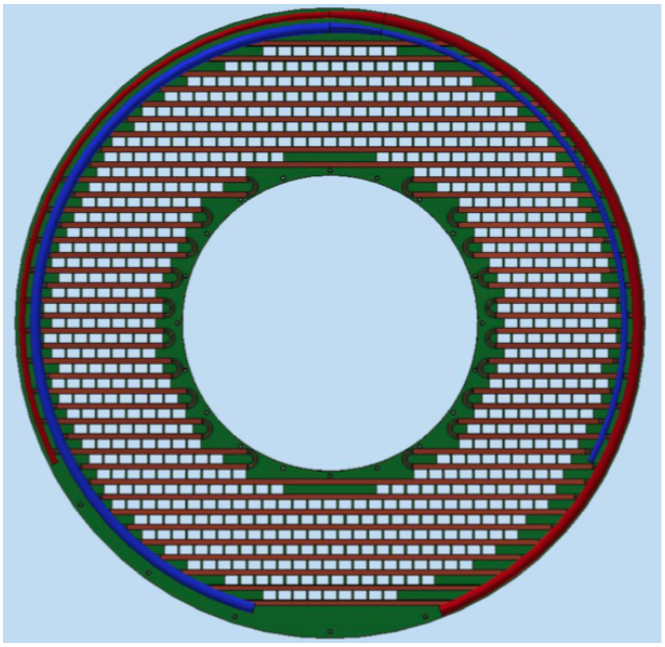

Figure 3.2: CAD view of the 38 pipes network on 1 calorimeter disk back plate.

Is important that the fluid does not leak inside the cryostat because this would deteriorate the vacuum level, as well as produce other environmental problems. Also the cooling lines are brazed to their cases with a similar procedure using a pure silver foil 0.15 mm thick.

3.3.2 DAQ cooling geometry

The cooling channels of the DAQ electronics are directly milled inside the lateral panels of the DAQ crates (fig. 3.5). The reason for this design is not only to improve the cooling but also for space efficiency. The crates are quite close to each other and have many features on their sides where external cooling channels would be cumbersome (see fig. 3.6).

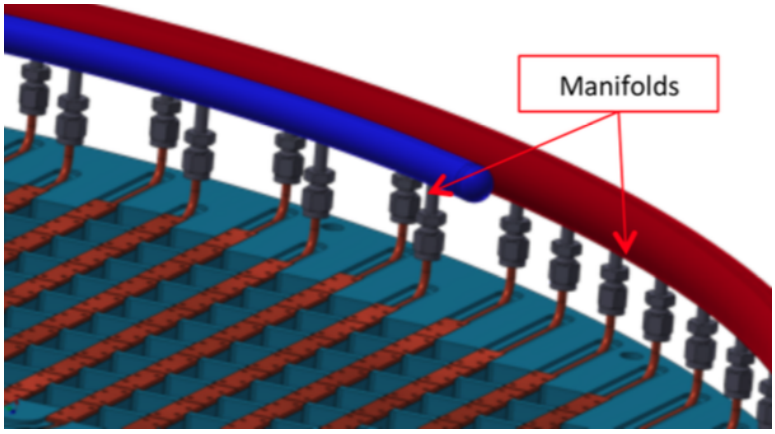

Figure 3.3: CAD details of the manifolds (blue for inlet, and red for outlet) and their connections with the pipe network.

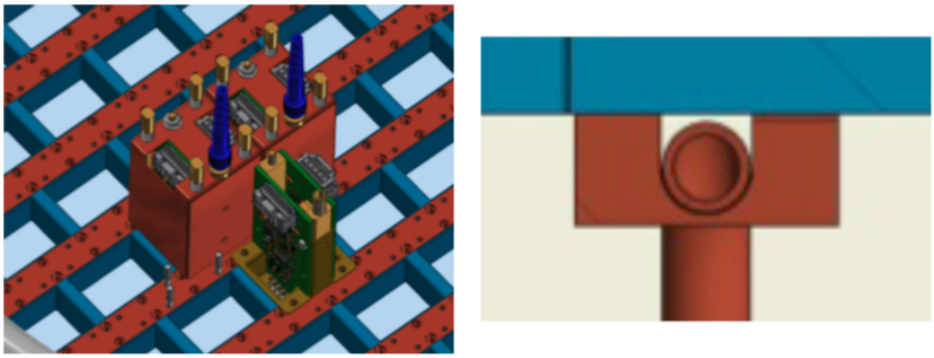

(a) CAD model showing three front end units fixed to the pipe cases and the plate. A Faraday cage covers two of the tree units.

(b) CAD model showing the contact between pipe case and the backplate. To reduce the thermal contact with the plate, the mechanical contact between this and the pipe cases is limited to small areas.

Figure 3.4: CAD overview of the front end unit cooling system (Mu2e Datacenter).

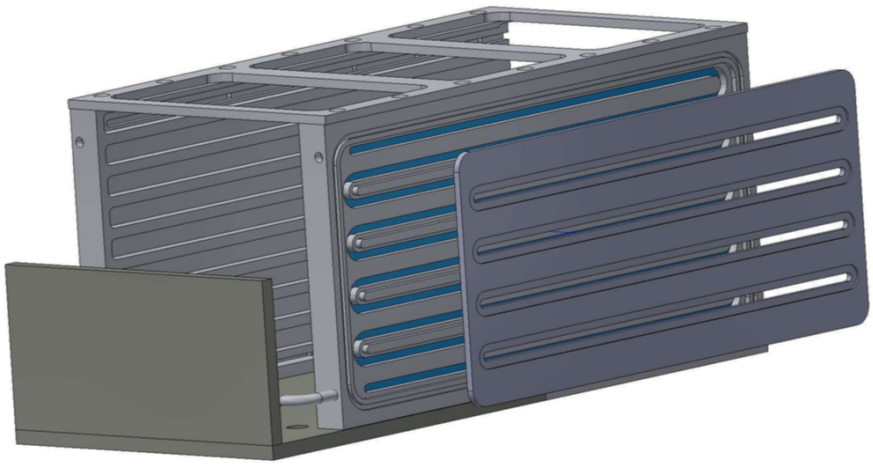

Figure 3.5: View of the internal cooling channel in a crate CAD model.

Each crate is connected to the inlet and outlet manifold in parallel by means of Swagelok connectors. The manifolds are then connected to the main DAQ line which supplies the cooling fluid at the right temperature and rate.

Once the geometry in proximity of the target components is determined the next step is to design a flow schematic for the process to supply the right amount of fluid at the right temperature and properly cool the system.

To do this we have estimated the temperature at which the fluid must flow close to the components as well as its thermodynamic properties and flow rate.

To calculate these temperatures we need a thermal model of every heat exchange of interest: one for the FEE electronics, and one for the DAQ. The goal of any thermal model is the calculus of thermal resistance between points of interest. One point of interest is where the fluid is as close as possible to the component, and the other one is the component's critical point (where the temperature is maximum).

Thermal resistance is analogous to the electrical resistance, and is physically defined in the following way:

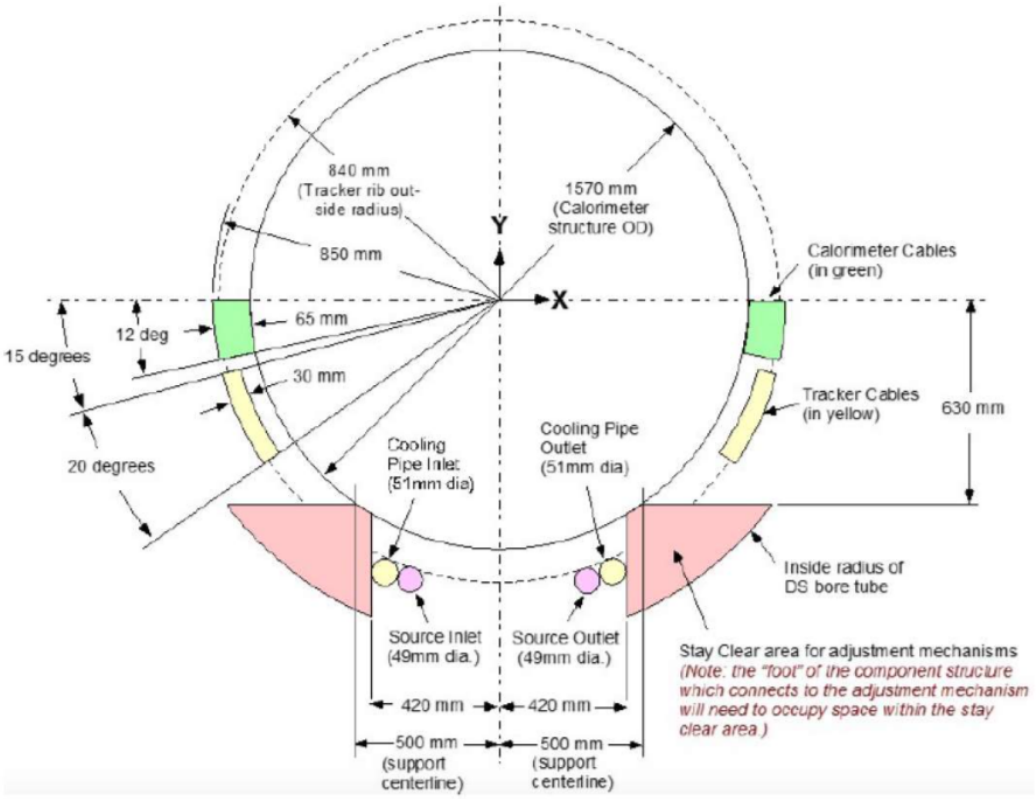

Figure 3.6: Schematic view of the calorimeter face geometry, including the volumes reserved to the electric cables and cooling pipes.

$$R_{th} = \frac{\Delta T}{\dot{Q}}$$

In other words it is the resistance that the material opposes to the heat flow occurring between two points with different temperature. For example, a path connecting two points at 1 $°C$ of difference that allows 1 W of heat power transmission, has a thermal resistance of $1°C/W$.

This type of thermal resistance (conductive) is a characteristic of the material geometry involved in the heat flow path. For a system with defined materials and geometry the resistance is uniquely determined (except for temperature and other minor variations that affect some properties of the material).

If every thermal resistance of interest is determined, as well as the heat flow, what remains to be computed is the temperature difference between points of interest:

$$\Delta T = \dot{Q} R_{th}$$

This allows to evaluate the temperature of the material in contact with the fluid in order to properly cool the right elements. This procedure is described in Chapter 4, and the results will be useful data for the cooling system design, shown in Chapter 6.

The estimate of the electrical resistance for 3D models is not so easy to accomplish. Heat can flow in any direction and the involved equations become

too difficult to be solved manually. The general problem of heat conduction in a solid is described by the well known partial differential equation [8]:

$$\frac{1}{\alpha}\frac{\partial T}{\partial t} = \nabla^2 T$$

Where $T(x, y, z, t)$ is function of the thermal diffusivity α of the material. We are interested in an equilibrium configuration for the system, so we can study the simpler steady state equation:

$$\nabla^2 T = 0$$

The analytical solutions for this problem is known only for simple geometries and boundary conditions. For the general case of 3D geometry and different boundary conditions numerical methods must be adopted. Such numerical methods are embedded in the so called *Finite element methods (FEM) softwares*[3].

For this project the most used FEM program has been *Ansys Workbench*. It has been used to estimate the following temperature distributions:

- Front end unit temperature distribution, in particular to estimate the temperature variation between the fluid and SiPM;
- DAQ temperature distribution in order to estimate temperature variations between the fluid and the critical electronic components.

In Chapter 4 all the thermal results coming from simulations will be briefly summarised to find important data for the cooling system design.

[3]The finite element method is a numerical method for solving problems of engineering and mathematical physics. Typical problem areas of interest include structural analysis, heat transfer, fluid flow, mass transport, and electromagnetic potential. The analytical solution of these problems generally require the solution to boundary value problems for partial differential equations. The finite element method formulation of the problem results in a system of algebraic equations.

Chapter 4

Thermal models

The purpose of this chapter is the determination as accurate possible of the temperature distribution between points of interest. This results in a lumped parameter model (shown in fig. 4.1), in which the heat path is treated as an electrical circuit.

The temperature difference between two points (or two bodies) plays the role of electrical voltage, while the heat flux is analogue to the current. The corresponding relation to the Ohm's law becomes:

$$\Delta T = \dot{Q} R_{th}$$

Where R_{th} is the thermal resistance between two determined points, ΔT is the temperature difference between them, and $\dot{Q}$ is the total heat flowing from the warmer point to the colder one. Following this methodology we can obtain important parameters for the system design. Knowing the maximum allowable temperature of SiPM and the heat power produced it is a straightway the calculus of components temperature that mediate this exchange.

The power to be transmitted depends on the configuration of the system during its lifetime[1]. The goal is to find a design able to withstand all the possible configurations of the system in the cheapest, and most reliable way.

[1]Several configuration are foreseen during the life cycle of the calorimeter. They are descripted in the requirements chapter

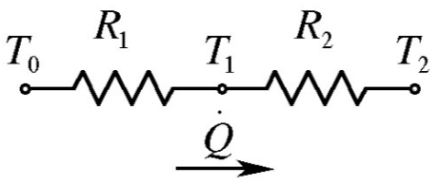

Figure 4.1: Example of a 3 bodies lumped parameter model. The three bodies in series are represented by T_0, T_1, T_2. The thermal resistance between the bodies are R_1, R_2, and the heat flowing is $\dot{Q}$

4.1 Thermal model of the front end electronics

The first category of points of interest is represented by the front-end electronics (composed by the front end boards and the SiPM). The temperature must be low enough to let the SiPM work properly, as well as the front end boards.

The complete thermal simulations and experimental verifications can be found in [4] and [17]. In this section we only present some important result of the simulations. The goal is to understand the thermal behavior of the various parts during operation. The simulation had to be as accurate as possible, since that the electronic components are fully functional only within a limited range of temperatures. Furthermore, their reliability and lifetime strongly depend on the operating temperature. The physical access to the detector for repairs or maintenance will be limited to few weeks per year. This means that every effort improving the system reliability is very precious.

Electronic components vendors usually specify the critical temperature below which the electronic components have to be maintained. The SiPM is the most critical part, and attention will be focused on it. It also has a strong dependence on operational temperature, which has to be maintained below $-10°C$ in the worst conditions. The simulations results of the front-end unit are presented in three different sections:

1. Results of one single SiPM simulation;
2. Results of a complete front-end unit;
3. Summary of the results.

4.1.1 SiPM thermal model

The SiPM adopted for Mu2e calorimeter is custom produced by the Japanese company Hamamatsu^{TM}. The company reports a value of the *Overall Thermal Resistance (OTR)* per unit surface of:

$$OTR = \frac{s}{k} = 4.9 \cdot 10^{-4} \ \frac{m^2 K}{W}$$

Where s is the thickness of SiPM, and k its thermal conductivity. Knowing the SiPM cross section ($A = 14 \cdot 19.4 = 272 \ mm^2$), the overall SiPM thermal resistance is

$$R_{SiPM} = \frac{OTR}{A} = 1.8 \ K/W$$

Fig. 4.2 shows the SiPM model used in the simulation, which includes the G10 support, the metal, the underfill resin and the silicon sensor.

Table 4.1 reports the values of thermal conductivity and thickness of every SiPM part.

(a) *Back side of the SiPM .*

(b) *Front side of the SiPM .*

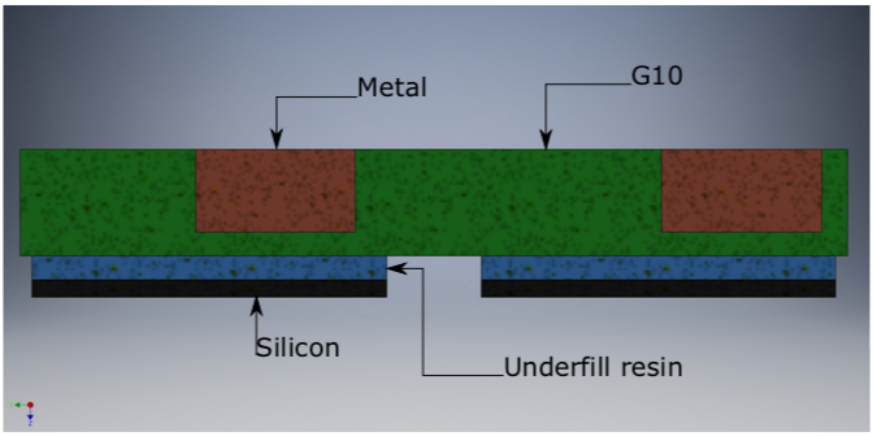

(c) *Section of the SiPM .*

Figure 4.2: Schematic representation of a SiPM [4].
a) SiPM back side with the metal ring;
b) SiPM front side with the six adjacent silicon layers;
c) main SiPM components: the sensitive silicon layer, the underfill resin layer, the G10 body and the asymmetric metal contact.

Since the SiPM are very thin elements, the finite element method may have meshing[2] problems. In order to have a reliable and numerically stable result, at least two mesh elements should always be used in the thickness direction, but it's also good practice to not use tiny elements because of numerical problems. A possible solution is to multiply both the thickness s and thermal conductivity k by the same numerical factor. This artificially increases the dimensions of the finite elements, allowing the insertion of more mesh elements without changing the results. In the case of these simulations the real parameters have been doubled during the simulation.

Table 4.2 shows the virtual thickness and conductivity values used in the model. As a consequence of this procedure, the components that once were isotropic (the metal, the underfill resin and the silicon) now have an anisotropic thermal conductivity[3].

[2]Mesh generation is the practice of creating a mesh, a subdivision of a continuous geometric space into discrete geometric and topological cells. Mesh cells are used as discrete local approximations of larger domains. Meshes are created by computer algorithms depending on the complexity of the domain and the type of mesh desired. The mesh should also be fine in areas that are important for the subsequent calculations.

[3]The materials can have different thermal conductivity depending on the heat flow direction.

Table 4.1: Thermal properties of SiPM components.

Components	**Thickness** $[mm]$	**Thermal conductivity** $[W/m^2K]$
G10	0.9	$k_\perp = 0.3$ $k_\parallel = 0.9$
Metal	0.7	200
Underfill resin	0.2	2.4
Silicon	0.15	148

Table 4.2: Thermal properties used for the simulations.

Components	**Thickness** $[mm]$	k_x $[W/m^2K]$	k_y $[W/m^2K]$	k_z $[W/m^2K]$
G10	1.8	0.9	0.9	0.6
Metal	1.4	200	200	400
Underfill resin	0.4	2.4	2.4	4.8
Silicon	0.30	148	148	296

4.1.2 Boundary conditions and results

Fig. 4.3 shows the boundary conditions used in the simulation. Any thermal simulation needs two possible types of boundary conditions:

- A first set of condition regards the imposition of a certain temperature field $T(x, y, z)$ along the boundaries of a body;
- Another set of condition regards the heat flow occurring at the external surface. This condition affects the temperature gradient $\nabla T(x, y, z)$ on the boundary. It can be of two types:
  - Via conduction with another attached body;
  - Via convection with an external fluid.

For the SiPM simulations the following boundary conditions have been used:

- The temperature of the back side of the SiPM has been fixed at 0 $°C$;
- On the silicon faces has been applied an overall uniform heat flux of 1 kW (4.3b);
- All the other surfaces are considered adiabatic. Their heat flux (or temperature gradient) has been set to zero.

The values selected for the boundary conditions are not important by themselves, but to compute the thermal variations of the SiPM apparatus. In other words: once we have the right value of thermal resistance (or alternatively the

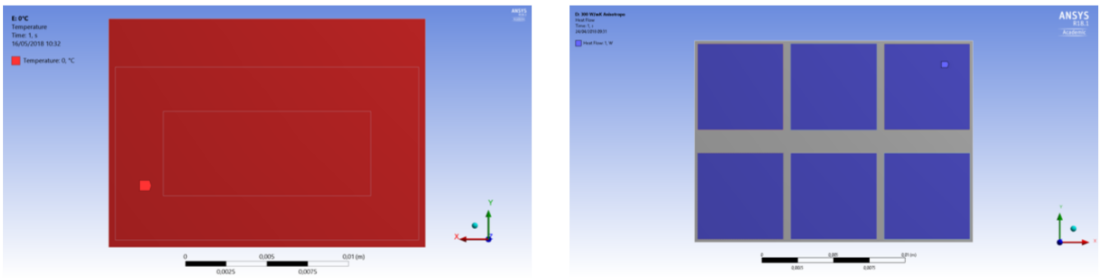

(a) *Constant temperature on one face.*

(b) 1 W *power on the silicon pieces.*

Figure 4.3: Boundary conditions for SiPM simulation.
a) uniform temperature on the back side of 0 $°C$;
b) uniform heat flux on SiPM faces of 1 kW.

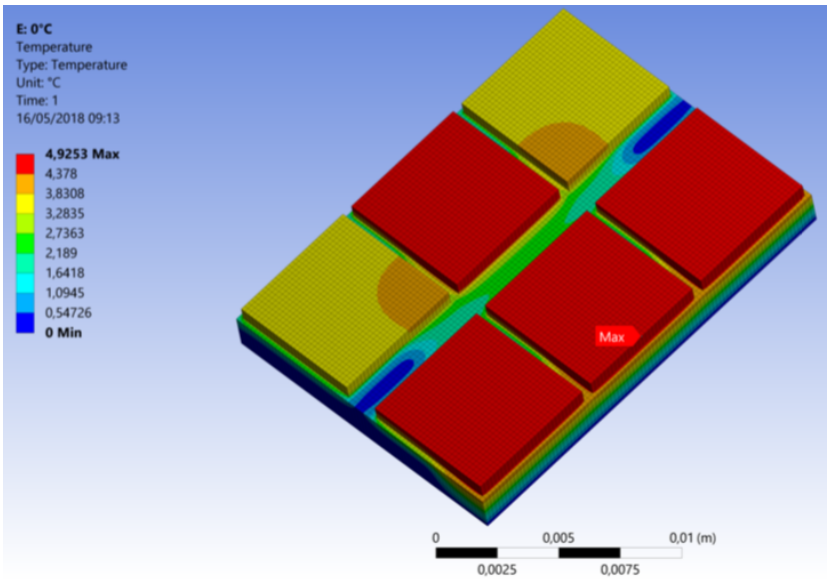

Figure 4.4: Result of SiPM simulation. The critical point is at 5 $°C$ higher temperature than the backsurface of SiPM.

temperature difference, once the resistance is determined) from the back surface towards the SiPM faces we can establish the temperature requested to the back surface of SiPM in order to keep the photosensors at the right temperature.

Fig. 4.4 reports the temperature distribution between the cooled surface (the back surface) and the SiPM critical points (the hottest ones).

The maximum temperature value on the silicon surface is not coherent with the OTR value provided by Hamamatsu. If the power dissipated by the SiPM were 1 W, the temperature difference between the silicon surface and the G10 surface should be $\Delta T = 1.7\ °C$, not consistent with the value of 5 $°C$ coming from simulations. This is probably due to the limited accuracy of the modeled SiPM, and that we do not know exactly how the OTR had been calculated by Hamamatsu. Even though the value of provided by the manufacturer is obviously more accurate than this SiPM model, it will be used to obtain conservative estimates of the temperature field. This value of 5 $°C$ will be used later together with other

temperature variations in order to obtain the researched design parameters: the overall temperature difference between the cooling fluid and the SiPM.

Along the heat path between the fluid to the SiPM are also present convective resistances. They cannot be determined only by the materials and geometry because they depend on the cooling fluid and flowing properties (temperature, velocity, etc...). It can be demonstrated that in this series the convective resistance plays a little role. It means that if we slightly changed the dynamics properties of the flow, the overall resistance of the thermal path would not change very much. We can then consider the temperature jump associated with the convection between fluid and pipe almost a constant value. Once we'll have a satisfactory design we'll simply verify this assumption.

In this way becomes possible to select the temperature for the fluid in particular locations. Once we decide what temperature we want for the SiPM, we simply have to subtract the ΔT of reference and obtain the temperature that the coolant should have in that position. When we obtain a significant map of temperature key points we'll be able to design a system. As soon as the first design is obtained, we'll verify whether or not the requirements and the assumptions are respected. In case they didn't pass the verification analysis, iterations on the system will be done until a satisfactory design comes out.

Another important result coming from the simulations is the importance of the glue used to stick the SiPM to the backplate. Glue distribution can modify the temperature field inside the sensor significantly, thus attention will be mandatory in this part of assembly. Further information on different glue distributions can be found in [4].

4.1.3 Front end unit modeling

The design of the cooling lines has been discussed in chapter 3, and is reported in fig. 3.4. In order to compute the thermal resistance from the cooling line to the front-end board is important to set some parameters prior to calculate the right boundary conditions:

- **Type of fluid**: the fluid selected for the simulation was *35% glycol* because it was expected to be used. The choice of the cooling fluid will be fully explained in chapter 5;
- **Velocity of the fluid**: this quantity, together with the cooling channel diameters, provides the cooling performance of the line. In other words it's needed to calculate the convective resistance between the fluid and the pipe inner walls;
- **Temperature of the fluid**: needed to calculate the thermodynamic properties of the fluid at the right conditions of employment.

The velocity and initial temperature of the cooling fluid have been fixed respectively to 3.5 m/s and $-10\ ^{\circ}C$. From these data we can compute the convection film coefficient h_c. The friction coefficient can is obtained with *Colebrook-White correlation* [9]:

$$f = \left[1.14 \cdot 2\log_{10}(\frac{\varepsilon}{D_h} + \frac{21.25}{R_e^{0.9}})\right]^{-2}$$

Where $\varepsilon = 30\ \mu m$ is the mean rugosity of the channels, $D_h = 3\ mm$ is the inner diameter of the pipes and $R_e = \frac{\rho V D}{\mu} = 87010$ is the Reynolds number in the duct.
The Nusselt number for a turbulent flow (since that $R_e = 87010$) can be estimated with the *Dittus-Bolter correlation* [13]:

$$Nu = \frac{1}{8} f R_e P_r^{1/3}$$

Where P_r is the glycol Prandtl number at -10 $°C$.
From the definition of Nusselt number we can obtain the heat convective coefficient in this way:

$$h_c = \frac{kN_u}{D}$$

The found value for the convection film coefficient is:

$$h_c = 5590\ \frac{W}{°C \cdot m^2}$$

This value is needed as boundary condition at the interface between the cooling fluid and inner pipe walls, because it determines the temperature of the inner pipe walls once the heat flow is determined:

$$T_{pipe} - T_{fluid} = \frac{\dot{Q}}{Ah_c}$$

Where A is the contact surface, and $\dot{Q}$ is half of the total heat power coming from the front end unit (2 SiPM and 2 front end boards). Only half of it is used because each front unit is cooled by 2 cooling lines.

Since the temperature variation of the cooling fluid along a pipe is negligible and the thermal conductivity of the back plate material (PEEK) is low, only one front end unit has been included in the analysis model. The simplified CAD model is reported in figure 4.5.

The boundary conditions used for the simulation are the following:

- Two film convection boundary conditions at the interface between the inner surface of pipes and cooling fluid. This means attributing the previously found value of T_{pipe} to the pipe surfaces in contact wit the fluid;
- The heat flow conditions to simulate the power dissipated from both the SiPM and electronic boards. All this power must flow towards the fluid. This condition sets a value on the temperature gradient in proximity of the fluid (by the Fourier's law of heat transfer $\vec{q} = -k\nabla T$);
- Adiabatic conditions for all other surfaces, being them in vacuum. This impose a zero gradient on the temperature field on those boundaries.

The thermal conductivity of involved materials is listed in table 4.3

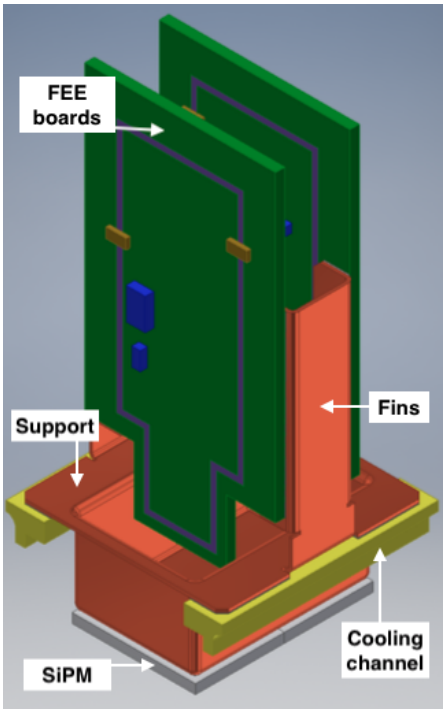

Figure 4.5: Simplified CAD model of the front end unit used for the simulation.

Table 4.3: Thermal conductivity of the front end unit materials.

Component	**Material**	**Thermal conductivity** k $[W/°Cm]$
Support	Copper	401
Glue	Boron nitride	1.2
Bridge resistor	Aluminum nitride	156
Pipe case	Copper	401
FEE board $\parallel$	FR-4+Copper	1.1
FEE board $\perp$	FR-4+Copper	0.36

4.1.4 Front end unit results

The analysis results are reported in fig. 4.6. The front-end boards are not critical components since that the allowable temperature is 125 $°C$, while the maximum reached temperatures in the simulation are approximately of 80 $°C$. These results have been experimentally verified with good coherence [17].

The temperature difference between the cooling fluid and the front end board is estimated to be:

$$\Delta T_{FEE-BOARD} = 90 \ °C$$

This means that whatever the temperature and type of fluid used in the cooling system (not too different from the ones used in the simulation), the critical point of the front end board will be approximately at 90 $°C$ higher temperature than

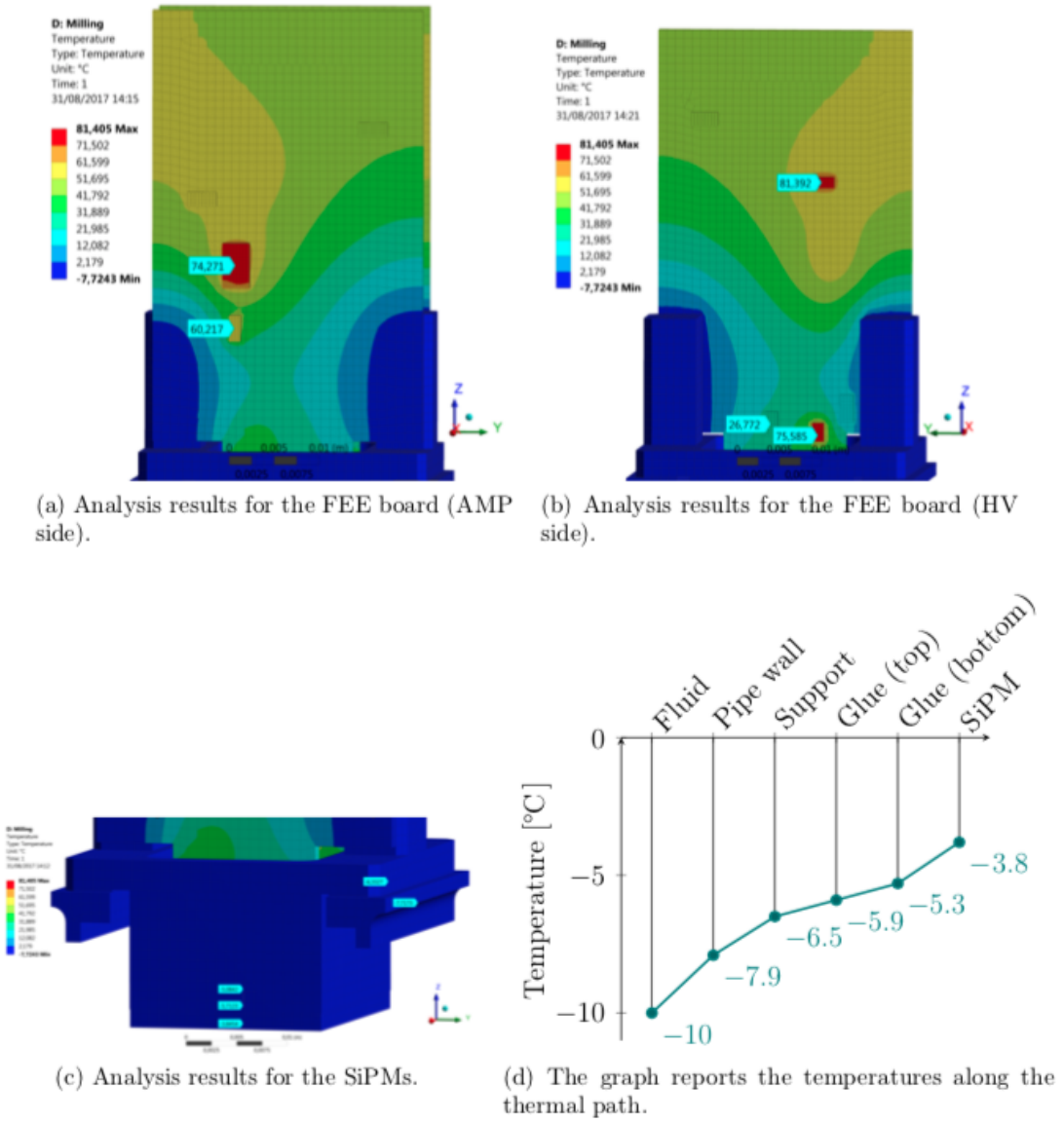

(a) Analysis results for the FEE board (AMP side).

(b) Analysis results for the FEE board (HV side).

(c) Analysis results for the SiPMs.

(d) The graph reports the temperatures along the thermal path.

Figure 4.6: Results of the front end units simulation.

the coolant. Obviously the real system will have slightly different temperatures[4], but that difference is assumed to be negligible for a first approximation design. Once the system will be fully designed new simulations and experiments will verify whether or not these assumptions were true.

4.1.5 Summary

After simulations and experiments of SiPM and front-end boards we can get important data for the system design. Recalling that a determined heat flow and

[4]This happens because some resistance depends on the temperature and the cooling system layout.

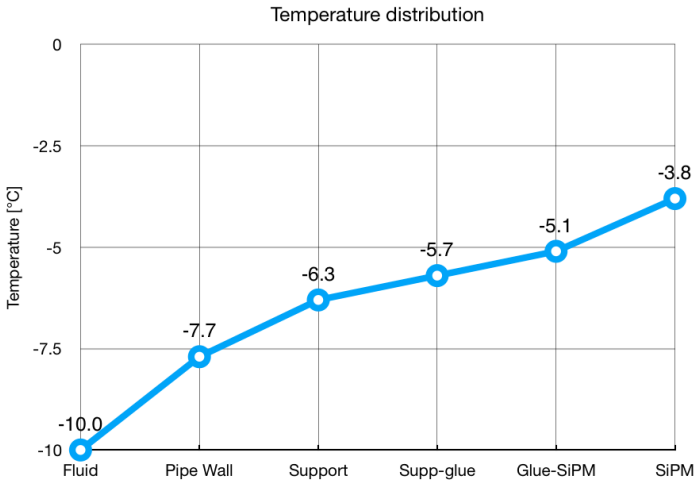

Figure 4.7: Temperature distribution from fluid to SiPM.

a fixed set of thermal resistances[5] imply a fixed ΔT among points of interest we can draw some important chart in order to easily visualize the results.

Fig. 4.7 reports the temperature difference between the fluid and the SiPM. The last temperature gap between glue-SiPM and SiPM is only 1.3 $°C$ instead of the predicted 5 $°C$ found in the single SiPM simulation. In order to be conservative we'll use the bigger value, even though 1.3 $°C$ almost perfectly matches with the value provided by Hamamatsu (1.7 $°C$).

We obtain in this way the overall temperature difference predicted between the fluid and the SiPM:

$$\Delta T_{SiPM} = 5 + 6.2 = 11.2 \ °C$$

The other important ΔT in the front end unit is the one connecting the fluid to the front end board. From fig. 4.6:

$$\Delta T_{FEE-BOARD} = 90 \ °C$$

These two quantities will be used for the design of the cooling circuit, described in chapter 6, in order to select the main parameters of the system.

Other types of heat exchange phenomena have been studied: for example the radiation heat exchanged between bodies at different temperature. None of them have produced significant modifications to the thermal model, and then will be neglected.

[5]Recall that if fluid and flowing properties change, the resistance associated with convection varies, but doesn't affect so much the global path resistance. As a first guess we can assume those values almost constant. Later they will be verified.

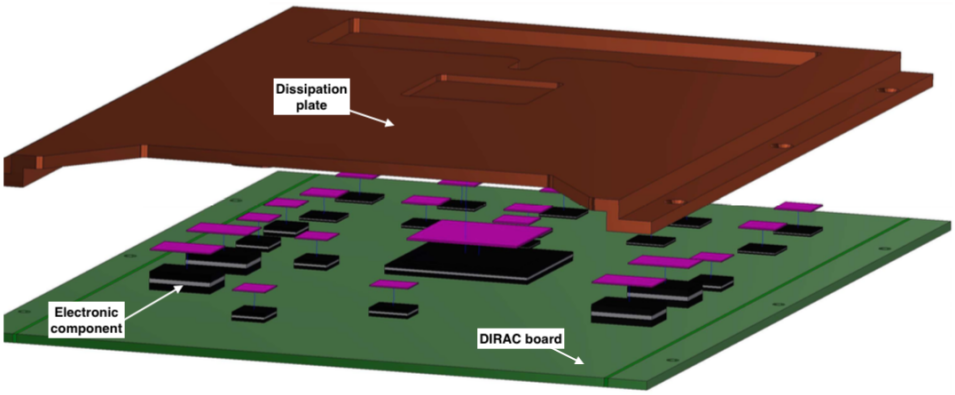

Figure 4.8: CAD model of the DIRAC board used in the simulation.

4.2 Thermal model of the DAQ crates

In this section we report the thermal simulation of the DIRAC boards and the DAQ crates (further information in [26]). The study of the junction temperature[6] of these components is the purpose of the problem, because allows the determination of cooling system characteristics. It's been decided to set the maximum allowed junction temperature of each component at 50% of the maximum operating junction temperature reported in the components data sheet. In this way the components should have temperatures lower than 60 $°C$

During the first analysis of the problem, simulations and experiments were carried out together in order to validate the thermal models used in the simulation. This happened because the thermal properties of electronic components were not equal to the data sheet ones; and this produced incoherence between simulation and experimental results. After "calibration" of the thermal model, the simulations got always more accurate. In the next section we'll see the results of the latest simulations.

4.2.1 DIRAC board model

In order to perform the thermal simulation, it's been produced a simplified model of the DIRAC board in which all the little geometric features were not present. That is a general guideline always suggested in order to reduce meshing problems and simulation time. The CAD model used for the simulation is represented in fig. 4.8.

The dissipation plate (made of copper) has been introduced after some time, when it was found that without it the temperature distribution was unacceptable. The plate was introduced to improve the thermal exchange between the electronic chips and the cooling lines. The DIRAC board is in thermal contact along its sides with the cardlocks[7], and on its upper surface with the dissipative plate, which

[6]The junction temperature is the temperature at the interface between the board and the electronic component. Vendors of electronic components give allowable values for such quantity.

[7]Is the device that fix the boards to the crates side walls.

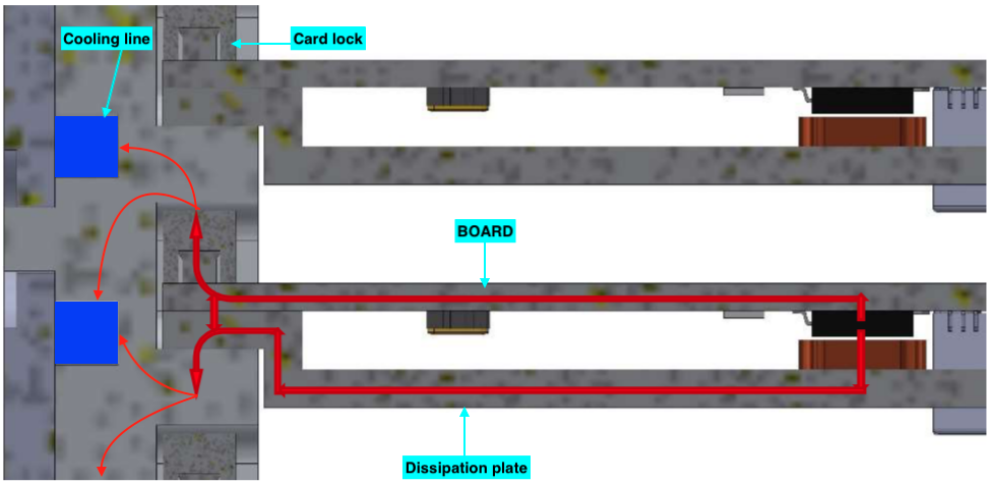

Figure 4.9: Cross section of the DAQ crate assembly. The red lines reproduce possible thermal paths, while the blue squares represents the cooling lines (the heat sinks). The heat source is the black electronic components.

in turn is in contact with the crate internal walls. The physical model and the equivalent electrical circuit of the DAQ crate and board is reported in fig. 4.9 and fig. 4.10, where the possible heat flow paths are in red color.

The resistances of fig. 4.10 represent:

- R_1: resistance between the junction and the thermal dissipation plate;
- R_2: between the junction and the edge of the board;
- R_3: resistance of contact between board and thermal plate (Cu-Cu contact);
- R_4: due to the contact Cu-Al between the board and the card lock;
- R_5: internal resistance of the card lock;
- R_6: due to the contact Al-Al between the card lock and the crate wall;
- R_7: due to the contact Cu-Al between the thermal plate and the crate wall.

R_1 and R_2 have been estimated with only the thermal simulations of the dissipation plate and board, assuming a one-dimensional heat flux directed towards the crate wall. By solving the circuit they estimated the heat flow through each resistance and the ratio between the power flowing through the dissipation plate and through the bottom of the board with respect to the total power. The result is that about 95.5% of the heat flows through the thermal plate, and just 4.5% through the cardlock. That's the reason for what the dissipative plate was introduced. That is obvious considering that the thermal plate has a thermal conductivity which is two orders of magnitude larger than the one of the fiberglass board.

This information allows a more precise simulation of the crate wall, differentiating the power exchanged between the various parts of the contact surfaces. The set of boundary conditions is represented in fig. 4.11.

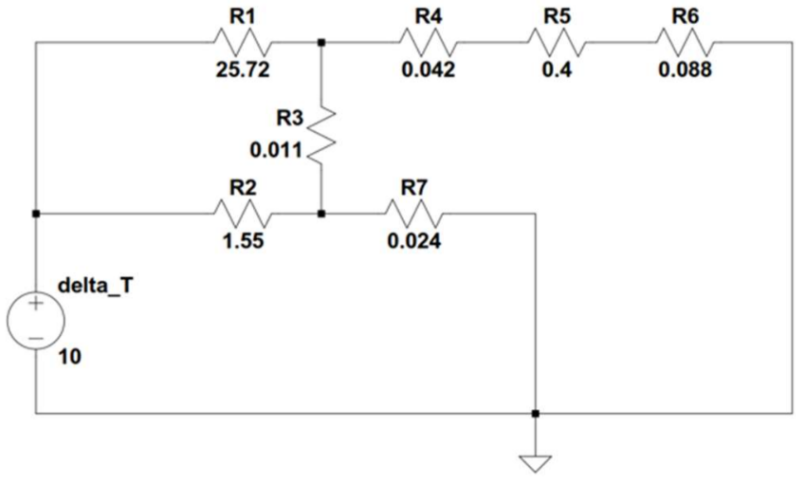

Figure 4.10: Equivalent thermal circuit of fig. 4.9. A temperature difference of 10 $°C$ is applied in order to compute all the important resistances. The numerical values refer to the units $[°C/W]$.

4.2.2 DIRAC board results

Simulations were accompanied by experimental tests. This because many important parameters were not well known during first calculations, and there was the need for experimental verification. We'll give only the final results of the analysis without many information on the experiment setup that can be found in [17].

After the calibration of boundary conditions and thermal parameters the final results are shown in fig. 4.12 and fig. 4.13.

From fig. 4.13 the hottest component is the jitter cleaner, going up to 31 $°C$. The cooling fluid temperature used was -10 $°C$. This means that the most unlucky component undergoes a temperature increase from the fluid of around:

$$\Delta T_{DAQ} = 41 \ °C$$

Again, this value will be used as a design parameter, and once a design will be ready, verifications will be made on this assumption. Although the results seem to be good, is important to note that the electronics and the firmware implemented in the FPGA have not been finalized yet. However we already know the total dissipated power by the DIRAC will increase. Because of this we have to foresee temperature margins. Furthermore, the dissipated power will increase as a consequence of the radiation dose absorbed by the electronic components. Actually, these results show that the thermal plate may not be necessary for the cooling of the electronic components at the beginning of Mu2e data taking, but it will be employed anyway, thanks to its good performance and simplicity.

Finally, except for huge power modifications, we should not encounter any problems since the lowest allowable temperature of components is around 100 $°C$. The margin fo safety is promising.

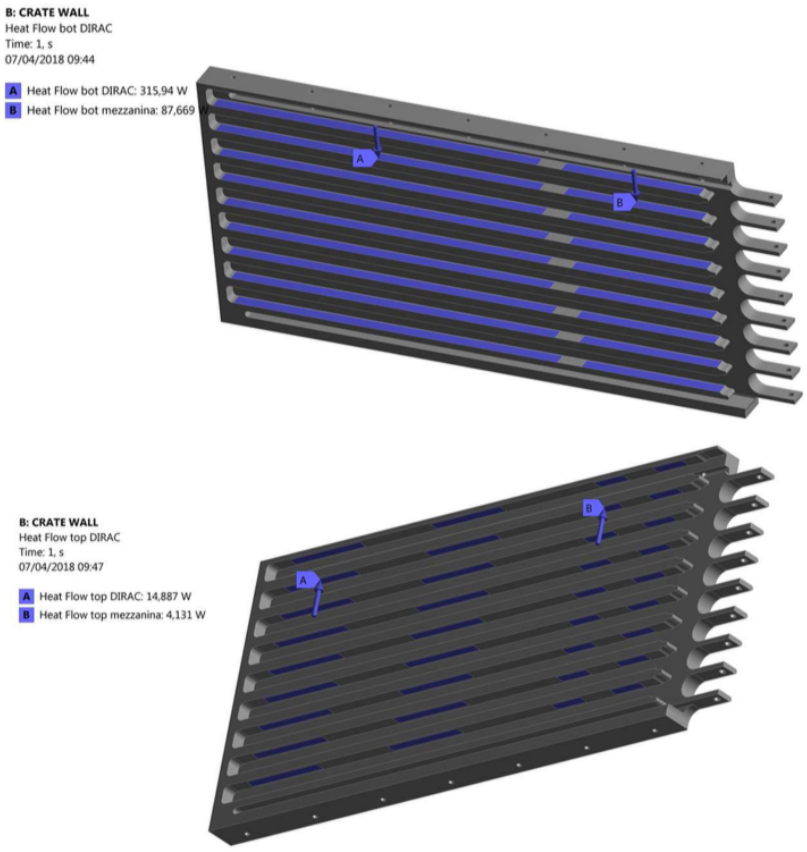

Figure 4.11: Boundary conditions applied to the crate walls. The proportions of heat flux coming from different surfaces is derived from the thermal circuit previously studied. The walls without an applied heat flow are considered adiabatic.

4.3 Conclusion

In this chapter we summarize the previous results, in order to gather the important data. The simulations and experimental tests were accomplished together to validate each other accordingly. Only the most important parts have been investigated (SiPM and electronic boards) considering that the mechanical parts have no problems at the expected temperatures.

From the results of previous sections we can take the following information:

- The most critical component is the SiPM. Due to its low temperature requirement is important to have a very cold fluid. The electronics could stay well above this range of temperature;

- The characteristics of the coolant and its flowing properties don't matter very much[8] as long as they don't differ too much from the values used in the analysis. What really matters is the temperature at which the fluid gets in contact with the component of reference;

[8]Of course they are important in many other things: cost of the plant, chemical compatibility, efficiency etc ...

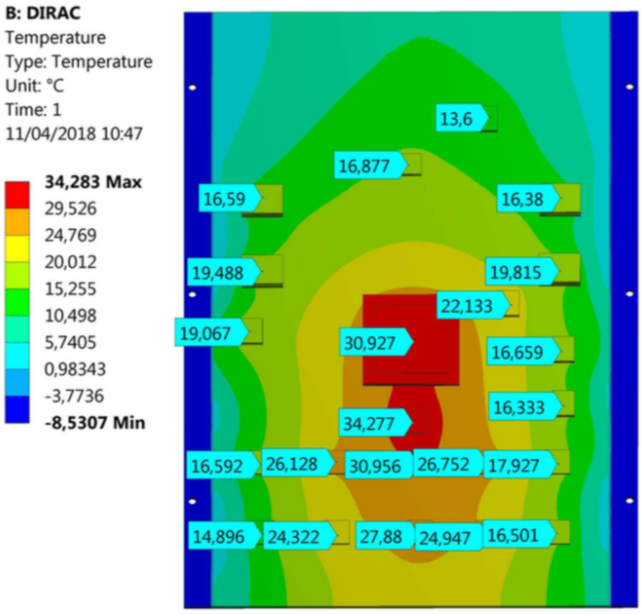

Figure 4.12: Simulation result of the DIRAC board showing temperature of the main components.

Table 4.4: List of the temperature variations between the fluid and the important electronic components.

Component	**Allowable Temperature** $[°C]$	ΔT **from fluid** $[°C]$
SiPM	-10	+11
FEE board	125	+90
DAQ board	60	+41

- In order to design the system the most important parameter is the temperature of the fluid at certain locations. This allows us to design a system enveloping these temperature key-points.

Based on the last item, we report a table (4.4) in which we summarize the important temperature differences estimated between coolant and components. These values are only indicative for a preliminary design, and need a final verification prior to set up the real system.

From tab. 4.4 is clear that the most critical component is the SiPM, having temperature requirements $-10\ °C$. In order to keep it at the right temperature is necessary a coolant temperature of at least $-20\ °C$ in that zone. This will be the general guideline for the system design.

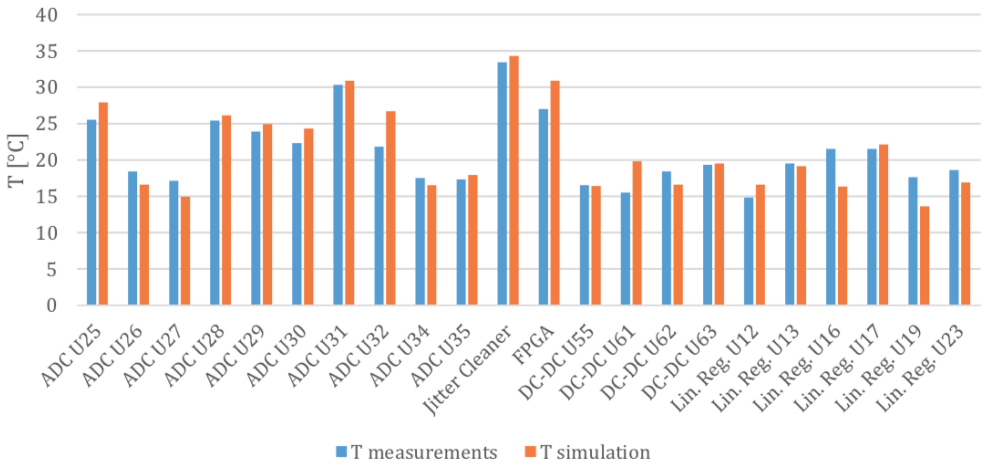

Figure 4.13: Comparison between simulation and experimental results for every board component.

Chapter 5

Selection of the cooling fluid

We have taken into consideration several cooling fluids with different characteristics. After a preliminary examination of many possible alternatives, only the two following categories turned out to be the most adequate ones:

1. **Propylene glycol**: this is an organic compound with chemical formula $C_3H_8O_2$. It is mainly used for two purposes: as raw material in the manufacture of polyester fibers and for antifreeze formulations. It is an odorless, colorless, sweet-tasting and viscous liquid;

2. **PF-5060**: PF stands for *performance fluid*. it is a fluorocarbon (produced by 3M NOVEC^{TM}), having chemical formula C_6F_{14}. It is also known as *modified freon* or *perfluorohexane*. It is a derivative of the hexane, in which all hydrogen atoms are replaced by fluorine. It is used in some formulations as electronic cooling liquid/insulator fluorinert for low-temperature applications, due to its low boiling point of 56 $°C$ and freezing point of -90 $°C$. It is odorless and colorless.

In the following sections we will describe the two fluids and explain their advantages and disadvantages.

5.1 Propylene glycol

The major use of glycol is as a medium for convective heat transfer in automobiles and liquid cooled computers. Glycol is also commonly used in chilled water air conditioning systems[1]. It is used in systems with coolant temperatures below the water freezing point. In geothermal heating-cooling systems, this is the fluid that transports heat through the use of a geothermal heat pump[2]. The glycol either

[1]Systems in which the glycol is used to cool the water, that in turn cools down an air stream for air conditioning purposes.

[2]A heat pump is a device that transfers heat energy from a source of heat to what is called a heat reservoir. It moves thermal energy in the opposite direction of spontaneous heat transfer, by absorbing heat from a cold space and releasing it to a warmer one. In order to do that it uses external power, such as electric motors.

gains energy from the source (lake, ocean, water well) or dissipates heat to the sink; this depends on whether the system is being used for heating or cooling.

Pure glycol has a specific heat capacity about one half that of water. So, while providing freeze protection and an increased boiling point, it also lowers the specific heat capacity of water mixtures (relative to pure water). That is a negative effect, since a large heat capacity is a fundamental property of any coolant fluid. A 1:1 mass mixture with water, called 50% glycol, has specific heat of 3140 $J/kg°C$, three quarters that of pure water, and freezes at -32.5 $°C$. Thanks to the low freezing temperature, glycol is commonly used as a de-icing fluid for windshields and aircraft, as an antifreeze in automobile engines, and as a component of vitrification mixtures for low temperature preservation of biological tissues and organs.

The use of glycol not only decreases the freezing point of aqueous mixtures, but also elevates their boiling point. This results in the operating temperature range for the fluid being broadened on both ends of the temperature scale. The increase in boiling temperature is due to pure glycol having a much higher boiling point and lower vapor pressure than pure water, typical of most binary mixtures of volatile liquids. However, it must be taken into account that higher proportions of glycol also increase the viscosity of the mixture. The right percentage of glycol is then a result of trade-off studies for each application.

Many types of different glycol concentrations have been investigated. Their physical properties are reported in tab. 5.1.

From the table we can note important things:

- The dynamic viscosity μ plays an important role in the circuit head loss. Note that it is really sensible to temperature variations. The head loss would change significantly after small temperature variations, and this could produce unacceptable effects;
- Since the SiPM required temperature is -10 $°C$, and from chapter 4 $\Delta T_{SiPM} =$ 11 $°C$, glycol should stay around -21 $°C$ in proximity of the SiPM. This means that the minimum concentration needed for glycol becomes 45%. Lower glycol concentrations would not be able to work at -21 $°C$;
- 45% glycol at -20 $°C$ has a relatively high viscosity. This means that could be unacceptable for head loss and electric power reasons;
- 35% glycol would be a really good choice in case the coolant didn't go below -10 $°C$. The viscosity wouldn't be too high and the performance as coolant would be great.

At the beginning of this project, the requirement for the SiPM temperature was only 0 $°C$, and the 35% glycol was the first choice as coolant. Then we found out that SiPM performance degrades rapidly as a function of the absorbed radiation dose. We estimated that after one year of continuous calorimeter operation the SiPM will dissipate much more power than the initial period. We thus need the flexibility to decrease the SiPM operational temperature to -10 $°C$ to better control the negative effects of performance degradation. This implies glycol should

Table 5.1: Physical properties of monopropylene glycols at different temperature conditions

Glycol concentration	**Freezing point** T_{fr}	**Temperature** T	**Density** ρ	**Specific heat** c_p	**Dynamic viscosity** μ	**Thermal conductivity** k	**Vapour pressure** P_v
	$[°C]$	$[°C]$	$[kg/m^3]$	$[J/kgK]$	$[mPa \cdot s]$	$[W/Km]$	$[Pa]$
35%	-17	-10	1040	3759	4.331	0.429	253
		-15	1042	3751	5.286	0.426	169
40%	-21.6	-10	1045	3789	4.938	0.413	247
		-15	1047	3779	6.075	0.411	164
		-20	1049	3769	7.565	0.409	108
45%	-26.7	-10	1051	3618	5.717	0.398	239
		-15	1053	3607	7.096	0.397	160
		-20	1055	3595	8.921	0.396	104
		-25	1056	3583	11.371	0.395	67
50%	-32.5	-10	1056	3548	6.738	0.382	231
		-15	1059	3535	8.448	0.383	154
		-20	1061	3521	10.738	0.383	101
		-25	1062	3507	13.847	0.383	65
		-30	1064	3493	18.134	0.384	41

be circulated in the circuit at the temperature of -20 $°C$, but this would produce large head loss due its high viscosity. Several studies confirmed that this solution would also have been unacceptable for electric budget reasons [19]. The high viscosity of the fluid would require big pumps and consequently too much electric power. We do not know yet if the SiPM degradation will require such a low operational temperature. While waiting for more conclusive studies we selected the coolant accordingly to the worst predictions.

5.2 PF-5060

PF-5060 is a clear, colorless, fully-fluorinated liquid. Like other 3M performance fluids, PF-5060 fluid is chemically and thermally stable, practically non-toxic, and nonflammable. The high dielectric strength, excellent materials compatibility, chemical and thermal stability make PF-5060 fluid useful in a wide range of applications, such as lubricant deposition, reaction media and heat transfer. It is compatible with most metals, plastics and elastomers. Its most important characteristic is the -90 $°C$ freezing point, that makes of him a good candidate as cooling fluid for low temperature operations.

PF-5060 fluid has zero ozone depletion potential (ODP). The material is exempt from the U.S. EPA and most State definitions of a volatile organic compound (VOC), and does not contribute to ground-level smog formation. The only problem is that, being a perfluorocarbon (PFC), has a high global warming potential (GWP) and a long atmospheric lifetime. As such, it should be carefully managed so as to minimise emissions. 3M recommends that users of PF-5060 fluid further limit emissions by employing good conservation practices, and by implementing recovery, recycling and/or proper disposal procedures. 3M offers a program in the U.S. for used fluid return. Guidelines for safe handling and use of this 3M product are provided in the material safety data sheet [1].

PF-5060 is a solvent, and in case of leaks it immediately evaporates and get absorbed by the vacuum system of the cryostat. After the evaporation it does not leave any residue, because has been developed by 3M Company for delicate electronics washing. It is also used in many CERN experiments, such as CMS, ATLAS and LHC.

All these characteristics make of PF-5060 a good candidate for low temperature operation, but careful attention is required for storage and handling. The physical properties of the fluid are shown in tab. 5.2.

The important result coming from the table is this:

- The physical properties of the fluid do not depend very much on the temperature. This is very important in our project because the system could run in a range between -10 and -20 $°C$, and robustness is what is demanded in such situations. It allows us to design a system able to work appropriately even at different temperature, without losing too much efficiency after temperature variations.

Table 5.2: Physical properties of PF-5060 at different temperature conditions. $T_{fr} = -90\ °C$.

Temperature T	**Density** ρ	**Specific heat** c_p	**Dynamic viscosity** μ	**Thermal conductivity** k	**Vapour pressure** P_v
$[°C]$	$[kg/m^3]$	$[J/kgK]$	$[mPa \cdot s]$	$[W/Km]$	$[Pa]$
0	1740	1014	0.946	0.060	8634
-5	1753	1006	1.03	0.061	6528
-10	1766	998	1.13	0.061	4867
-15	1779	991	1.24	0.062	3576
-20	1792	983	1.37	0.063	2586
-25	1805	975	1.52	0.063	1838
-30	1818	967	1.7	0.064	993

5.3 Comparisons and selection of the coolant

In this section we present a comparison among the possible coolant alternatives. As it is well known an ideal cooling fluid is characterized by:

- **High specific heat**: it produces low fluid temperature variations along the circuit. This is really important for SiPM cooling, since they are sensitive components and non uniform temperature may lead to degraded reading performance (the main goal of the calorimeter itself);

- **High density**: a dense cooling fluid will occupy less volume than another less dense. This could be a design parameter because the room used for the mechanical components is not so large, and everything must fit inside specific volumes;

- **Low viscosity**: it means having low head loss through the system, that in turn means small pumps and low electric power. Achieving the same cooling result with less electric power can save a lot of money during the life cycle of the detector (expected 3 years);

- **Good chemical compatibility**: the fluid has to be chemically compatible with the devices encountered along the circuit. It also must not produce corrosion phenomena;

- **High thermal conductivity**: having a good conductivity allows the fluid to easily exchange heat via convection. This permits the use of lower velocities and smaller heat exchangers, resulting in lower head loss and electric power;

- **Low temperature sensibility**: the fluid will undergo many temperature variations along the circuit. If it were very sensible its properties would change a lot from the ones in which the circuit would have been optimized. It would deteriorate the efficiency of the system, increasing losses and operational costs;

- **Low cost [$\$/kg$]**: cost can change very much between different types of coolant. Therefore it must be always taken into account;

- **Eco-friendly**: a good coolant does not damage the environment if it leaks outside the system. There are two scientific indexes relative to this characteristic:

  - the ozone depleting potential (ODP);
  - the global warming potential (GWP).

  A good coolant fluid should have the minimum possible value (possibly zero).

The specific heat, viscosity and conductivity can be combined in a single property called the *Prandtl number* (P_r). It is defined as the ratio between the momentum and thermal diffusivity. The thermal diffusivity can be interpreted as the measure of the fluid thermal inertia. In a substance with high thermal diffusivity, heat moves rapidly through it without heating it too much. It happens because the substance conducts heat very quickly with respect to its heat capacity. It is defined as:

$$\alpha = \frac{k}{\rho c_p}$$

While the momentum diffusivity, also known as *kinematic viscosity*, measures the capacity of the fluid molecules to exchange momentum among them. It is defined as:

$$\nu = \frac{\mu}{\rho}$$

Combining the previous formula we obtain the Prandtl number in terms of specific heat, viscosity and conductivity:

$$P_r = \frac{\nu}{\alpha} = \frac{c_p \mu}{k}$$

Since in the previous equation the three important parameters are mixed together, the Prandtl number can help us in selecting the best choice only if the compared fluids had at least one equal parameter. Between two fluids having one equal parameter, the best choice would be the one with lower P_r.

Before comparing the fluids is important to understand the operating conditions of the system. It is obvious that the plant will have at least two cooling zones: the DAQ line, and the FEE line. The DAQ line will cool the crates, while the FEE line the front-end boards and the SiPM. The temperature requirements for these two zones are quite different. The SiPM need to stay (in worst conditions) at -10 $°C$, and this means a fluid passing there at least at -20 $°C$. The DAQ line is instead less compelling from this point of view, since that the electronics can safely withstand 60 $°C$, and the fluid could stay at temperatures in the range of ($15 \div 20$ $°C$). This produces a trade-off problem for the physical layout of the system. There are mainly two possibilities:

- **Single system**: this is a layout in which only one system will be designed. The coolant flow splits between the two cooling zones, and join back together after them. In this way the numbers of pumps, valves, tanks, chillers, and all other equipment would be halved (even though the single components would be a bit bigger);
- **Double system**: in this case there will be two separate systems providing fluid to the cooling zones. In this way every single circuit would be more optimized compared to the other case[3], but the number (and total cost) of

[3]When versatility is introduced the efficiency always decreases. In this case the selection of the lowest temperature for both the circuits would produce an "oversized" cooling system for the DAQ line.

components would be higher.

A possible requirement for the system is to have the DAQ line at higher temperature than the FEE line. This is due to the possibility for the crates to exchange heat via radiation with the closest components of the tracker detector. The real problem is that no one has been able to estimate the equilibrium temperature of the irradiated tracker, and it is a really fragile detector. It has very thin and weak straws that could break if their temperature is not exactly the expected one. The design temperature of the straws is 25 $°C$, and if the crates (in proximity of the last tracker panels) went down to -20 $°C$ there would be 45 $°C$ of ΔT able to produce heat exchange.

The heat exchanged with radiation scales with the fourth power of the temperature difference, since that its basic relation is described by the *Stefan-Boltzmann law* [10]:

$$J = \sigma T^4$$

Where J is the heat flux emitted by a black surface $[W/m^2]$ and T is the temperature of the surface $[K]$. The general heat flow exchanged between a crate surface and a tracker surface is:

$$\dot{Q} = \varepsilon A_{cr} F_{cr-tr} \Delta T^4$$

Where ε is the crate surface emissivity, a number between 0 and 1, accounting for real surface not perfectly black. F_{cr-tr} is the factor of view from the crate to tracker, and takes into account the geometrical problem of irradiation from one surface to another. ΔT^4 is the fourth power of the temperature difference between the two surfaces.

The amount of heat exchange between tracker and calorimeter has been estimated in the order of few watts, but few watts is also the power exchanged by the tracker with the soil (the detector is insulated on any contact surface). This means that we end up with a thermal power balance between infinitesimal quantities and it is almost impossible to estimate in a reliable way the equilibrium temperature of the system. Even few watts could produce large temperature variations in time, that could compromise the tracker detecting capabilities. Some screening device between tracker and calorimeter has been foreseen, but more detailed information will be needed for the final set up of the system. Until then we will develop two different solutions for the crates temperature, introducing as much flexibility as possible in the system.

The operating conditions foreseen until now are the following ones:

1. **A single system running at -20** $°C$: the lines going to DAQ and FEE electronics would be roughly at the same temperature. Initially it will be sufficient to keep the SiPM at 0 $°C$, until they will require lower the temperature due to radiation damage. This configuration may lead to radiation problems for the tracker, but some solution is possible, and it will be explained later;

2. **Two separate systems at different temperature**: In this case the FEE system runs at -20 $°C$, and the DAQ at higher temperature. The working temperature of the DAQ line would be regulated in order to not impact the tracker.

In order to choose the best option, is important to note that the single circuit cannot afford to have two branches at different temperature. This is due to the power needed to heat up, and consequently cool down a certain amount of flow rate. Later we will show that heating up the DAQ line of only 10 $°C$ requires a power consumption in the range of 40 kW. The overall alcove power budget is only 25 kW, which makes impossible the single system design in the eventuality of different temperature lines.

A solution for the tracker problem in the single system would use the DAQ line at the same temperature of FEE line, but with a such low mass flow rate that the crates would stay at higher temperatures. As it will be shown later, this will lead to select a Reynolds number for the DAQ exchanger in the transitional regime of flow[4]. A lot of uncertainty would be present, but could be a smart solution.

- **Case A**; the single system will be used whereas the DAQ line can run at cold temperatures (in the range of -20 $°C$), or in the case of transitional flow in the crates channels. In this way the system will be more compact, and everything will fit inside the mechanical alcove without any problems;

- **Case B**: the double system will be realized if the DAQ line cannot be mantained at similar temperatures to the SiPM. In this case the separate systems will run at different temperatures, and probably with different coolants.

This Thesis is mainly focused on the first perspective, since it seems the most probable one. Anyway, some indications will be given also for the double system, in order to have ready important indications whereas the requirements will change unexpectedly.

Assuming for good the previous assumptions, the fluid will need to work efficiently in the range $-20 \div -10\ °C$. The available coolants in liquid form at those temperatures are:

1. **45% glycol**;

2. **PF-5060**.

50% and higher percentage glycols will not be considered because at equal temperature have higher viscosity than the 45%. 40% has been discarded because of the proximity of its freezing temperature with operating conditions. Tab. 5.3 reports a comparison of the main fluid properties:

[4]Transitional flow is a mixture of laminar and turbulent flow, with turbulence in the center of the pipe, and laminar flow near the edges. In this flow regime there are a lot of uncertainty and empirical correlations don't give reliable results..

Table 5.3: Comparison of main properties of 45% glycol and PF-5060. The properties are given at condition -20 $^{\circ}C$

	45% glycol	**PF-5060**
ρ $[\frac{kg}{m^3}]$	1055	1792
c_p $[\frac{J}{kg \cdot ^{\circ}C}]$	3595	983
μ $[mPa \cdot s]$	8.921	1.37
C_p $[\frac{kJ}{m^3 \cdot ^{\circ}C}]$	3793	1762
k $[\frac{W}{m \cdot ^{\circ}C}]$	0.396	0.063
P_r	81	21

From the comparison is clear that glycol would have far better coolant properties than PF-5060. The thermal capacity $C_p = \rho c_p$ of glycol is more than twice that of PF-5060. The big problem is the high viscosity, that makes of him an inefficient fluid. Others before me [19] demonstrated that 45% glycol running at -20 $^{\circ}C$ requires too much power, thus rejecting this solution. The only fluid able to work efficiently at those temperatures is PF-5060. It has problems related to safe handling and storage, since no leaks are permitted because of its global warming potential. Nonetheless it's been used several times in CERN experiments, and we'll carry on a system based on it.

Chapter 6

Design of the cooling circuit

The previous Chapters report on the expected performance of the cooling system we are developing. We are now ready to design a preliminary project. The design of the circuit should include all the necessary components (tank, pumps, valves etc...). This will allow to perform a preliminary estimate of all the important characteristics and verify if the system satisfies the requirements expressed in section 3.1. If the result is negative, we will have to modify the flow parameters or act directly on the flow schematics. We will iterate this procedure until we achieve a satisfactory solution. Fig. 6.1 shows this logical process.

The steps shown in fig. 6.1 can be easily explained in the following way:

- **Guidelines**: keeping in mind the important guidelines draw a certain flow diagram:
  - the Reynolds number above a threshold ($R_e > 10000$) is the standard request to have an efficient heat exchange: this is due to the convective cooling that increases with the turbulence of the flow (almost linearly in turbulent conditions). In a laminar flow regime ($R_e < 3000$) heat exchange is extremely limited. Between 3000 and 10000 the flow is quite unpredictable because in a transitional condition;
  - the cooling fluid temperature should be of the order of -20 $°C$ in the SiPM proximity. The circuit temperature map[1] will be calculated starting from that point;
  - an important suggestion is to have a slow fluid along the circuit ($V_{fl} < 4.5\ m/s$) because the head loss is proportional to the square of the velocity ($\Delta P = f\frac{L}{D}\rho\frac{V^2}{2}$);
- **Assume**: produce a certain system layout, assuming the important geometric parameters (lengths, diameters, etc...);
- **Calculate**: calculate all the significant circuit characteristics, for example head loss and temperature distribution. All these things could not be computed in previous works due to missing data;

[1] The temperature distribution along the circuit.

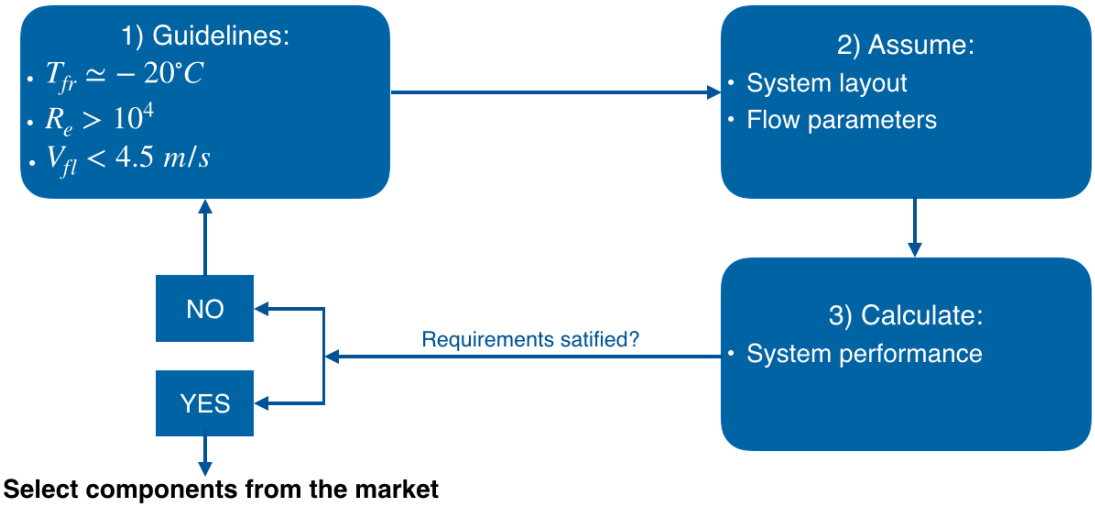

Figure 6.1: Iterative method used to design the cooling system.

- **Check the results**: compare the estimated circuit performances with those requested. If they agree we can proceed and select real components from the market. Otherwise it is necessary to modify the design and follow again the design steps and then iterate until the results are satisfactory.

My work has taken into consideration the preliminary version of the project developed in previous works [23], [17]. This Chapter reports the flow diagrams I obtained by inserting the necessary modifications to the previous version of the design, taking into account the evolution of system constraints.

6.1 Introduction to PFD and P&ID

We have used the standard tools named respectively PFD and P&ID[2] to visualize the conceptual design of the hydraulic cooling system.

- The PFD provides a simplified view of the global architecture of the hydraulic system. It shows the main lines and bypasses usually marked with an arrow to show the direction of the liquid flow. The PFD also shows the most relevant circuit components, such as pumps, filters, measurement instruments and valves. Each component is represented with a coded symbol.

  To summarize, the PFD reports only the necessary features to understand the logic of the hydraulic circuit and is the first step in a circuit design. In order to produce a real system we need the P&ID that reports many more details;

- The P&ID is usually developed only once the PFD is well understood and agreed. The P&ID is a complete scheme reporting every line and component employed in the circuit. Every item is underlined in a proper way. Unlike

[2]PFD and P&ID are standard acronyms in use in piping systems. They stand respectively for *process flow diagram* and *piping and instrumentation diagram*

the PFD, the P&ID is not only a qualitative and logic scheme, but also a quantitative diagram. It reports quantitative information, for example the measurements of pressure, mass flow rate, pipe diameters and temperatures taken at significant points of the circuit.

Personally I reviewed the preliminary diagrams of the circuits and improved them in a continuous collaboration with INFN and Fermilab engineers. I also designed the circuits shown in section 6.8, referring to the possible use of a double circuit system. The diagrams shown in the next pages are the latest ones in a chronological time-scale, but they are not final yet. They could be modified again before the final assembly of the system.

6.2 PFD of the single system

We begin by showing the first PFD for a single system to explain the components function on a simple system. In the next section we will show the evolution of the PFD in the most recent P&ID. The simplest logic for the cooling purpose is shown in Fig. 6.2.

The components functions are the following:

- **Cooling station**: it cools down the fluid every time it is heated up in the circuit. It is the unique part of the system where heat is extracted from the fluid and not introduced. It is made of a chiller[3] and other equipment needed to discard the heat absorbed from the fluid. The chiller function will be discussed more in detail in section 7.1;

- **Pumping station**: it gives the fluid the necessary energy to win all the head loss encountered in the circuit. It is composed of a pump and relative equipment needed to regulate the flow. The pump function and selection will be discussed in section 7.2;

- **Filters**: the filters remove residual particles from the fluid before they can damage the system. The front-end lines are 3 mm diameter pipes, that can easily get chocked by particles coming from other zones;

- **2 parallel lines**: the two lines running in parallel and bringing the right amount of fluid to the front-end units and crates. They will be called FEE line and DAQ line;

- **Heater**: The heater in the DAQ line was foreseen in order to heat up the fluid for temperature regulation purpose. As previously explained this idea will not be used because it requires excessive electric energy. Anyway the heater can always be used for fine regulations of circuit temperature.

[3] A chiller is a machine that removes heat from a liquid via a vapor-compression or absorption refrigeration cycle. This liquid can then be circulated through a heat exchanger to cool equipment, or another process stream (such as air or process water). As a necessary by-product, refrigeration creates waste heat that must be exhausted to the environment, or for greater efficiency, recovered for heating purposes.

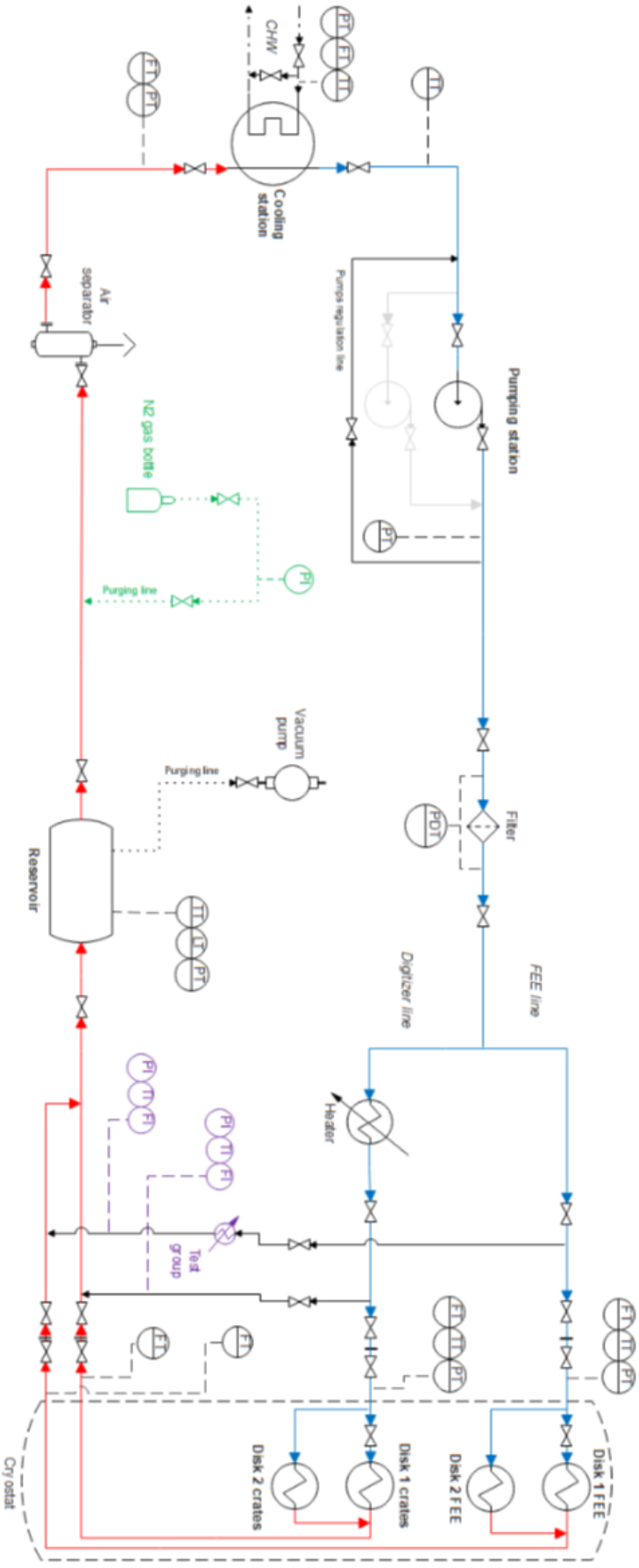

Figure 6.2: A preliminar PFD of the cooling system ([17]).

Detailed information about the temperature regulation will be given in section 6.6.2;

- **Test group**: the test group allows for testing procedures before data taking begins. It is composed of a heater that simulates heat production from the calorimeter itself, in order to test the system with comparable thermal loads, and a series of instruments to measure the system performance;
- **Tank**: it is the reservoir that collects the fluid from the cooling lines located outside the cryostat. It must allow for fluid expansions and gas venting coming form the purging system;
- **Purging system**: it is the line that purges the system making use of nitrogen. The goal of any nitrogen purging system is to cleanse pipes and other parts that contain harmful contaminants for the system;
- **Air separator**: this components removes residual gas particles from the fluid;
- **Instruments**: several instruments are needed for the system operation (flow, temperature and pressure transmitters). They will be used both for initial calibration and for system monitoring.

Once the PFD of the system is well understood and agreed, we can move on to the P&ID. It will have much more information and will be useful to verify the system performances.

6.3 P&ID of the single system

A preliminary version of the P&ID is reported in [17]. Fig. 6.3 shows the final version I designed during my permanence at Fermilab. The drawing shows the hydraulic diagram of the circuit (i.e. valves, transmitters, indicators) and the numerical values of the main parameters (pressure, temperature, mass flow rate) measured where necessary. All the items have been assigned a unique codes among those available in use at Fermilab to identify also different devices of the same typology.

The legend of the symbols used in the diagram is shown in fig. 6.4. Most valves installed inside the mechanical alcove and along the routing lines are shut-off valves normally open[4], which can be manually set. During data taking it will be not necessary to close them. Manual shut-off valves normally closed[5] are opened only during particular operations, such as maintenance, testing activities or shutdown.

Actuated valves[6] can be controlled at any moment, also during data taking. In the following list we will explain the function and the position chosen for the most important components.

[4]Normally open means that under normal conditions the valves are open. The fluid passes without any problem.

[5]The opposite of normally open valves

[6]Valves controlled and actuated by electronic control system and mechanical actuators.

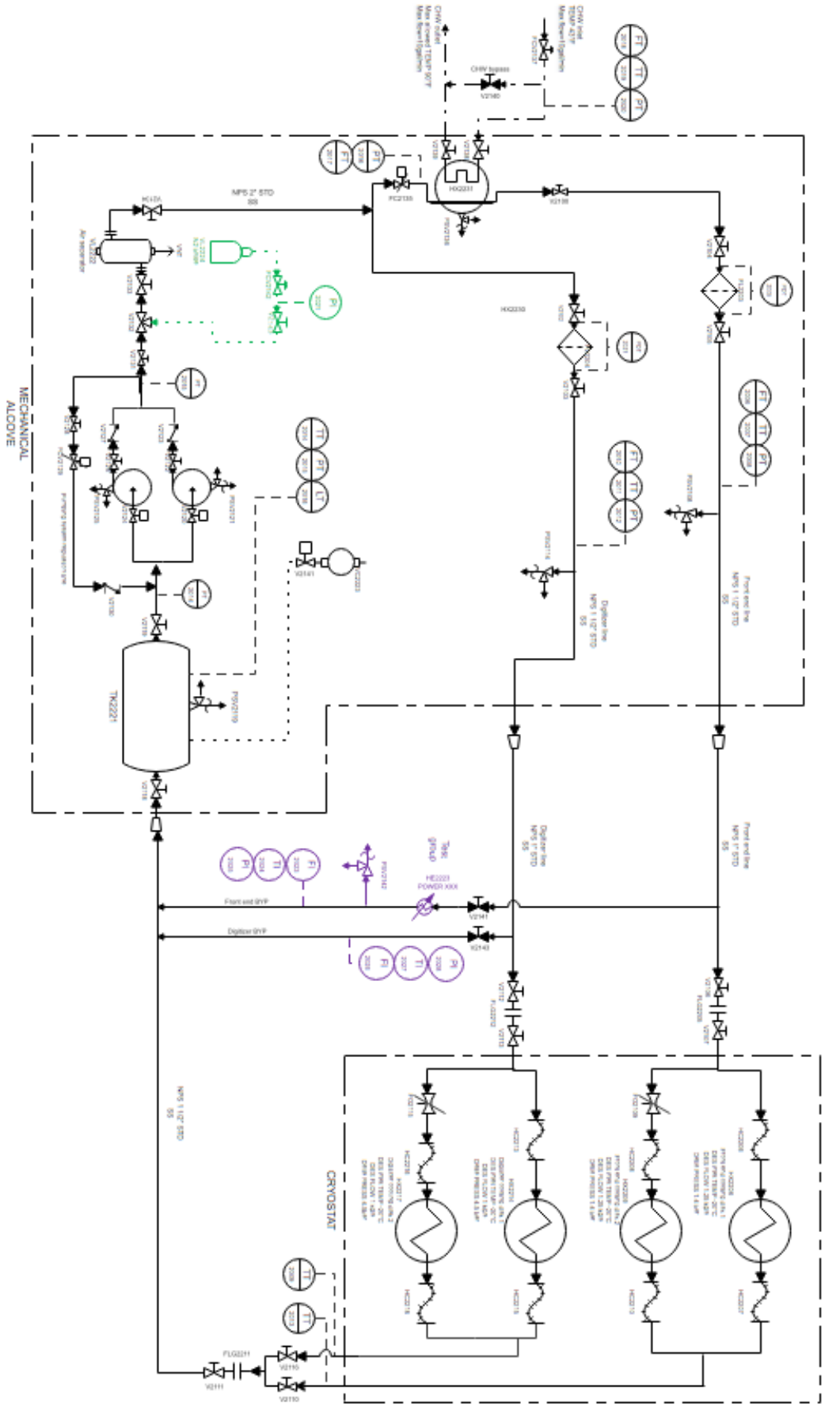

Figure 6.3: P&ID of the single system [17].

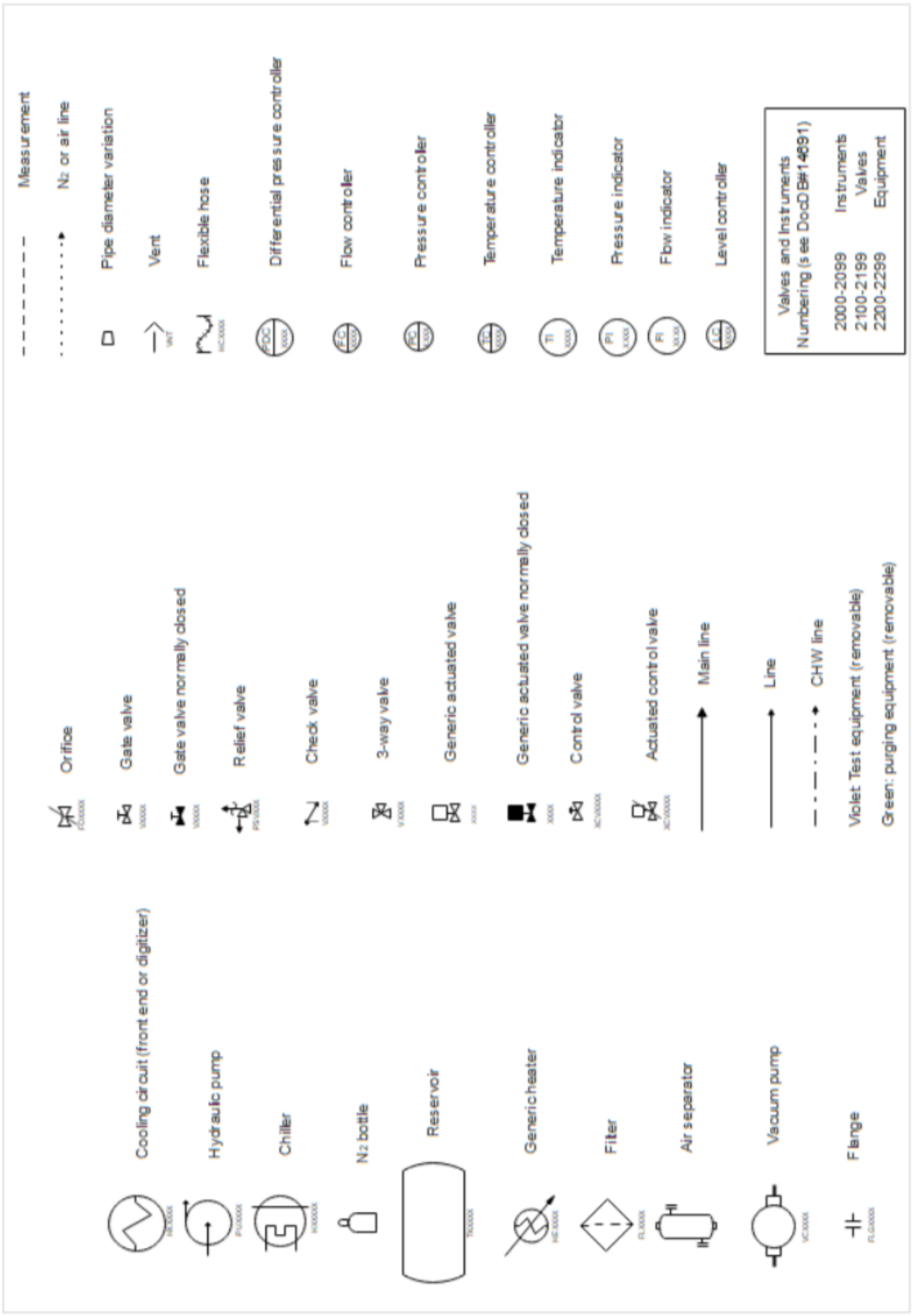

Figure 6.4: PFD of the system [17].

- The pumping group in the outlet line is made of two parallel pumps to implement a redundant system. In this way the circuit can be operational even though one pump fails. The pumps will work alternatively and share a common bypass line for flow regulation. Since the hydraulic system is a closed loop circuit, the pumping group is mainly necessary to balance the head loss due to the impedance[7] of the whole circuit.

  The actuated valves are shut-off valves activated from the control panel and not manually. It is not possible to manually open or close them because their frequency of use is much higher than the maintenance frequency of the pumping group.

  Each pump and relative valves are expected to function for one month every two, while maintenance is done almost once per year. Nevertheless, they do not work as control valves: it is not recommended to regulate the flow upstream of a pump, because this could generate problems at the pump inlet. Check valves are located only where a flow in the wrong direction may be generated. The actuated control valve located on the bypass line regulates the mass flow rate downstream of the circuit. If any serious problem affects the valve, the flow regulation is not possible anymore;

- The filters should be placed upstream of the cryostat to prevent possible failures due to dust, debris and other kinds of dirt. They preserve cooling lines that do not have the automatic bypass in case of clogging. The filters are fundamental components, although they produce a significant pressure drop;

- The actuated control valve located in the front-end line is another essential component of the system. Its aim is to regulate the mass flow rate directly into the front end line and, as a consequence, in the DAQ line. In case of severe problems, the flow regulation upstream of the cryostat is not possible anymore with the current design;

- A bypass for the FEE and DAQ line has been foreseen for testing procedures. During the commissioning of the system, a set of valves and heaters can be assembled along these lines in order to simulate the losses and thermal incomes of the calorimeter itself. It allows to test the whole circuit in the operational conditions, except for the calorimeter disks;

- The amount of equipment inside the cryostat has been minimized. There are only two orifices that adequately balance the pressure drops between the parallel lines. Orifices are simpler objects, without any moving parts, and in the cryostat they provide a better performance than flow regulation valves. Once the orifices are set and the cryostat insulated, it is not possible to modify them anymore. Flexible hoses are necessary because the two disks have to be axially moved along their horizontal rails during maintenance.

[7] It has the same meaning of an electric impedance. Hydraulic impedance is the factor relating the flow rate to the resistance of the circuit. The term impedance means that also phase shifts are possible within a general unsteady hydraulic circuit.

Moreover, they are more convenient than pipes when space is limited, and allow to compensate misalignments;

- The tank has internal pressure approximately at the same level as the atmosphere. During the experiment a certain amount of nitrogen will be located inside the vessel, in contact with the fluid surface. The reservoir is inserted in the main line and allows to perform the following tasks:

  – set point of the circuit pressure;
  – refill automatically the circuit in case of micro leaks;
  – host the whole circuit fluid in case of complete draining.

  The atmospheric pressure is a reference point and not a technical specification. If the measured value of pressure slightly differs from the environmental one, there is no need to set alarms. The reservoir also contains the opening to fill up the circuit;

- The vacuum pump is permanently connected to the reservoir and is used to evacuate the circuit from air before the cooling fluid fills it up. This prevents the generation of air bubbles and pockets which may not allow to properly fill the system in the highest positions;

- The purging system of the fluid is based on nitrogen, which is less chemically aggressive than compressed air and leads to a more compact system. This gas is particularly useful before the filling of the circuit to remove residual air particles from the pipes. The three way valve is a manually actuated shut-off valve.

6.4 Preliminary definition of the single system

The P&ID of the system allows to estimate circuit performance. First of all it is important to find, assume and select some quantities needed as starting data:

- **Mass flow rate**: it determines pressure drops and temperature variations. It affects the losses because they are roughly proportional to the square of the fluid velocity, and the flow velocity is directly related to the mass flow rate once the fluid type and pipes diameter are determined. The value of the mass flow rate will be selected later according to constraints driven by the project guidelines;

- **Diameters**: the diameters of the pipes affect directly the losses of the circuit. For an equal flow rate a larger diameter implies lower velocity and lower losses. On the other hand, larger diameters imply higher cost and encumbrance for the piping system;

- **Temperatures**: the choice of the operational temperature is important for several reasons. First of all a lower fluid temperature will produce

lower temperature on the cooling targets. This in turn produces higher thermal load on the system because the larger difference between the fluid and environment temperature increases the environmental heat entrances. Furthermore, colder fluids increase also the head loss of the circuit, since that density and viscosity increase at low temperatures.

6.4.1 Mass flow rate selection

The mass flow rate is a design parameter. It must be selected independently for the FEE and DAQ lines. According to the following equation, it impacts directly the variation of the fluid temperature:

$$\Delta T_{ij} = \frac{\dot{Q}_{ij}}{\dot{m}_{ij} c_p}$$

- ΔT_{ij} is the fluid temperature variation along the path from point i and j. It is an important parameter because in many situations large ΔT could not be acceptable due to other constraints (for example a certain temperature uniformity for some electronic device);
- $\dot{Q}_{ij}$ is the heat power absorbed by the fluid during the path between the generic circuit points i and j. It depends on what type and how many electronic components the fluid goes through;
- $\dot{m}_{ij}$ is the mass flow rate in the line connecting points i and j. Obviously a higher mass flow rate will undergo lower temperature variations after crossing the heat sources;
- c_p is the specific heat of the fluid (PF-5060 in our case). Its value depends mainly on the temperature, and care must be taken to insert the correct quantity depending on fluid conditions.

Several assumptions have been made to select a good value for the mass flow rate. As previously said, a good cooling system should satisfy the following guidelines:

1. Good convective efficiency;
2. Low head loss.

The convective efficiency mainly depends on the boundary layer condition of the fluid. It is well known that a turbulent boundary layer improves the mixing capability of the molecules, improving the heat exchange with the walls [13]. This dependence will be explained later during the mass flow rate definition. Therefore a good convective efficiency is ensured by a turbulent flow. The turbulence evaluation of a certain duct flow can be performed by simply calculating the Reynolds number, and knowing that good entities of turbulence are present for $R_e > 10000$. Good turbulence could also be present in the range between 2300 and 10000, but in that case it would be dependent on several initial conditions of

the fluid (agitation, vorticity, etc...), and would practically impossible to predict accurately.

To be conservative, we will consider a duct flow being turbulent only if $R_e > 10000$. The Reynolds number definition for a duct flow is the following:

$$R_e = \frac{\rho V D}{\mu} = \frac{4\dot{m}}{\mu \pi D}$$

Where D is the *hydraulic diameter* of the pipe. It is a definition based on convenience which provides reasonable results also for non circular ducts. Its expression is [11]:

$$D = \frac{4A}{P}$$

where A is the cross section of the duct, and P the perimeter. For square channels the hydraulic diameter coincides with the square side. Low head loss means that low mechanical power is needed to force fluid circulation. This means that not only the viscous dissipation is low (decreasing the dissipated heat), but also that smaller pumps can be used. This is good both for economical and encumbrance reasons. The fluid mechanical power dissipation depends roughly on the square power of velocity, and is directly related to the mass flow rate, once the diameters are selected.

$$\Delta P = f \frac{L}{D} \frac{1}{2} \rho V^2 = 8 f L \frac{\dot{m}^2}{\rho \pi^2 D^5}$$

By looking at the Reynolds and head loss equations, we can see that the two guidelines are in opposition each other: turbulence is increased by the mass flow rate (for fixed geometry) but at the same time high mass flow rates produce large dissipations.

It is important to note the dependence of the head loss on the inverse fifth power of the diameter. This means that for a selected mass flow rate, the system loss depends very much on diameter variations. The selection of pipes diameter is then a difficult process, usually made by experts in the piping sector.

6.4.2 FEE line mass flow rate selection

The design of the geometry of the FEE line has been performed taking into account the encumbrance of the system. The little copper pipes running through the backplate and cooling the SiPM and FEE boards, have a diameter of 3 mm. Tab. 6.1 reports all the pipes dimensions. The network nomenclature is reported in Fig. 6.5.

With this geometry determined, the mass flow rate through the FEE line can be estimated in the following way:

1. **Arbitrarily select a mass flow rate**: choose a reasonable value for the FEE line mass flow rate. This value will be equally divided between the 2 disks, and will be the value used as first estimated value;

Table 6.1: Lengths of the pipe network. The inner diameter is 3 mm for all of them. The groups named t and b are straight pipes, while the ct group has 180 degree elbows. The pipes classification refers to fig. 6.5.

Pipe	**Length** $[mm]$
1t	511
2t	658
3t	771
4t	863
5t	941
6t	1009
7t	1068
8t	1120
9t	1165
1ct	905
2ct	760
3ct	734
4ct	694
5ct	673
5cb	673
4cb	694
3cb	734
2cb	760
1cb	905
9b	1165
8b	1120
7b	1068
6b	1009
5b	941
4b	863
3b	771
2b	658
1b	511
6cb	905
7cb	760
8cb	734
9cb	694
10cb	673
10ct	673
9ct	694
8ct	734
7ct	760
6ct	905

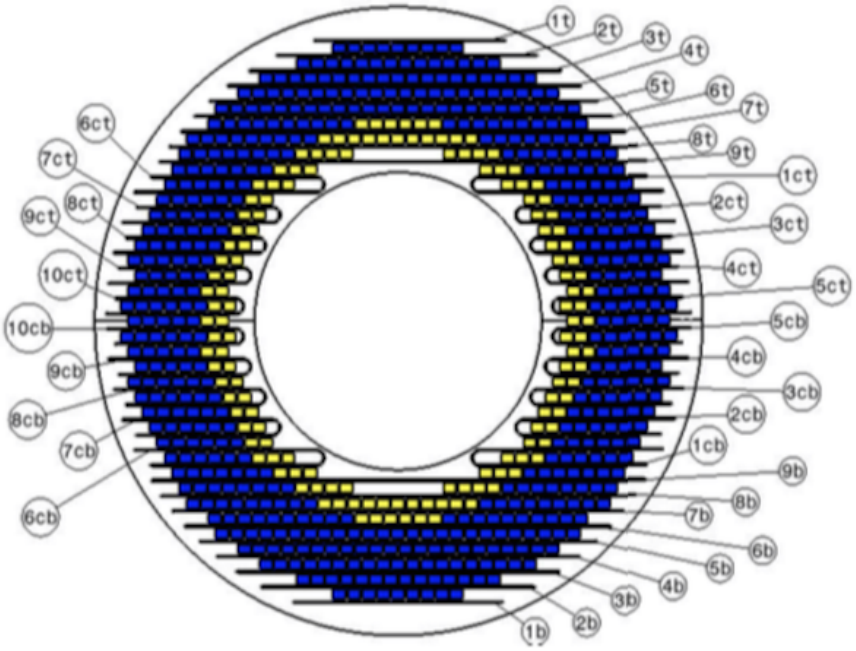

Figure 6.5: Legend used for pipes classification. The groups named t and b are straight pipes, while the ct and cb groups have 180 degree elbows.

2. **Calculate the maximum ΔT of the network**: the mass flow rate selected in point 1) for a disk splits in the pipe network according to the loss of every tube. Since that the various pipes of the network are linked together in a parallel way their final head loss must be the same. The pipes are all of different length and curves, so in order to have the same head loss the mass flow rate will adjust in a non symmetric way. In other words the flow won't split equally among the 38 pipes. Moreover the quantity and type of SiPM encountered is not equal for every pipe, producing different heat power absorbed.

   Following an algorithm called *Hardy Cross Method*, explained in appendix A, is possible to calculate the head loss and temperature increase for every branch of the network. In this way we can find the most unlucky pipe in terms of temperature raise and head loss;

3. **Calculate the SiPM temperature**: Once we have the hottest pipe, we can evaluate the most unfortunate SiPM temperature using the results of chapter 4;

4. **Analysis of the results**: check if the critical SiPM temperature satisfies the requirements, and also if this guarantees a good temperature uniformity. In particular observe the difference between the hottest SiPM in the last portion of the hottest pipe, and the coldest one in the first position of the coldest pipe.

   If the results are not satisfactory change the value assumed for the mass flow rate and iterate again.

We report here the results obtained from the last iteration:

- With a mass flow rate of $\dot{m} = 1.25\ kg/s$ per disk, the maximum $\Delta T = 1.1\ ^\circ C$ occurs at pipes *8t* and *8b* (which have the same geometry and heat absorption). This is in agreement with simple intuition since these pipes are in contact with the largest number of more powerful SiPM (yellow color in fig. 6.5). This temperature difference between inlet and outlet of the hottest pipe is considered acceptable. The flow averaged temperature difference for the whole network is:

$$\Delta\bar{T} = \sum_{i=1}^{38} \frac{\dot{m}_i \Delta\dot{T}_i}{\dot{m}_{tot}} = 0.65\ ^\circ C$$

  Where $\dot{m}_i$ is the mass flow rate passing through pipe i, and $\Delta\dot{T}_i$ is the related temperature increase. It is also a good indicator of temperature uniformity;

- Now that we have the flowing properties of the hottest pipe we can estimate the temperature of the critical SiPM. Taking into account a calorimeter disk inlet temperature of -20 $^\circ C$, the fluid temperature at the outlet section of the critical pipes is:

$$T_{cr} = -18.9\ ^\circ C.$$

  By means of the Hardy Cross Method also the mass flow rate through the critical pipes is known. It is:

$$\dot{m}_{cr} = 0.03\ kg/s$$

  With these values of mass flow rate and diameter, the fluid velocity is:

$$V_{cr} = \frac{\dot{m}_{cr}}{\rho A} = 2.4\ m/s$$

  and the related Reynolds number:

$$R_e = \frac{\rho V_{cr} D}{\mu} = 10118$$

  The friction factor is given by the *Colebrook-White's correlation*:

$$f = \left[1.14 \cdot 2\log_{10}\left(\frac{\varepsilon}{D_h} + \frac{21.25}{R_e^{0.9}}\right)\right]^{-2} = 0.04$$

  Where $\varepsilon = 20\ \mu m$ is the mean rugosity of the tube. The Nusselt number is given by the *Dittus-Bolter correlation*:

$$N_u = 0.023 R_e^{0.8} P_r^{0.4} = 141.9$$

The convective heat coefficient is then:

$$h_c = \frac{N_u k}{D_h} = 2942 \ W/m^2 K$$

From the *Newton's law* of convective heat transfer:

$$\dot{Q} = A h_c (T_{wall} - T_{cr}).$$

and knowing the heat power that must be exchanged, we can determine the temperature of the pipe inner walls:

$$T_{wall} = T_{cr} + \frac{\dot{Q}}{h_c A} = -15.1 \ ^\circ C$$

With the pipe wall temperature, and the results coming from fig 4.7 about the thermal difference between pipe wall and SiPM (3.9 $^\circ C$), we can evaluate the temperature of the most unlucky SiPM.

$$T_{SiPM} = T_{wall} + \Delta T_{wall-SiPM} \simeq -11 \ ^\circ C$$

This value is in agreement with the requirements for SiPM temperature.

Although this is not critical, we can also determine the temperature of the hottest component of front end boards T_{hc}. From fig. 4.6:

$$T_{hc} = T_{wall} + \Delta T_{FEE-BOARD} \simeq 75 \ ^\circ C$$

As expected the temperature of the front-end board is not critical at all (the maximum acceptable temperature is 125 $^\circ C$), and in the following pages we will neglect it compared to SiPM requirements. Nevertheless, we should always keep in mind that this solution is valid only if the system architecture remains the same. If the cooling circuit changed, this would not be necessarily true, and attention should be needed for the front-end boards.

From this section we can conclude that a total mass flow rate (supplying both the calorimeter disks) of:

$$\dot{m_{FEE}} = 2.5 \ kg/s$$

is sufficient to satisfy the front end unit requirements. It also produces turbulent Reynolds numbers in the network (the minimum is 10118) and low velocity (2.4 m/s) as requested by the design guidelines.

6.4.3 DAQ line mass flow rate

We will now estimate the mass flow rate through the DAQ line. In this way the overall circuit mass flow rate will be determined and this will allow to evaluate the global system performance.

The guideline for the DAQ mass flow rate is slightly different from the FEE line. Here we do not need a high temperature uniformity, since each electronic component on the boards can be at a different operational temperature. Measurements and results of the calorimeter itself would not be affected by modest temperature differences. Anyway, also the DAQ line must satisfy the cooling guidelines of good convection efficiency and low head loss.

The 20 crates are supplied by manifolds originated directly from the DAQ lines. The DAQ line splits in two inlet manifolds, that in turn split in 10 crates. After that, all the pipes gather together in two outlet manifolds and finally in the DAQ common line. The geometry of the crates cooling line is shown in fig. 3.5, but the size of the rectangular channels still needs to be defined in a convenient way. We used the following procedure:

1. **Assume a ΔT_{in-out}**: assume a certain value for the ΔT_{in-out} between crates inlet and outlet temperature. The value selected is:

$$\Delta T_{in-out} = 3 \ ^{\circ}C$$

2. **Calculate the mass flow rate per crate $\dot{m}_{crate}$**: assuming that all the heat power generated in a crate goes directly into the fluid we can calculate the mass flow rate necessary in order to have a temperature variation of the fluid ΔT_{in-out}:

$$\dot{m}_{crate} = \frac{\dot{Q}_{crate}}{c_p \Delta T_{in-out}} = 0.1 \ kg/s$$

3. **Introduce constraints**: introduce constraints on the value of the Reynolds number and velocity in the channels. Good choices could be the following ones:

$$\begin{cases} R_e > 2500 = R_{e.min} \\ V < 3.5 \ m/s = V_{max} \end{cases}$$

The previous constraints can also be written in terms of the channel diameter, and recalling that for square channels the hydraulic diameter coincides with the square sides:

$$\begin{cases} D < \frac{\dot{m}_{crate}}{\mu R_{e.min}} = 29.2 \ mm \\ D > \sqrt{\frac{\dot{m}_{crate}}{\rho V_{max}}} = 4.2 \ mm \end{cases}$$

There are tight constraints on the available space in the region where the crates are located and to reduce the encumbrance of the cooling channels we have chosen the smallest available side length:

$$D_{crate} = 5 \ mm$$

4. **Check the results**: with mass flow rate and channel size selected, check all the results for the DAQ line.

   The velocity inside the channels is:

$$V = \frac{\dot{m}_{crate}}{\rho D_{crate}^2} = 2.2 \ m/s$$

   The Reynolds number is:

$$Re = \frac{\rho V D_{crate}}{\mu} = 14606$$

   The Nusselt number is:

$$N_u = 0.023 R_e^{0.8} P_r^{0.4} = 124.5$$

   The convective heat coefficient:

$$h_c = \frac{N_u k}{D_{crate}} = 1545 \ W/m^2K$$

   And finally the temperature difference between central fluid and inner channel walls:

$$\Delta T_{fl-w} = \frac{\dot{Q}_{crate}}{h_c A} = 3 \ ^\circ C$$

   Considering a fluid inlet temperature of 5 degrees higher with respect to the FEE line (-15 $^\circ C$ instead of -20 $^\circ C$ for reasons explained later), and assuming for safety reasons only the temperature at crates outlet:

$$T_{out} = -12 \ ^\circ C$$

   Adding ΔT_{fl-w} we can obtain a conservative estimate for the channel walls temperature:

$$T_{wall} = T_{out} + \Delta T_{fl-w} = -9^\circ C$$

This value of wall temperature implies that the most unlucky components of crate boards will be around[8]:

$$T_{max.daq} = T_w + \Delta T_{DAQ} = 32^{\circ}C$$

5. **Analysis of the results**: The maximum expected temperature for the electronic components is not critical. They could safely withstand 28 $^{\circ}C$ warmer temperatures. This is the reason for dividing the DAQ and FEE lines in two independent circuits. Another solution could be to decrease the flow in the crates, in order to raise the crates walls temperatures, and subsequently the electronic boards. This solution would also decrease the head loss of the system.

   There is no reason to keep the crates so cold, since the only tight requirement is on the SiPM. Moreover, it is not yet clear if cold crates could produce problems of irradiation towards the straw-tracker. A good solution in this case would be to design two separate circuits with the circulating fluid at two different temperatures. The DAQ cooling circuit could be safely used at higher temperature than the FEE circuit. Another advantage of two separate circuits would be to use another fluid for the DAQ cooling. At higher temperature also water could be used, as well as glycol. This would reduce the environmental damage potential of PF-5060 leakages, since a smaller amount of fluid means smaller amount of possible leaks.

   Nevertheless, we should notice that the available space inside the mechanical room is limited. Having two separate circuits implies two sets of equipment: tanks, chillers, pumps, valves etc... This could be a problem if the space inside the room turned out to be insufficient. This trade-off study is very important, and while the requirements get always more defined, the most convenient solution should always become more clear.

As a conclusion we have selected for the DAQ line a total mass flow rate of:

$$\dot{m}_{crate} = 2 \ kg/s$$

This value will be used to design the whole circuit in the next section.

6.5 Definition of the single system

In this section we develop a cooling system taking into account the constraints and results highlighted in the previous section. The goal of the design is to respect the previous guidelines in order to satisfy the cooling requirements. We report here a brief summary of the requested flow characteristics:

[8] In this calculation ΔT_{DAQ} comprises also a ΔT contribution from fluid to pipe already accounted in previous values. The real ΔT between walls and electronic component will be a little smaller than that.

- The mass flow rate for the FEE line is:

$$\dot{m}_{FEE} = 2.5 \ kg/s$$

- The front end inlet temperature is:

$$T_{FEE.in} = -20 \ ^{\circ}C$$

- The mass flow rate for the DAQ line is:

$$\dot{m}_{DAQ} = 2 \ kg/s$$

- The DAQ crates inlet temperature is around:

$$T_{DAQ.in} = -15 \ ^{\circ}C$$

The system will be designed in order to satisfy the previous constraints.

Since the mass flow rates are selected for both the FEE and DAQ line, the total mass flow rate is:

$$\dot{m}_{tot} = \dot{m}_{FEE} + \dot{m}_{DAQ} = 4.5 \ kg/s$$

Starting from the PFD logic of fig. 6.2 the hydraulic circuit P&ID of fig. 6.3 has been designed. As it can be seen from the diagram, there are some important features we want to highlight:

- The cooling station is crossed only by the FEE line. This means that only the fluid going towards the front-end unit is cooled down to -20 ° C. The DAQ line is simply recirculated in the system because it does not need cold temperatures. Furthermore, having only one line passing through the chiller reduces its complexity and reduces the cost. The DAQ fluid will have slightly higher temperatures than the FEE fluid, until they get out from the cryostat and mix together. At that point the fluid temperature will be the flow averaged temperature.

  However, the heat power to be extracted from the system remains practically the same[9]. There are not advantages from that standpoint. Suitable chillers will be discussed in section 7.1;

[9]The slightly higher temperature of the DAQ line decreases the heat power entering into the fluid from the environment by a negligible quantity.

- Both the FEE and DAQ lines need an appropriate filter upstream of the cryostat. Using a single filter in the outlet routing line would have produced a simpler system, but for safety reasons is not recommendable. Filters always have to be upstream of the critical locations;

- All other equipment is obviously located on the routing line, where single components are sufficient. Particular attention should be posed on the relative position of tank and pumping group. It can be seen from the sketch of the mechanical alcove that the tank will be mounted with a hydrostatic head with respect to the pump. This is always a good guideline because the hydrostatic pressure reduces the possibility of cavitation[10] at pump inlet blades. A cavitation validation analysis will be performed during the performance analysis of the system;

- Several instruments have been foreseen for the good operation of the system. There are essentially three types of them:

  1. **Flow transmitter (FT)**: sensor that measures the value of mass flow rate in a certain line;
  2. **Pressure transmitter (PT)**: sensor that measures the value of pressure in a certain line;
  3. **Temperature transmitter (TT)**: sensor that measures the value of fluid temperature in a certain line.

  They are used in order to manually calibrate the system during installation and first use. If the sensors show quantities different from the predicted ones, the operator will act on valves and calibrate the system. Several valves can be used to regulate the system, automatically or manually;

- We have not yet determined the diameters of routing lines and inside the mechanical room. In order to have low losses their diameter will be in the range between 1 and 2 inches. More information will be given in section 7.4

Prior to select the components from the market is important to carry out a detailed analysis of the system performance. That is the goal of the next pages.

6.6 Analysis of system performance

The analysis is made on the system relative to fig. 6.3. The goal is to calculate all the important quantities along the circuit, in order to select the right components. The significant quantities are of the following types:

[10] Cavitation is the formation of bubbles or cavities in liquid, developed in areas of relatively low pressure around an impeller. The imploding or collapsing of these bubbles trigger intense shockwaves inside the pump, causing significant damage to the impeller and/or the pump housing.

- Head loss between points of interest, and total head loss. These values are needed to calibrate the parallel branches and select the pumps;
- Temperature map of the system. This means having a distribution of temperature along the overall system. This is important to select the right chiller and to perform the final verification on the plant.

Before passing through the analysis we briefly summarize the formulas and concepts needed to carry out the analysis.

6.6.1 Thermo-fluid dynamic analysis

In a thermo-fluid dynamic analysis the quantities of interest are temperature, fluid velocity and pressure. The velocity is uniquely determined from the mass flow rate and pipe diameters, already defined in the previous Chapters. Therefore the quantities that still need to be calculated are the pressures and temperatures.

In a closed system the quantities that can be calculated are the variations of temperatures and pressure, not their absolute values. This means that we need to fix a set point value for them at a certain location in order to calculate the absolute values. Two assumptions will be made on the circuit set point:

1. The temperature at front end inlet is:

$$T_{FEE.in} = -20 \ ^{\circ}C$$

2. The tank is directly connected to the environment[11]. This means that the fluid in the tank has a pressure of approximately:

$$P_{tank} = 1.013 \ bar$$

All the relative variations (pressure and temperature) along the circuit will be taken starting from these two set points. The absolute value of pressure is not important by itself but to properly choose the components, since many hydraulic elements are sized accordingly to the internal fluid pressure. Other assumptions can be made thanks to the nature of the system:

- The flow is unidimensional and incompressible. This simplifies a lot the calculations, and is a realistic assumption compared to the requested accuracy;
- *Bernoulli's equation* is valid and the hydrostatic components are almost everywhere negligible.

[11] This can be changed is necessary. If the fluid for whatever reason (cavitation) needs to have higher pressures, the tank can be closed and pressurized at the requested level. In absence of justified motivations it would be silly to raise all the circuit pressures.

Knowing the set points of the circuit we can evaluate the system characteristics. In order to do that is important to show how to calculate head loss and temperature change.

- **Head loss**: it is a loss in pressure head $[Pa]$ due to the viscosity of the fluid and obstructions to a certain flow, such as pipe elbows, valves, etc... By knowing the head loss, we can calculate the absolute or relative pressure of all the other circuit points. It is extremely important because the pump will be sized and selected accordingly. As demonstrated in all fluid dynamics books, and in particular in [16], the head losses are proportional to the square power of velocity:

  $$\Delta p \propto V^2$$

  In hydraulic circuits there are mainly two types of head loss. The first type is the loss along a tube due to wall friction, and is called distributed head loss ΔP_d. The second type of loss is due to particular components, such as valves and other fittings, and is called concentrated head loss ΔP_j. They can be calculated in the following way, in which we added the formulas in terms of mass flow rate for simplicity:

  $$\Delta p_d = f\frac{L}{D}\rho\frac{V^2}{2} = 8\frac{fL}{\rho\pi^2 D^5}\dot{m}^2$$

  $$\Delta p_j = K_j\rho\frac{V^2}{2} = 8\frac{K_j}{\rho\pi^2 D^4}\dot{m}^2$$

  the meaning of the terms is:

  - f is the friction factor, and a good estimate is given by the empirical *Colebrook-White's correlation*:

    $$f = \left[1.14 \cdot 2\log_{10}(\frac{\varepsilon}{D_h} + \frac{21.25}{R_e^{0.9}})\right]^{-2}$$

  - K_j is the *irreversible loss coefficient* of the localized pressure loss j. It depends on the kind of obstacle that the fluid has to run through:

    $$K_j = f(geometry, R_e)$$

    It is a quantity specifically defined by the manufacturer of the equipment, or can be estimated with procedures shown in [16].

- **Temperature change**: the temperature variations are mainly due to heat absorption in the passage in a piping section. All the circuit can be divided in sections, each of which has its own heat power discharged into the fluid.

Once the heat power introduced into the fluid is known, as well as flow characteristics, we can estimate the temperature change in this way:

$$\Delta T_{ij} = \frac{\dot{Q}_{ij}}{\dot{m}_{ij} c_p}$$

Where i and j refers to two particular points of the circuit taken as reference.

Using the previous information, the overall estimate of circuit head loss is shown in fig: 6.6.

It is important to note that the DAQ line undergoes a head loss of around 2.4 *bar* higher than that of the FEE line. This means that in order to calibrate the system we have to artificially increase the head loss in the FEE line of the same amount. Otherwise the circuit would be unbalanced and the total mass flow rate would split in a wrong way between the 2 lines. This artificial head loss will be introduced closing partially a control flow valve on the FEE line, and will be done during the initial calibration of the system. This produces a dissipation of mechanical energy that could be avoided by designing two independent circuits.

Another important aspect is that the overall head pressure loss of the system is 7.5 *bar*, where approximately 4.5 *bar* is due the dissipation in the crates channels. During experimental tests [26] we found a large difference between calculations and measurements of the crates head loss. There was a difference of 4.6 *bar* between them. In order to be conservative we will add this difference to the calculated values, until new experiments will verify or not this prediction. Moreover, 0.5 *bar* will be added as a safety margin, since we have not accounted yet for losses of the fluid passing through the chiller coils. Doing so, we end up with a total circuit head loss of:

$$\Delta p_{TOT} = 12.5 \ bar$$

The temperature map of the circuit is reported in fig. 6.7.

The important temperatures in fig. 6.7 are relative to chiller inlet and outlet ports (respectively $T_{ch} = -16.1°C$ and $T_c = -20.1°C$), and the front end outlet temperature ($T_5 = -19.4°C$).

The latter temperature value satisfies the previously assumed desired guidelines, therefore the system can be considered acceptable for what concerns the cooling function.

6.6.2 Regulation of the system temperature

In section 3.1 we mentioned the possibility to run the system in two different ways. During the first period the system could work with fluid temperatures around -10 $°C$ (and SiPM at 0 $°C$), and after a certain irradiation time it should lower the temperature at -20 $°C$ because of SiPM degradation. The system described in section 6.5 has been sized to work in the critical condition of -20 $°C$, but it must be provided with regulation systems able to shift the overall circuit temperature.

The circuit temperature is defined by the energy balance between absorbed and discharged thermal powers. We can take into consideration a system composed

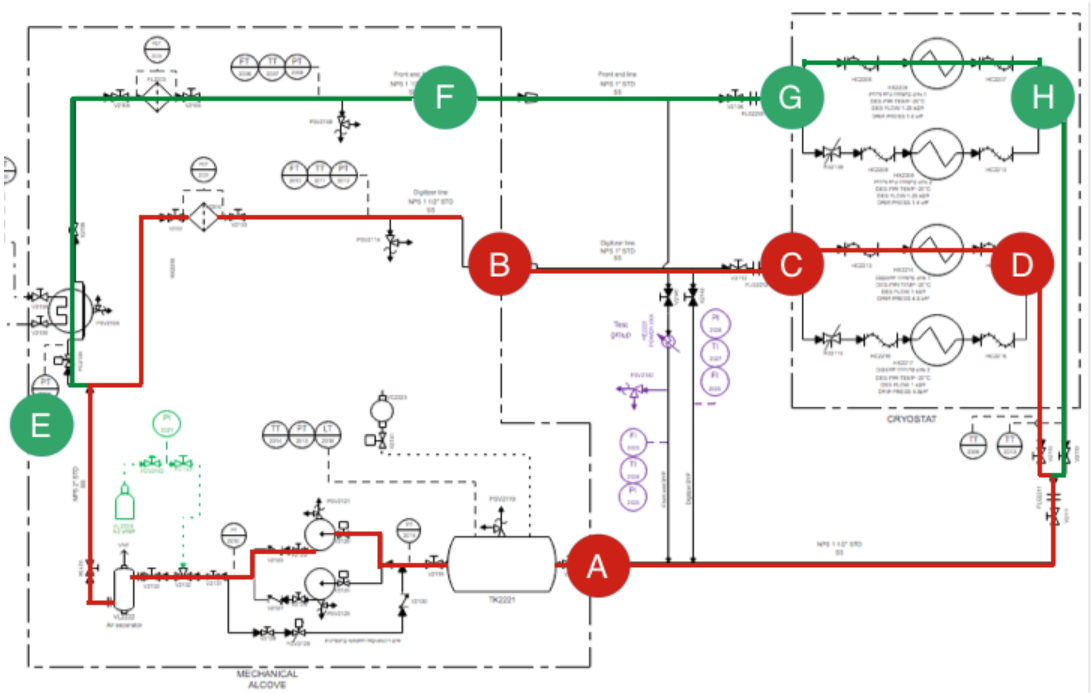

FEE PATH	HEAD LOSS [bar]
Mechanical alcove **A-E-F**	0.23
Routing FEE line **F-G**	1.56
FEE cooling line **G-H**	1.43
Common outlet line **H-A**	0.34
Valves & equipment	1.04
Margin of safety	10%
TOTAL	**5.1 bar**

DAQ PATH	HEAD LOSS [bar]
Mechanical alcove **A-B**	0.23
Routing DAQ line **B-C**	0.99
Crates cooling line **C-D**	4.45 (9.1*)
Common outlet line **D-A**	0.34
Valves & equipment	1.04
Margin of safety	10%
TOTAL	**7.5 bar (13.6*)**

Figure 6.6: Head loss summary for the single system running at -20 $°C$. The (*) value, relative to 9.1 *bar* loss in the crates cooling line D-A, refers to the quantity measured in experiments [26].

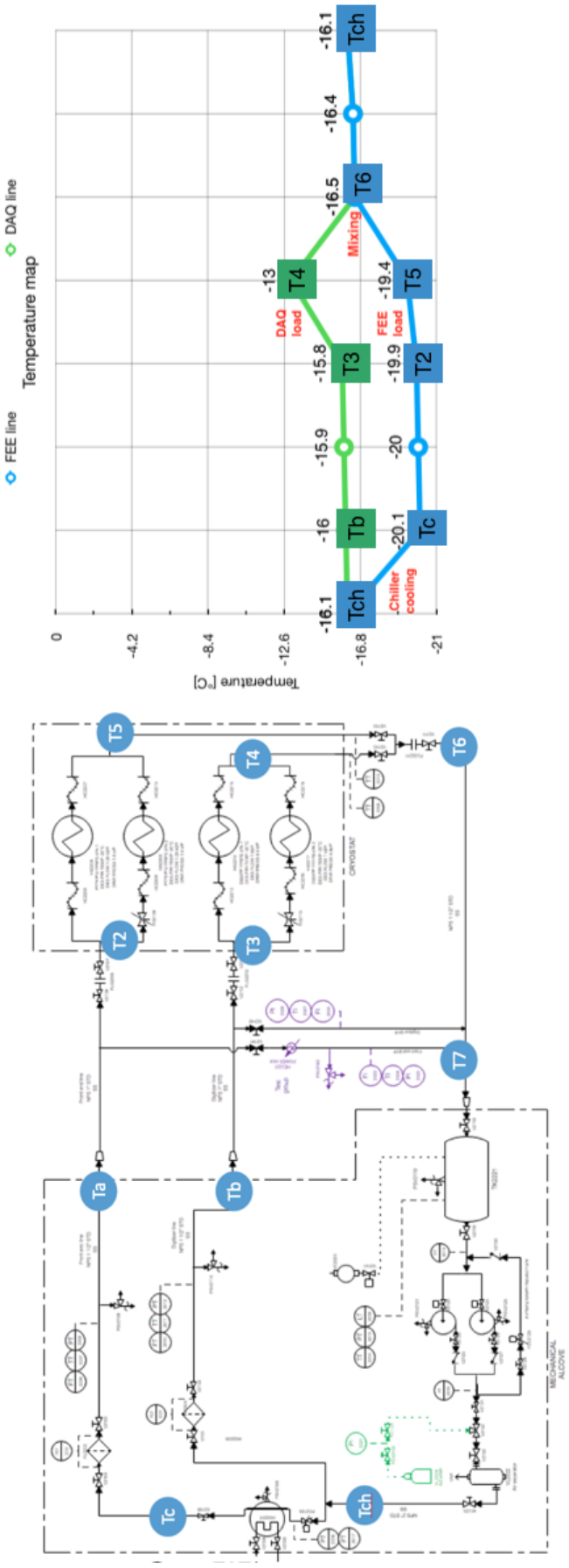

Figure 6.7: Temperature map for the single system running at -20 $^{\circ}C$ at front end inlet.

only by the fluid contained in the hydraulic circuit.
Let us assume that the system is running steadily at exactly -10 $°C$ (FEE inlet temperature). This means that there is a balance between input and output thermal powers. The input thermal power comes from the electronics and outer environment (heat sources), while the output is due to the chiller power extraction (heat sink).
At a certain time instant assume to increase the thermal load the chiller is extracting from the circuit. In that case there would be a net outgoing power from the system towards the environment. This power gap decreases in time the energy of the system, and subsequently the fluid temperature; until a new equilibrium temperature is reached. The equilibrium is reached once the environmental entrances increase at the level in which they perfectly balance the previous gap (since we can consider the electronics input as a constant term).

From the system enthalpy equation [11], (assuming for simplicity constant c_p and $\dot{Q}_{in}$; together with uniform fluid temperature) we can write:

$$m_{tot} c_p \frac{dT}{dt} = \dot{Q}_{in} - \dot{Q}_{out}$$

Where m_{tot} is the total mass of fluid contained in the system, c_p is an average of the specific heat between maximum and minimum temperature of interest, and $\dot{Q}_{in}$ ($\dot{Q}_{out}$) is the average of the incoming (outgoing) heat power during the time of observation.[12]

The enthalpy equation can be easily integrated (considering all constant terms for simplicity) in:

$$\frac{\Delta T}{\Delta t(\dot{Q_{in}} - \dot{Q}_{out})} = \frac{1}{m_{tot} c_p}$$

This formula shows how quickly the temperature increases/decreases depending on the amount of net incoming/outgoing thermal power. For our system $m_{tot} = 740\ kg$ and $c_p = 980\ J/kg°C$. The result is:

$$\frac{\Delta T}{\Delta t(\dot{Q_{in}} - \dot{Q}_{out})} = \frac{1}{m_{tot} c_p} = 1.38 \cdot 10^{-3} \quad \frac{°C}{s \cdot kW}$$

This means that a power thermal gap of 1 kW produces an approximate temperature change of 10 $°C$ in around 2 hours. Obviously this solution is very much approximated, since that in real situations the various terms are not constant. This was only to explain the physics and catch the trend of the process. In reality, once the desired temperature is reached, a fine regulation will be necessary to keep the equilibrium on that temperature. Nonetheless the level of approximation, this is a pretty good solution, because during operation a quick temperature change will not be necessary and the necessary power will be low.

[12]There are several assumptions made on the previous formula only in order to be simplier. Some quantities change with the temperature, and for accurate calculations the right behavior of parameters should be taken into account.

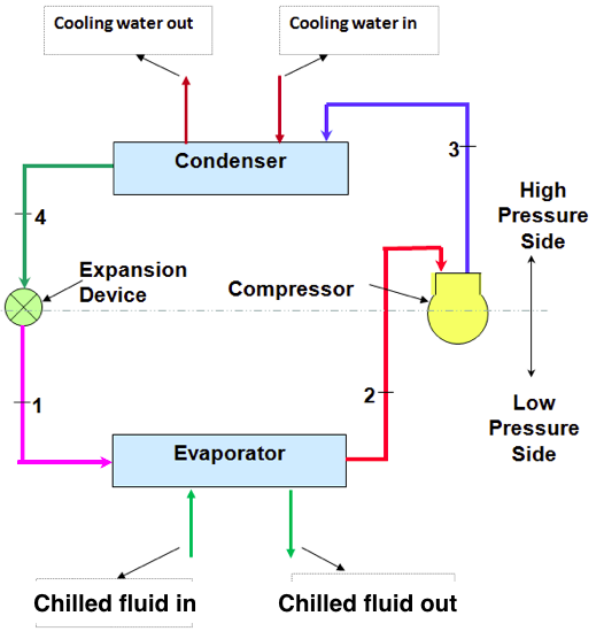

Figure 6.8: Schematic view of the internal refrigerant circuits of simple chillers.

The two selected equilibrium temperatures are -10 $°C$ and -20 $°C$. In order to size a system able to shift between them we have to estimate how much the energy balance changes in different conditions.

The input powers of the system are:

- Heat produced in the calorimeter electronics;
- Environmental heat.

The calorimeter electronics heat can be assumed almost constant. Therefore, changes in input power depend only on the environment, which in turn depend on the system temperature. Considering the environment more or less always at the same temperature, if the system decreased its temperature contemporaneously would increase the difference with outer environment. Therefore the environmental heat inputs increase.

Now that it is clear that the system temperature can be changed only modifying the terms relative the energy balance, we can think at various methods to do that efficiently. During my internship at Fermilab I thought to different ways to do that:

- **Option 1 (Adjustable chiller)**: this is the most accurate method to change the temperature of a system. Chillers are machines with their own internal refrigerant circuits (shown in fig. 6.8).

  The amount of absorbed power depends on the flow rate of internal refrigerant. That quantity is controlled by the compressor, which in turn can be controlled by means of a *variable frequency driver*[13] (VFD).

[13] A variable-frequency drive (VFD), also known as inverter, is a type of adjustable-speed drive used in electro-mechanical drive systems to control AC motor speed and torque by varying motor input frequency and voltage.

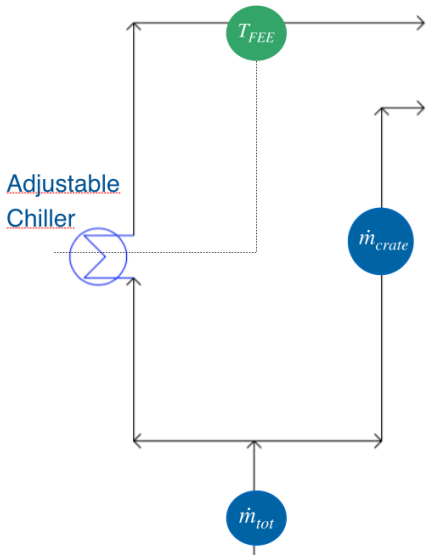

Figure 6.9: Schematic representation of option 1 for temperature regulation.

The regulation method is schematically represented in fig. 6.9. The sensor reads the temperature T_{FEE} and the control system adjusts the chiller thermal load accordingly.

This method can be very accurate, but attention should be focused on the fact that VFD are expensive devices, and the system could work in acceptable ways even with cheaper solutions;

- **Option 2 (Adjustable thermal resistance)**: this method implies the introduction of one (or more) thermal resistances in the circuit. An example is shown in fig. 6.10.

  The thermal resistance makes use of simple Joule effect to produce heat, defined by:

$$\dot{Q} = RI^2$$

  Where $\dot{Q}$ is the heat produced, R is the electrical resistance, and I is the current crossing the resistance. In this case the regulation would be done adjusting the amount of current crossing the resistance (or changing the resistance keeping a constant current) with a simple electronic controller. This method provides a very simple and cheap solution, even though increases the electric expense of the mechanical room. This is one of the most common method of regulation already embedded in chiller machines;

- **Option 3 (Chiller bypass)**: this method foresees to bypass a certain amount of flow from the chilled line (6.11).

  In this case the chiller would be designed to work efficiently with a chilled fluid mass flow rate of $\dot{m}_{FEE} = 2.5\ kg/s$. If a certain percentage of it got bypassed, the chiller would operate with a flow rate different from the design

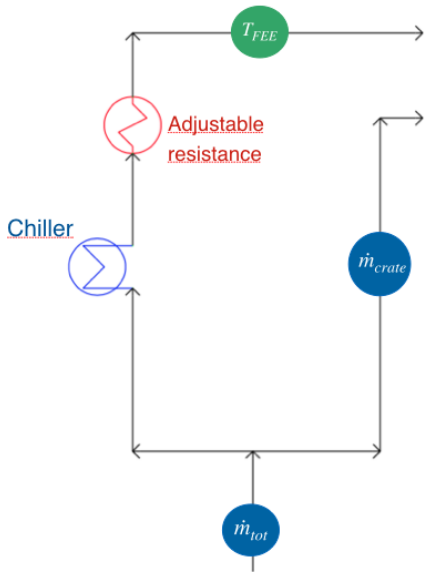

Figure 6.10: Schematic representation of option 2 for temperature regulation.

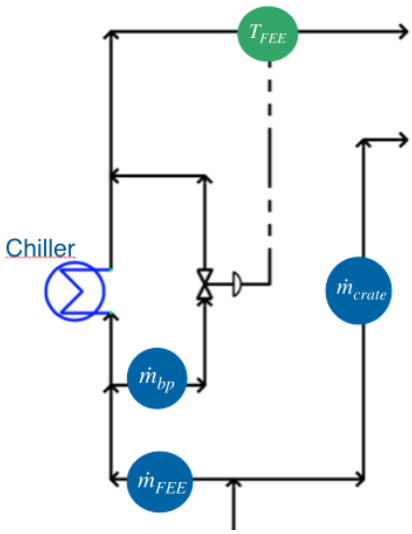

Figure 6.11: Schematic representation of option 3 for temperature regulation.

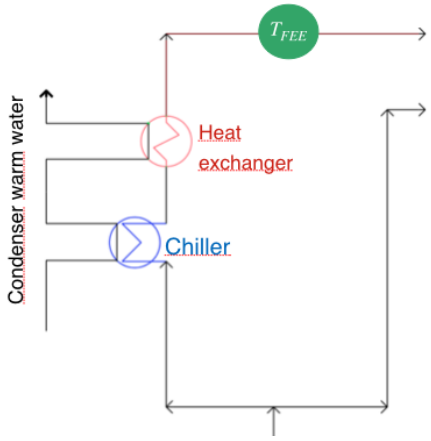

Figure 6.12: Schematic representation of option 4 for temperature regulation.

value. In that case the machine would work slightly worse, decreasing the thermal load absorbed from the system.

This would be a "for free" regulation, because the necessary energy would be only the one relative to the regulation of bypass control valve. The problem is that to design a reliable system like this we must have a very good knowledge of chiller characteristic diagrams, not easy to be obtained;

- **Option 4 (Condenser water heat recovery)**: this method makes use of the temperature difference between the cooling fluid and the chiller cooling water (fig. 6.12).

  As shown in the chiller functional scheme (fig. 6.8) the water leaving the condenser has a certain temperature higher than the chilled fluid. Exploiting this temperature difference in a heat exchanger (shell and tube type for example) could introduce the right amount of heat in the system practically for free. This solution is not so simple and cheap because it needs a customized exchanger, but can become a smart solution in case we ran out of electric power.

All the regulation methods can also be used in the case of double circuit system. The logic would be exactly the same even though the size of various machines would be different. The selection of the best method is of course matter of a trade-off study. The VFD driven chiller is the most accurate and performing method, but since the system requirements regarding the regulation ability are not so stringent could be convenient using another cheaper method.

The method described in option 2 would be sufficient to change the system temperature of 10 $°C$ in around 8 hours simply using a 250 W resistance. The cost would be negligible and the wasted energy not too large. Moreover, once the target temperature is reached only little amount of current would be needed to keep stable the equilibrium point. On the other hand, inverters can cost as much as 6000 $, (as explained in the section relative to chiller selection), weighing around 20% of the total chiller cost.

6.7 Single circuit running at -10 °C

In this section we report the performance analysis of the circuit during the first period of use. During the first period the circuit is expected to run at -10 °C (fluid temperature). Our goal is to demonstrate if the system designed to work at -20 °C still satisfies the technical requirements.

Following the same procedures of the previous case, we can calculate the head loss of the system. The results for the pressure drops are slightly lower than those of the colder case (because of a little decrease in the viscosity of the fluid). This is in agreement with the low temperature sensibility of PF-5060. Therefore, we can confirm that from the head loss standpoint there are no problems in running at 10 °C warmer temperatures.

Regarding the temperature map the results are shown in fig. 6.13

The Figure, shows the results of the system are essentially the same of the other working condition. This is true because in order to absorb a certain thermal power, the system will need to be colder of another amount dependent on the design of various components. Due to the system thermal insulation, at higher temperature the total power entering into the circuit is more or less the same than the -20 °C case. Therefore all the temperature variations remain more or less the same.

In the end, increasing the circuit temperature produces only a warmer set point[14].

This section has demonstrated the possibility to switch between −10 and −20 °C. During the first period the system should run at -10 ° until SiPM sensors reveal an increasing temperature, demanding for the reduction of fluid temperature. During the passage between working conditions the system will need to absorb more heat than that introduced from electronics and environment. During that period one of the options shown in section 6.6.2 can be used.

6.8 Double circuit system

In this section we want to give important information in case the double circuit system will be chosen. The preliminary definition of mass flow rates and temperatures follows the same procedure shown for the single circuit. In this way we found mass flow rates value of:

$$\dot{m}_{FEE} = 2.5 \ kg/s$$

$$\dot{m}_{DAQ} = 2 \ kg/s$$

While the assumed temperatures used for the analysis are:

$$T_{FEE.in} = -20 \ ^{\circ}C$$

[14]Of course this is true only for small temperature changes. It would be wrong in case of large temperature variations, that anyway should not occur in our system

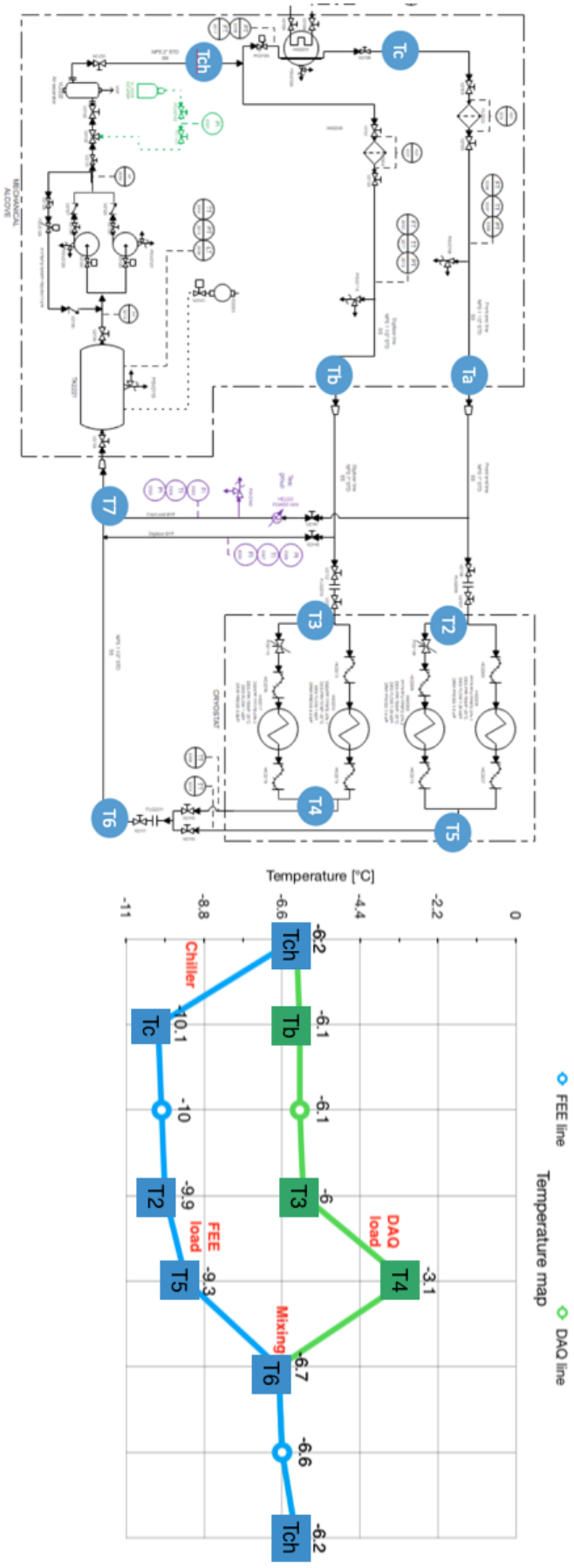

Figure 6.1.3: Temperature map of the system in the case of front end inlet temperature of -10 °C.

$$T_{DAQ.in} = -10 \ ^{\circ}C$$

The results are essentially modified forms of the single circuit. Fig. 6.14 reports the head loss for the FEE circuit running at -20 $^{\circ}C$, while fig. 6.15 the one relative to its temperature map.
Fig. 6.16 reports the head loss for the DAQ circuit running at -10 $^{\circ}C$, while fig. 6.17 the one relative to its temperature map.

From the figures is clear that also this type of design layout is compliant with technical requirements. The good point in it is the possibility to change one circuit temperature independently from the other. This could be the answer to the tracker problems, and must be kept in mind during final decisions.

6.9 Alternative solution to the Tracker problems

One of the main reasons to introduce the double system design was to provide an alternative solution to keep the DAQ line at higher temperature than the FEE line. This was meant to have warmer crates, in order to minimize any interference with the straw-tracker detector due to excessive heat radiation. An alternative solution could be to use the same hydraulic design of the single system, but with a lower velocity in the DAQ line. This would deteriorate the efficiency of the heat exchange, increasing the temperature of the crates group.

In this situation one problem arises: the flow enters in the transitional regime. With the parameters set in section 6.4.3 the flow in the crates channel was barely turbulent, and decreasing the velocity will take it to the transitional state and in the end into laminar conditions.

With the system designed in 6.4.3 the ΔT between the fluid and the pipe walls was 3 $^{\circ}C$. Since the maximum allowed temperature for the DAQ electronics has been set to 60 $^{\circ}C$, and the temperature variation between the channel walls and the hottest electronic component is around $\Delta T_{DAQ} = 41 \ ^{\circ}C$, the maximum allowable temperature of the cooling channel walls becomes 19 $^{\circ}C$. The fluid leaving the crates cooling channels has a temperature around -13 $^{\circ}C$. This means that the maximum allowable ΔT between fluid and pipe walls is 32 $^{\circ}C$. That is the maximum allowable temperature difference between the central fluid and the inner pipe walls.

The thermodynamic quantity important in the heat exchange between the fluid and the pipe is the Nusselt number (or equivalently the convective exchange coefficient h_c). It is a non-dimensional parameter that evaluates the amount of heat exchange, defined like this:

$$N_u = \frac{\dot{Q} D}{A k \Delta T}$$

$\dot{Q}$ is the heat exchanged, D is the hydraulic diameter of the duct, A is the surface area of exchange, k is the thermal conductivity of the fluid and ΔT is the temperature difference between central fluid and walls.
Knowing the Nusselt number for a certain heat exchange means knowing the temperature difference producing it (once the geometry and the other parameters

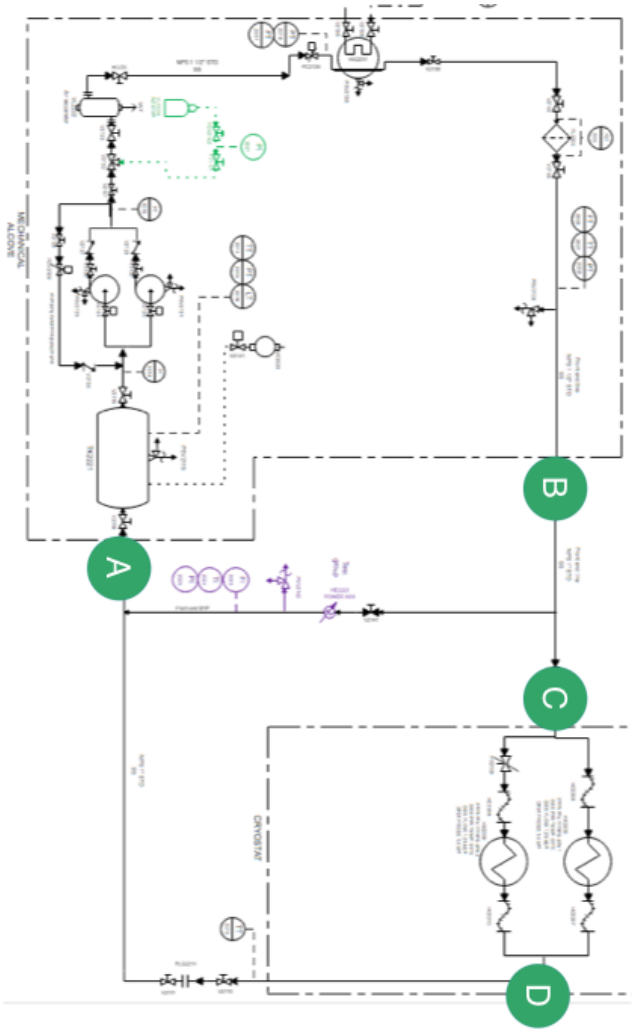

PATH	HEAD LOSS
Mechanical alcove **A-B**	0.26 bar
Routing FEE **B-C**	1.56 bar
FEE cooling line **C-D**	1.43 bar
Routing outlet line **D-A**	0.35 bar
Valves & equipment	1 bar
Margin of safety	10%
TOTAL	**5.1 bar**

Figure 6.14: Head loss of the FEE circuit at front end inlet temperature -20 $^{\circ}C$.

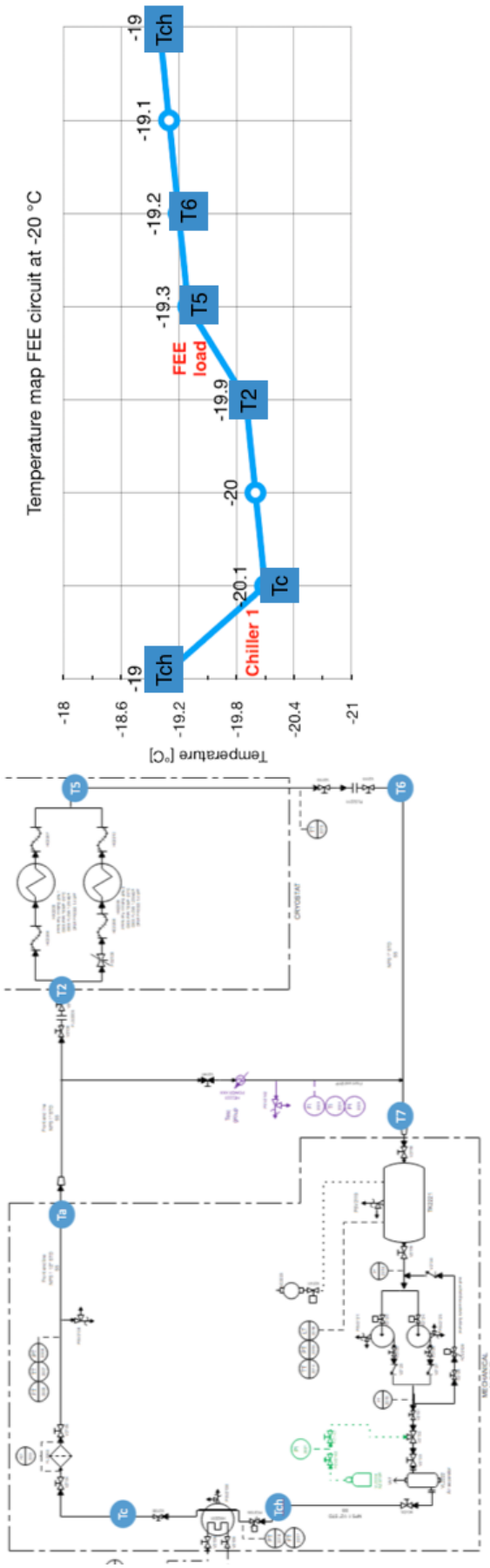

Figure 6.15: Temperature map of the FEE circuit at front end inlet temperature -20 $^{\circ}C$.

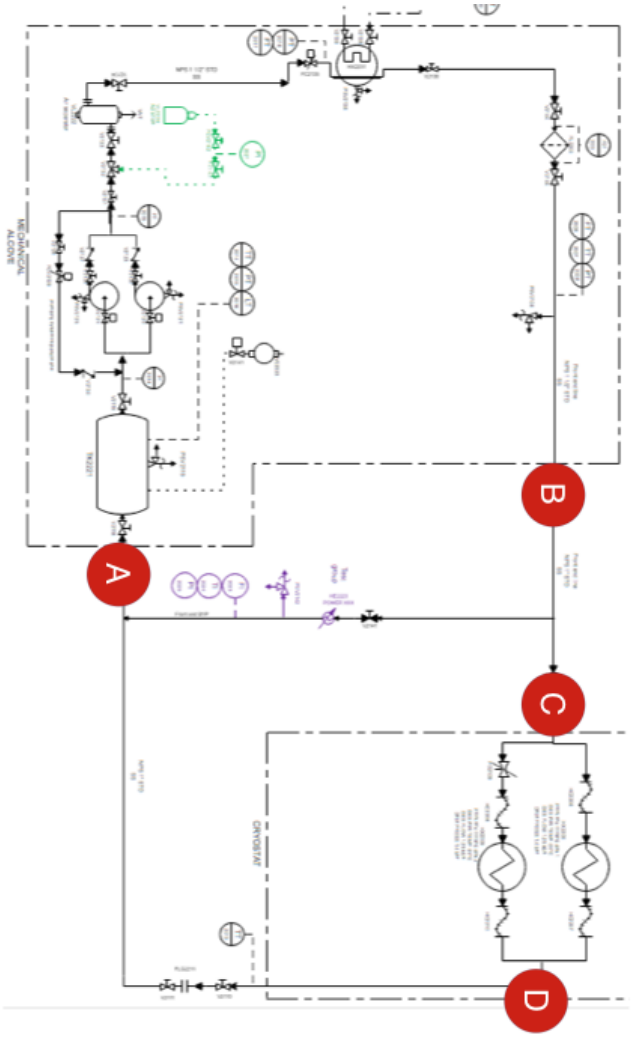

PATH	HEAD LOSS
Mechanical alcove **A-B**	0.22 bar
Routing DAQ **B-C**	0.96 bar
DAQ cooling line **C-D**	4.3 bar
Routing outlet line **D-A**	0.34 bar
Valves & equipment	1.03 bar
Margin of safety	10%
TOTAL	**7.5 bar**

Figure 6.16: Head loss of the DAQ circuit at crate inlet temperature -10 $^{\circ}C$.

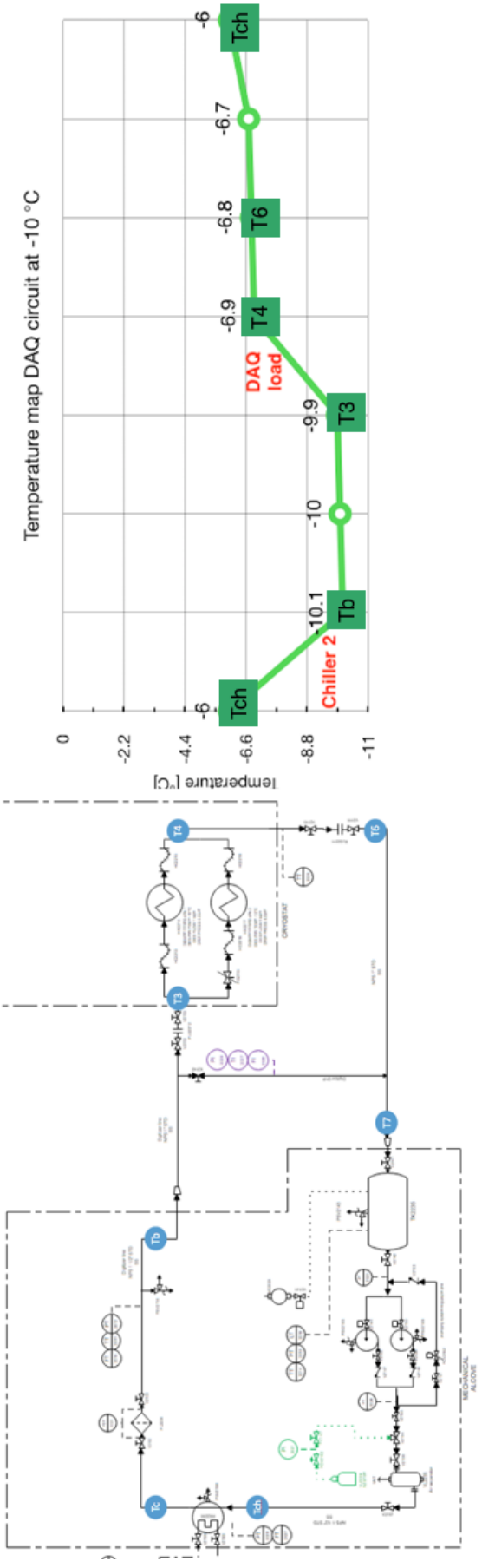

Figure 6.17: Temperature map of the DAQ circuit at crate inlet temperature -10 $°C$.

are fixed). The Nusselt number value depends on the flow conditions, and embeds all the fluid dynamics phenomena (descends directly from the *Navier-Stokes equations*, at least theoretically).

The analytical solution exists only under several simplifying conditions (laminar, one-dimensional, incompressible flow and simple geometry). In general situations, empirical correlations are necessary to obtain useful solutions. The empirical correlations give accurate estimates only for certain range of parameters. Always be careful to use them in the appropriate conditions. We'll see here the most commonly used correlations for the different flow conditions:

- **Laminar flow**: it's a flow regime where normally $R_e < 2300$. In this flow conditions the local Nusselt number is a constant throughout the fully developed region, but its value depends on the surface thermal condition (constant heat flux, or constant surface temperature). For a problem in which the amount of heat exchanged is fixed, and the temperature difference must be evaluated, the solution for the Nusselt number in a circular pipe is given by the *Hagen-Poiseuille* solution with constant heat flux [11]:

$$N_u = \frac{\dot{Q}D}{Ak\Delta T} = 4.36$$

  Where ΔT is the only unknown.
  For a square channel the laminar Nusselt number is 3.61. It is a bit lower than the circular solution, since the local convection coefficient varies around the periphery of a square tube, approaching zero at its corners. Hence, circular shapes are more efficient than polygonal figures.

  We can define an efficiency of the square shape compared to the circular one, in the following way:

$$\varepsilon = \frac{N_{U.square}}{N_{U.circle}} = 0.83$$

  This value will be the number relating the circular solutions (simpler to be found because many experiments have been done on them) to the researched square solutions (useful for our design). From the Nusselt number we can obtain the temperature difference between the walls and the central fluid:

$$\Delta T = \frac{\dot{Q}}{h_c A} = \frac{\dot{Q}D}{N_u k A} = 103 \ ^\circ C$$

  This means that under laminar conditions in order to exchange a heat flow per crate of $\dot{Q} = 296 \ W$ the temperature difference between the central fluid and the inner pipe walls shoulde be around 103 $^\circ C$.
  This is obviously an unrealistic solution because we used the properties of the fluid at -20 $^\circ C$, while the fluid inside the thermal boundary layer will be well above this temperature. A more accurate solution would use the fluid properties at the so called *film temperature* conditions.

In heat transfer and fluid dynamics, the film temperature T_{film} is an approximation of the temperature of a fluid inside a convection boundary layer. It is calculated as the arithmetic mean of the temperature at the wall, and the free stream temperature:

$$T_{film} = \frac{T_{wall} + T_{\infty}}{2}$$

The film temperature is often used as the temperature at which fluid properties are calculated when using Prandtl, Nusselt and Reynolds number to calculate a heat transfer coefficient, because it is a reasonable first approximation of the temperature within the convection boundary layer.

The research of the film temperature and final solution of ΔT would be an iterative problem, but we can note that ΔT depends on the inverse of the conductivity. PF-5060 fluid has a conductivity that decreases at higher temperature, therefore the final ΔT will surely be larger than the found value of 103 $°C$. Since that it is not acceptable for thermal requirements (it should be lower than 32 $°C$), is mandatory to increase the flow velocity, entering in the transitional regime. The final solution of our problem will certainly be between the laminar flow (that gives 103 $°C$) and the initial turbulent condition (3 $°C$).

- **Transitional flow**: transitional flow regime is a mixture of laminar and turbulent flow, occurring for $2300 < R_e < 10000$ with turbulence in the center of the pipe, and laminar flow near the edges. Each of these flows behave in different manners in terms of their frictional energy loss, and have different equations governing their behavior. The proportions between turbulent and laminar is almost impossible to predict because the turbulence onset phenomena depends on several initial conditions impossible to know adequately (initial agitation, initial vorticity, contaminants, etc...). This results in flow calculations with a lot of uncertainty, especially for the heat exchange.
  The effects of wall roughness and transitional flow for the Nusselt number evaluation may be considered using the *Gnielinski correlation* (valid for $0.5 \leq P_r \leq 2000$ and $3000 \leq R_e \leq 5 \cdot 10^6$):

$$N_u = \frac{(f/8)(R_e - 1000)P_r}{1 + 12.7(f/8)^{1/2}(P_r^{2/3} - 1)}$$

  This equation of course gives a Nusselt number increasing with the velocity. It means that the temperature difference between fluid and pipe decrease as long as the flow velocity increases. This correlation gives good values of the Nusselt number until the flow becomes fully turbulent. From that point, another correlation (Dittus-Bolter) is more accurate.

- **Turbulent flow**: In turbulent flows vortices, eddies and wakes make the flow analytically unpredictable. Turbulent flow happens in general at $R_e > 10000$.

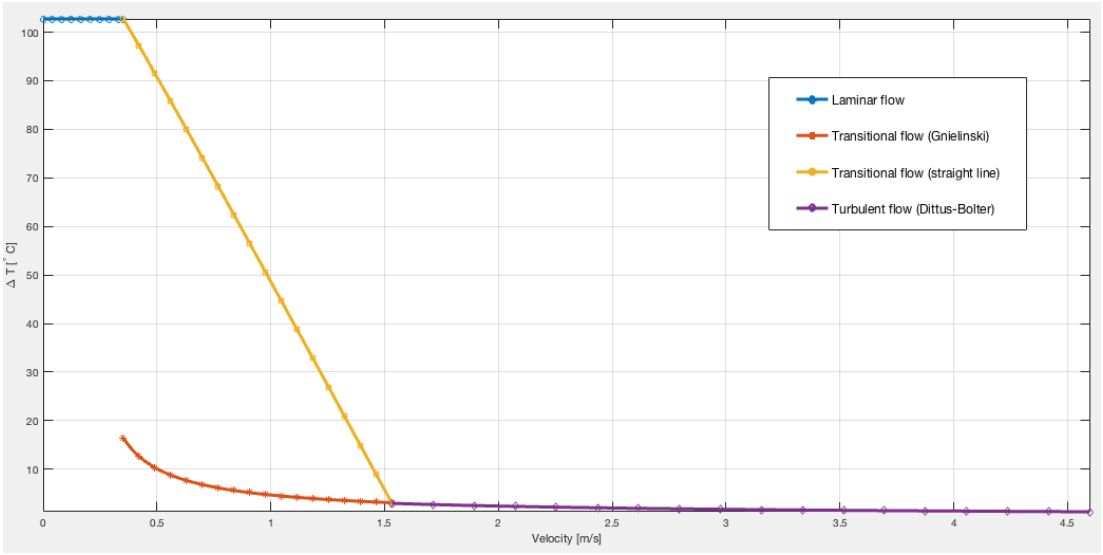

Figure 6.18: Temperature difference between central fluid and inner pipe walls in the crates cooling channel as a function of the flow velocity.

In this situations, experimentally more predictable than transitional regime, the Nusselt number is given by the *Dittus-Bolter correlation* (valid for $0.6 \leq P_r \leq 160$, $R_e \geq 10^3$ and $L/D \geq 10$):

$$N_u = 0.023 R_e^{0.8} P_r^{0.4}$$

Obviously also in the turbulent condition the temperature difference between fluid and pipe decrease with the increment of flow velocity.

In order to better understand the results as a function of the flow velocity we can draw a chart using the previous solutions (fig. 6.18).

The Gnielinski correlations is a good link between transitional and turbulent regimes, but is very distant from laminar solutions. For this reason we also used a simple straight line to link the laminar and turbulent solutions. Of course we need a more accurate solution for the range of interest.

Fig. 6.19 reports the solution for the Nusselt number in laminar and transitional conditions for a similar cooling application. We are looking for a maximum allowable $\Delta T_{max} = 32\ °C$. It is expressed by a minimum Nusselt number of:

$$N_{U.min} = \frac{\dot{Q} D}{A k \Delta T_{max}} = 11.6$$

The plot has been obtained for circular pipes. Therefore we have to use the efficiency parameter of the square shaped channel. This means that we must look for a minimum Nusselt number of:

$$N_{U.min} = 11.6/\varepsilon = 14$$

From fig. 6.19 we can see that $N_{U.min}$ intersects on the x-axis a value of:

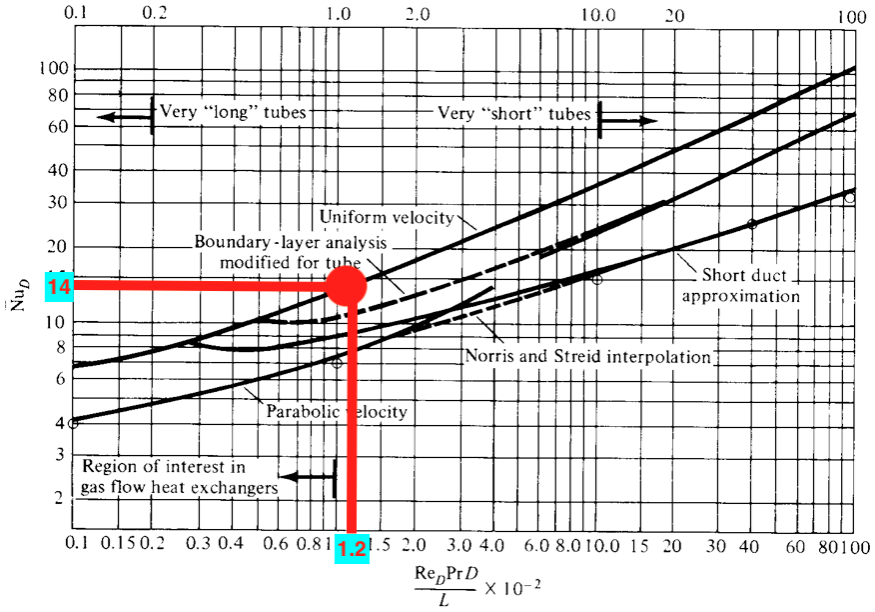

Figure 6.19: Heat transfer in transient flows through circular tubes at constant wall temperature (ASME).

$$\frac{R_e D P_r}{L} \cdot 0.01 = 1.2$$

which gives a Reynolds value of:

$$R_{E.min} = 7097$$

or, equivalently, a minimum velocity:

$$v_{min} = \frac{R_{E.min} \cdot \mu}{\rho D} = 1.1 \ \ m/s$$

Finally, we obtain a mass flow rate for the DAQ line exactly the half of the initial value of the single system:

$$\dot{m}_{DAQ} = 1 \ \ kg/s$$

Comparing the results of fig. 6.19 with those of fig. 6.18, we can see that this velocity produces a $\Delta T = 40 \ ^\circ C$ not too different from the one established with the straight line of fig. 6.19. This means that in the eventuality of this system configurations, a manual calibration of the circuit will be necessary, but the final flow selected for the DAQ line should be close to this value.

Important to note that a lower mass flow rate will decrease the head loss in the DAQ line (quadratically), as long as reducing the flow elaborated by the pump. This could be a really good improvement in system performances.

6.10 Final considerations on the system

We have obtained three possible configurations for the system. Two of them employ a single circuit, while the remaining one two independent circuits. The selection among them can be a difficult task, fruit of a trade-off study between efficiency and economical convenience.

Waiting for final decisions we pass now to select components among those available on the market in order to accomplish the most probable system functions.

Chapter 7

Components selection guide

The components selection is a delicate phase in a system design process. All the technical performance demanded to the system components must be converted in requested capabilities of certain devices, and a good critical sense is necessary to do it in a convenient way.

In the next pages we'll show examples of components selection for the circuit found among several companies of manufacturers. Firstly we'll describe the *sizing criteria* for every main component, and in appendix B we'll show the found data sheets.

7.1 Chiller selection

One of the most important component is the chiller (or cooling station). It is a machine that removes heat from a liquid via a vapor-compression or absorption-refrigeration cycle[1]. The liquid can then be circulated through heat exchangers to directly cool the target equipment, or another process stream (such as air or process water). As a necessary by-product, the refrigeration process creates waste heat that must be exhausted to ambience, or for greater efficiency, recovered for heating purposes. This heat is removed from the part defined *condenser coil*, shown in fig. 6.8 (an example of water cooled chillers).

A vapor-compression (the most common type) chiller typically uses one of four types of compressor: reciprocating compression, scroll compression, screw-driven compression and centrifugal compression. All these machines take power generally from electric motors. The cooling effect is provided via the *reverse-Rankine* cycle, also known as vapor-compression. The thermodynamic cycle is shown in fig. 7.1, where on the x-axis is reported the entropy of the fluid, and on the y-axis the temperature.

The simplest type of chillers work with the internal refrigerant fluid undergoing these thermodynamic transformations:

- **1-2**: The fluid in condition of dry saturated vapor, (point 1), gets compressed in the compressor leaving it in the conditions of a overheated saturated steam (point 2);

[1]Industrial chillers work mainly with one of these two type of thermodynamic cycles.

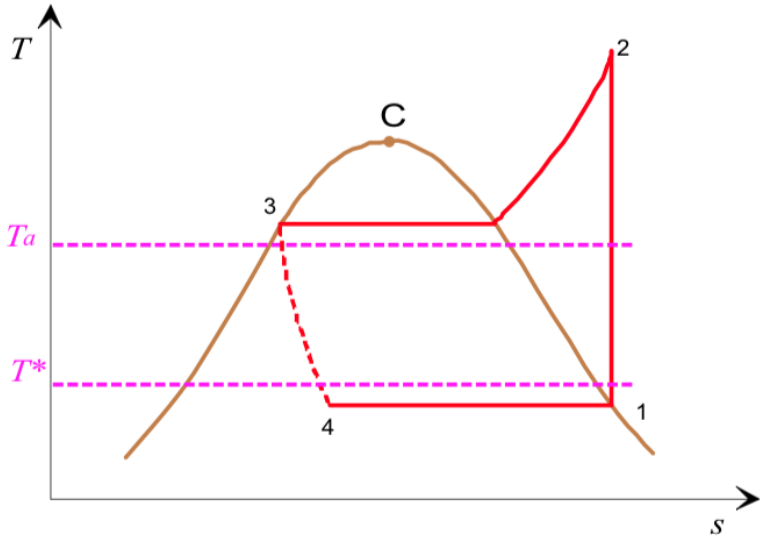

Figure 7.1: Thermodynamic cycle of a vapor-compression chiller. In the figure is represented the ideal cycle for simplicity, different from the real one because of unavoidable dissipations. [14] T_a and T^* represent in our application the temperature of the condenser water ($6\ ^\circ C$) and the chilled fluid ($-20\ ^\circ C$).

- **2-3**: The fluid, now at high pressure and temperature, passes through a condenser coil (a heat exchanger) where releases heat to the condenser fluid (water or air normally). The gas initially lowers its temperature until begins to condense. The transformation goes on until it becomes a saturated liquid (point 3). This transformation occurs almost at a constant pressure. Only little head loss occurs in the condenser passage;

- **3-4**: The saturated liquid passes through a lamination valve, where pressure is decreased very much, along with temperature. Doing so it becomes a saturated liquid at low temperature, ready to absorb heat from the chilled fluid (point 4);

- **4-1**: Now the fluid is able to absorb heat from the target fluid (PF-5060) passing through a heat exchanger called *evaporator*. Inside the evaporator it returns to its initial conditions of saturated vapor (point 1), ready to restart the cycle.

The condenser water function could be accomplished also by forced air ventilation. In our case, since the availability of a cold water source ($\simeq 38\ l/min$ at $6\ ^\circ C$), the best solution is a water cooled chiller.

In order to find a suitable chiller I wrote a list of requirements to be asked to chillers manufacturers:

- The machine has to be chemically compatible with the fluid PF-5060 (molecule C_6F_{14}, specific heat $982\ \ J/kg^\circ C$);

- The chiller must be provided with one cooling line, in which the flow designed is $2.5\ kg/s$;

- It has to absorb around 11 kW from a fluid having an inlet temperature of -16 $°C$ and a leaving temperature of around -20 $°C$;
- The chiller must be able to work also at 10 $°C$ higher temperature range. In that case the inlet PF-5060 temperature will be -6 $°C$, and the leaving temperature -10 $°C$;
- The range of thermal load regulation must be at least between 7 kW and 11 kW;
- The chiller must be cooled with water. The water source is defined by values of 40 l/min at 6 $°C$;
- The evaporator coils crossed by the chilled fluid must be rated for internal pressure up to 12.5 bar;

Along with requests I also asked them some questions:

- What is the electric power needed and the overall dimensions of the machine?
- Can you provide me some characteristic diagram of the machine? (efficiency, COP, range of regulation etc. . .)?
- Is the chiller adjustable? How large is the range of regulation, and how fine it is?

On of the most important parameters in the chiller selection is the *coefficient of performance (COP)*. It is a measure of the efficiency of the machine, defined as:

$$COP = \frac{\dot{Q_{out}}}{\dot{W_{in}}}$$

Where $\dot{Q}_{out}$ is the thermal power the chiller can extract from a system, and $\dot{W_{in}}$ is the total power necessary to the machine. The COP is usually a number larger than one, and good values are in the range between 3 and 4.

In section 7.1.1 and 7.1.2 are reported two chiller proposals that I received from american manufacturers.

7.1.1 Chiller option 1

The first proposed chiller is manufactured by the Cooling Technology Inc. company (fig. 7.2).

The machine is the model PCW-03LLTX, rated for a cooling capacity of 11.6 kW when operating at -20 $°C$. Attached here there are only some of the important characteristics. The complete quote is reported in appendix B.

- Max cooling capacity: 11.6 kW;
- Operating voltage: 460 V, 3 phase, 60 Hz;

Figure 7.2: PCW-03LLTX chiller model. (*Courtesy of Cooling Technology Inc.*)

- Condenser type: water cooled;
- Pressure drop at the evaporator: 0.6 bar;
- Capacity controller: hot gas bypass[2];
- Total chiller power: 4.4 kW;
- Chiller dimensions: 48" L X 36" W X 60" H;
- Cost: 28,869.00 $

The value of the total chiller power makes of this chiller a not very efficient one ($COP = 2.6$). Nonetheless it respects all the requirements with a medium cost (compared to other chillers). It can be considered as a valid option.

7.1.2 Chiller option 2

The second proposed chiller is manufactured by the Mydax Inc. company (fig. 7.2).

The machine is the CryoDax 16 model, rated for a cooling capacity of 13.1 kW when operating at -30 $°C$. Attached here there are some important characteristics, while the whole quote is reported in appendix B.

- Max cooling capacity: 13.1 kW;
- Operating voltage: 440/480 VAC, 3 phase, 60 Hz;
- Condenser type: water cooled;
- Capacity controller: Mydax systems use the *Advanced Temperature Control Technology*, from 0 to 100% proportional cooling and heating control;

[2]Hot gas is spilled from the internal circuit of the chiller and exchanges heat with the fluid

Figure 7.3: CryoDax 16 chiller model. (*Courtesy of Mydax Inc.*)

- Chiller dimensions: 74" H X 41" W X 53" D;
- Cost: 59,750.00 $

This chiller option is more expensive than option 1, mainly because of the patented control system. The company has not provided me a value for the COP of the machine, which probably will be similar to the first option.

This chiller could be a valid option but the high cost is maybe not well justified by the circuit requirements. There is not the need for such a control system performance.

7.2 Pump selection

Another fundamental component of every hydraulic circuit is the pump. The pump is the device that moves fluids (liquids or gases), or sometimes slurries, by mechanical action. Pumps can be classified into major groups according to the method used to move the fluid:

- Direct lift devices;
- Displacement pumps;
- Velocity pumps;
- Buoyancy pumps;
- Impulse pumps.

Pumps operate by means of some mechanism (typically reciprocating or rotary), and consume energy to perform mechanical work moving the fluid. There are several possible energy sources, including manual operation, electricity, engines, or wind power. A preliminary evaluation of the most suitable type is based on two parameters:

- How much pump head is needed;
- How much fluid must be pressurized;

These are the two parameters that define the most the pump type for a certain application. The radial machines use the centrifugal force to accelerate the fluid radially, which in turn gets decelerated in appropriate channels where it converts the just gained kinetic energy in pressure. Axial machines use a series of blades to push the fluid into regions of always higher pressure.

As described in [12], the first evaluation of the pump type (radial or axial type) can be made in the following way:

1. Calculate the performance requested to the pump. In our case:

$$\Delta P = 12.5 \ bar$$

$$\dot{m} = 4.5 \ kg/s$$

2. Calculate the hydraulic power. That is the mechanical power given to the fluid:

$$P_h = \frac{\dot{m}\Delta P}{\rho} = 3.1 \ kW$$

3. Calculate the pump *specific speed* Ω_s, knowing the requested pump head ΔP, the mass flow rate $\dot{m}$, and the maximum angular velocity of the impeller Ω (usually not higher than 3600 rpm for normal pumps):

$$\Omega_s = \frac{\Omega\sqrt{(\dot{m}/\rho)}}{(\Delta P/\rho)^{3/4}} = 0.12$$

4. With the found value of the specific speed look at fig. 7.4 and find the suggested type of pump geometry (radial, or axial).

   From fig. 7.4 is clear that our requirements involve a large pump head with a low mass flow rate, giving as a result an extremely radial machine. The best pump efficiencies are obtained when the specific speed is close to 1, because of the fluid dynamics nature of the machine. An extreme radial machine has very high viscous losses, while excessive axial machines suffer the problem of the *stall*[3].

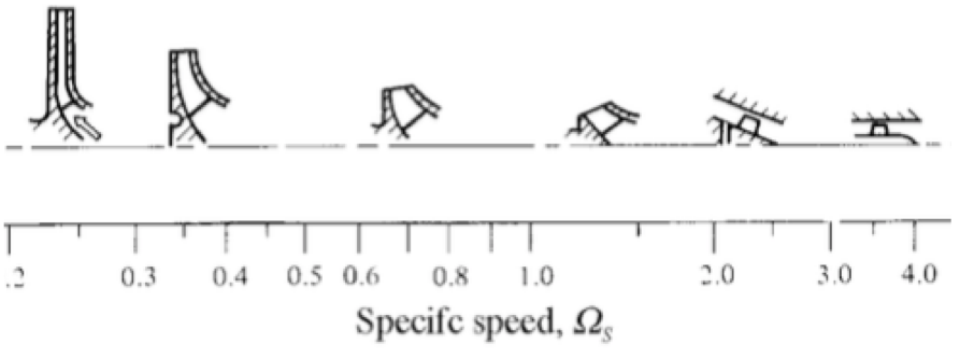

Figure 7.4: Guideline for pump type selection.

A good design would foresee a pumping group having all the pumps working with specific speed close to 1. In order to do so, for systems in which the mass flow rate is low, and the pump head is high, a common methodology is to use a many pumps in series. Each pump provides only a part of the whole head, thus working in better conditions. In order to have a specific speed value as close as possible to one, we can note that:

$$\Omega_s \propto \frac{1}{\Delta P^{3/4}}$$

It's simple to show that the head pump requested to obtain a unitary specific speed per pump would be around 1 *bar*. It is obvious that this would imply too many pumps (or stages), and then a trade-off study must be done between the compactness and efficiency of the pumping group. In the proposed options we'll see that passing from one single pump to two pumps in series increases the overall efficiency from 20% to 55%, while passing from two to three pumps does not produce significant gains.

Prior to show the proposed pumps is important to note the fluid to be pumped is the PF-5060. It is extremely important for such a fluid to don't leak out of the system, because of environmental effects. The pumps are devices that more or less always have some leakages, in particular due to the coupling seal between the motor shaft and the impeller shaft. To reduce this problem a type of pump called *Magnetic drive pump* has been developed by several manufacturers.

A magnetic drive pump (fig. 7.5) uses a balanced magnetic field to create the rotation of the fluid impeller. Unlike a traditional centrifugal pump which has a direct drive connection between impeller and motor, a magnetic type eliminates the direct drive mechanism and replaces it with a magnetic coupling between two magnets.

An outer magnetic bell housing is mounted on the end of the pump shaft. This outer bell is aligned on the outside of the rear casing. The pump impeller is connected to a smaller magnet assembly and rides on an internal shaft and bushing assembly. The liquid end parts are all isolated within the fluid head of the

[3]Is a fluid dynamics condition in which the boundary layer detaches from the blades suction side because of the too high load imposed. It is an upper limit to blade loading, and then to pump head.

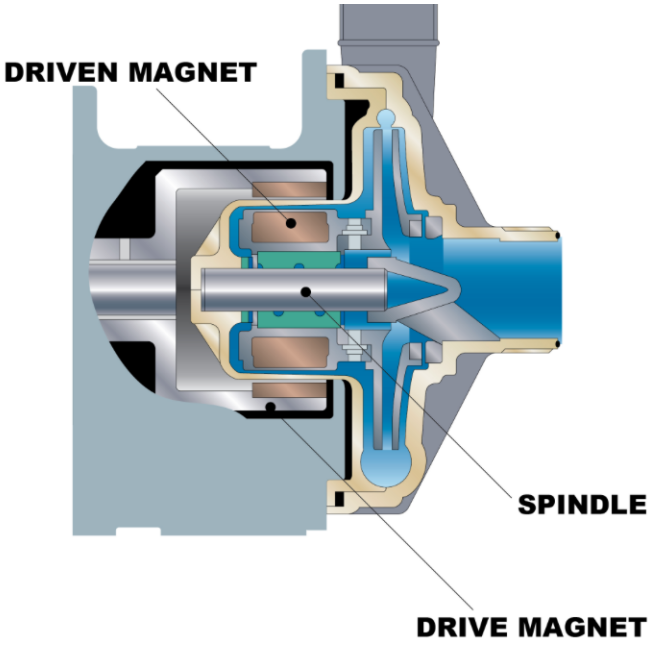

Figure 7.5: Internal schematic view of a magnetic drive pump.

pump without the need for a mechanical seal. When the pump motor is started the outer bell housing begins to rotate. As the outer bell rotates, the rotating magnetic field effects the inner impeller magnet. As the two magnets begin to turn together, the impeller begins to turn and displace the fluid.

We'll focus the pump research on this particular type of pumps, due to the extreme importance of leaks in our system. In order to find a suitable pump for the system I wrote a list of requirements to be asked to pumps manufacturers, that in turn sent me information on pump models:

- The machine must be chemically compatible with the PF-5060 fluid;
- The pump must elaborate 4.5 kg/s of PF-5060 at around -18 $°C$;
- The pump must provide a pressure head of at least 12.5 bar at nominal conditions;
- The requested $NPSH_r$ must be lower than the available value of $NPSH_a = 1.1\ bar$[4].
- Electrically driven pump, 440/480 V, 3 phase, 60 Hz;
- The pump must be of the sealless type (magnetic driven), in order to reduce the leaks.

Unlike the chiller case, for the pump is not important to be adjustable. The mass flow rate must always be the same, while little unbalance between head loss of

[4]NPSH stand for *net positive suction head*. It is a measure of the suction capability of certain fluid prior to the cavitation onset phenomena. To avoid cavitation is always recommended that the pump requested $NPSH_r$ is lower than the available $NPSH_a$ at the pump inlet port.

the circuit and the pump head will be covered closing partially some control valves. In this way the circuit characteristic will perfectly match the pump characteristic, and the results will be exactly the desired ones.

Now we'll show some pumping options I found during my internship at Fermilab. These are not final decisions, but can help in the final choice working as guidelines. Since that in the pump industry the SI units are not so used[5], we'll convert our requirements in the most used type of units: gallons per minute regarding the volumetric flow rate (instead of mass flow rate), and the meters (of water column) for the pump head:

$$\dot{m} = 4.5 \ kg/s \Rightarrow \ \dot{V} = 39.8 \ gal/min$$

$$\Delta p = 12.5 \ bar \Rightarrow \ \frac{\Delta p}{\rho g} = 127 \ m$$

These units will simplify very much the research of pumps on manufacturers catalogue.

7.2.1 Pump option 1

First of all we looked for a solution using a single pump. This would have simplified and improved the compactness of the system.

Unfortunately, the most efficient pump I found had a very low efficiency, around 30%. The efficiency relates to amount of electric power absorbed from the pump P_{el} to the hydraulic power transmitted to the fluid P_{hyd}:

$$\eta = \frac{P_{hyd}}{P_{el}}$$

Low efficient pumps absorb large amount of electric power compared to the mechanical power transmitted to the fluid. This happens because the flowing parameters of our system (flow rate and pressure rise) are very distant from the common ones requested on the market; therefore the commercial pumps are not designed to work well with these conditions. This results in bad values of efficiency. All this problem could be avoided using a custom made pump, but the cost would be very high for such a machine, and considering to employ a couple of pumps it is not a good idea.

Fig. 7.6 reports an example of a single pump providing all the circuit pressure rise.

The pump performances are:

- **Flow rate**: $\dot{V}$ =40.1 gal/min (requested is 39.8);
- **Head**: ΔP =12.6 bar (requested is 6.2);
- **Requested NPSH**: $NPSH_r = 0.3 \ bar$ (available is 1.1);

[5]The Imperial System is often preferred to the International System of Units in hydraulic fields. Mass flow rates are converted in volumetric flow rates taking into account the real density of the fluid.

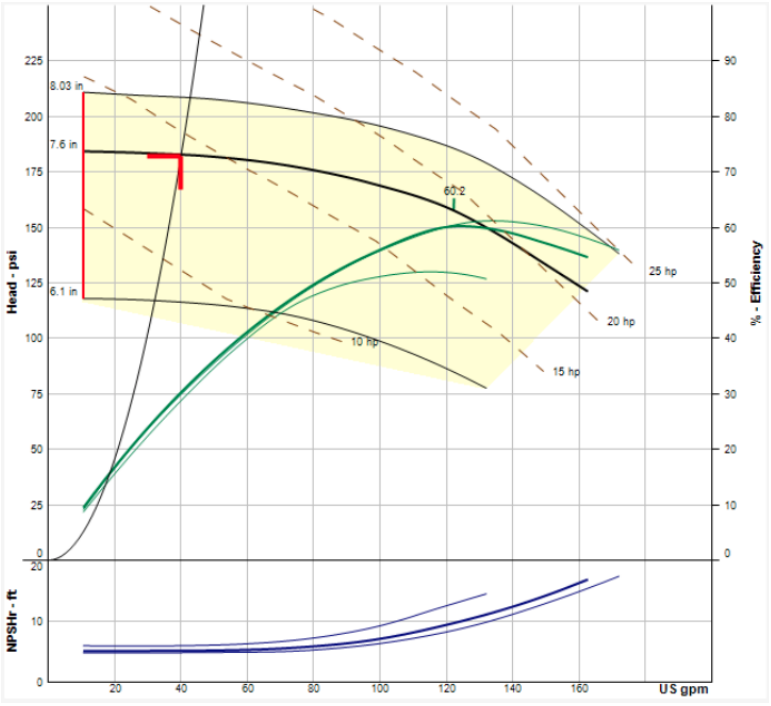

Figure 7.6: Characteristic curve of the Magnatex MHL42 model (*Courtesy of Magnatex Pumps Inc.*)

- **Efficiency**: η =30.1 %
- **Electric power**: P_{el} =10.5 kW

The 30% efficiency value is considered unacceptable because the electric budget could not be large enough to afford it, and even though it was, a lot of money would be wasted during the expected lifetime of the pump (3 years). This reason led us to think at pumping systems working with series of pumps. In the next section is shown an option using 2 pumps in series.

7.2.2 Pump option 2

This time we search pumps with the same characteristics than the previous single pump, but with a halved head. Using two pumps in series allows the reduction of pressure rise requested to the single pumps. In this way we should get close to common requested values of flow parameters, hoping for higher efficiency pumps.

Let's take for example fig. 7.7, which shows the characteristics of the Magnatex MP421 model.

The pump performances are:

- **Flow rate**: $\dot{V}$ =40.8 gal/min (requested is 39.8);
- **Head**: ΔP =6.3 bar (requested is 6.2);
- **Requested NPSH**: $NPSH_r = 0.3$ bar (available is 1.1)

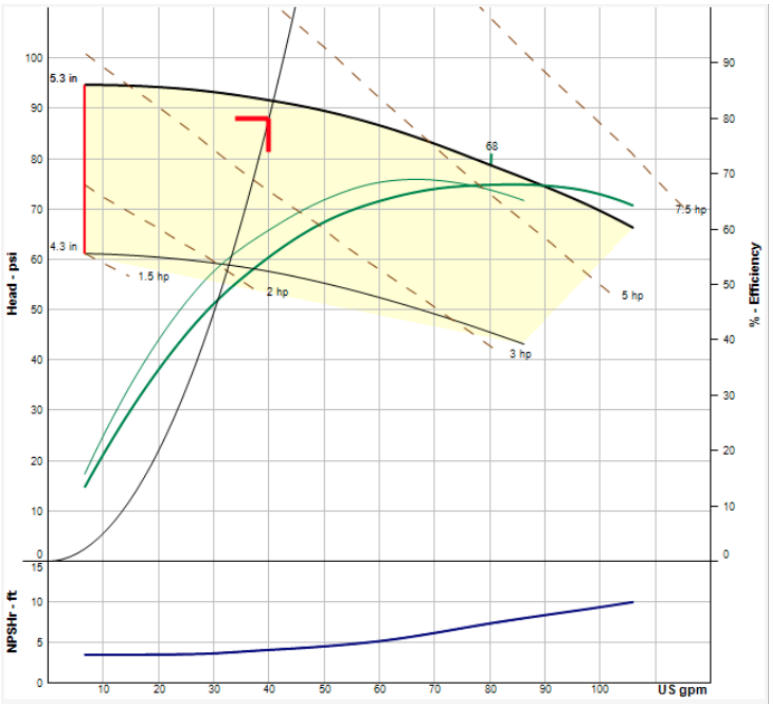

Figure 7.7: Characteristic curve of the MP421 model (*Courtesy of Magnatex Pumps Inc.*)

- **Efficiency**: η =55.3 %
- **Electric power**: P_{el} =5.8 kW

In order to achieve the whole pressure rise requested, two of these pumps would be employed together on the same line (and a third one as a redundancy). The electric expense is around the half of the single pump solution (the efficiency almost doubles, increasing from 30% to 55%), producing a big improvement in the pumping system simply passing from one pump to a series of two pumps.

Also systems with three pumps in series could be studied, but the efficiency would not improve significantly, while the system compactness would get worse. It is believed that the best configuration for the pumping group is given by two pumps in series. The model just shown could be a good option for that purpose.

7.3 Reservoir sizing

This objective of this section is to find the minimum allowable size for the reservoir. The size can be estimated as a function of the volume of the plant and the mass flow rate expected. The size is measured in volumetric units. A properly designed reservoir for a hydraulic system must be correctly sized so that it can supply the right amount of fluid to the system at all times, and can accomodate the effects of thermal expansions. Moreover, the size of the reservoir must ensure that the fluid in circulation has a reasonable dwell time to allow it to settle out the particulate contaminations, dissipate heat as quickly as possible, suppress any turbulence in the return fluid, and release the entrained air.

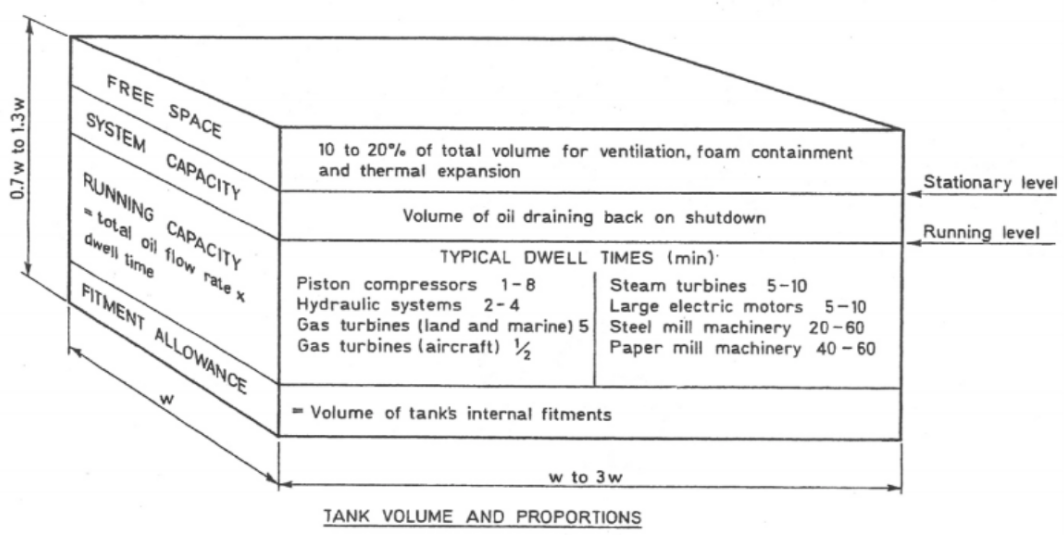

Figure 7.8: Guideline for reservoir sizing. Taking for example simple hydraulic systems applications, the suggested dwell time is in the range $2 \div 4$ minutes. [6]

As explained in [6], from fig. 7.8 the volume of the reservoir is given by the sum of several contributions:

- **Running capacity**: it is the part of volume always full of fluid that ensures a good dwell time depending on a certain flow rate. For cooling applications we can use typical values used in hydraulic system of 2 minutes. Since the design mass flow rate is 4.5 kg/s, the dwell time produces a running capacity of $\simeq 300\ l$;

- **System capacity**: this is needed because the reservoir should be used also for circuit draining purposes. In that case all the fluid contained in the circuit must find place to be stored inside the reservoir. The total system volume evaluation is reported in table 7.1;

- **Fitment allowance**: it is the volume occupied from the tank's internal fitments, for example baffles and sensors. This volume can be safely estimated as the 5% of the total volume;

- **Margin of safety**: a certain amount of free space is necessary for safety reasons, flashes, foams, ventilation and thermal expansions. We can select 10% for it.

Prior to size the tank is necessary to calculate the important system volumes, since they will be used for the system capacity evaluation. In table 7.1 are reported all the important system volumes.

Now we can evaluate the reservoir volume following the guideline expressed in fig. 7.8. All the important reservoir contributions are calculated and displayed in table 7.2.

Given the density of PF-5060 (1.792 kg/l), and the total reservoir volume (560 l), the minimum amount of fluid to have is then $\simeq 1004\ kg$. Given the price of

Table 7.1: Summary of the system volumes. The total represents the system capacity data for the reservoir sizing.

Item	**Unit volume** $[l]$	**Number of items**	**Total Volume** $[l]$
Mechanical alcove piping	32.3	1	32.3
Routing inlet FEE	15.3	1	15.3
Routing inlet DAQ	14.9	1	14.9
Routing outlet	29.9	1	29.9
Crate channels	0.2	20	4
Crate manifolds	1.1	4	4.4
Front-end channels	0.2	2	0.4
Front-end manifolds	1.2	4	4.8
Filter	18	2	36
Air separator	25	1	25
Pump	10	2	20
		Total	187

Table 7.2: System reservoir sizing.

Contribution		**Volume** $[l]$
System capacity		187
Running capacity		300
Fitment allowance		24
Margin of safety		49
	Total	560

NPS	DN	OD in (mm)	Wall Thickness Inches (mm)					
			Sch 40S	STD	Sch 40	Sch 60	Sch 80S	XS / XH
1/8"	6	0.404 (10.26)	0.068 (1.727)	0.068 (1.727)	0.068 (1.727)	--	0.095 (2.413)	0.095 (2.413)
1/4"	8	0.540 (13.72)	0.088 (2.235)	0.088 (2.235)	0.088 (2.235)	--	0.119 (3.023)	0.119 (3.023)
3/8"	10	0.675 (17.15)	0.091 (2.311)	0.091 (2.311)	0.091 (2.311)	--	0.126 (3.200)	0.126 (3.200)
1/2"	15	0.840 (21.34)	0.109 (2.769)	0.109 (2.769)	0.109 (2.769)	--	0.147 (3.734)	0.147 (3.734)
3/4"	20	1.050 (26.67)	0.113 (2.870)	0.113 (2.870)	0.113 (2.870)	--	0.154 (3.912)	0.154 (3.912)
1"	25	1.315 (33.40)	0.133 (3.378)	0.133 (3.378)	0.133 (3.378)	--	0.179 (4.547)	0.179 (4.547)
1-1/4"	32	1.660 (42.16)	0.140 (3.556)	0.140 (3.556)	0.140 (3.556)	--	0.191 (4.851)	0.191 (4.851)
1-1/2"	40	1.900 (48.26)	0.145 (3.683)	0.145 (3.683)	0.145 (3.683)	--	0.200 (5.080)	0.200 (5.080)
2"	50	2.375 (60.33)	0.154 (3.912)	0.154 (3.912)	0.154 (3.912)	--	0.218 (5.537)	0.218 (5.537)
2-1/2"	65	2.875 (73.03)	0.203 (5.156)	0.203 (5.156)	0.203 (5.156)	--	0.276 (7.010)	0.276 (7.010)
3"	80	3.500 (88.90)	0.216 (5.486)	0.216 (5.486)	0.216 (5.486)	--	0.300 (7.620)	0.300 (7.620)
3-1/2"	90	4.000 (101.60)	0.226 (5.740)	0.226 (5.740)	0.226 (5.740)	--	0.318 (8.077)	0.318 (8.077)
4"	100	4.500 (114.30)	0.237 (6.020)	0.237 (6.020)	0.237 (6.020)	--	0.337 (8.560)	0.337 (8.560)
4-1/2"	115	5.000 (127.00)	0.247 (6.274)	0.247 (6.274)	0.247 (6.274)	--	0.355 (9.017)	0.355 (9.017)
5"	125	5.563 (141.30)	0.258 (6.553)	0.258 (6.553)	0.258 (6.553)	--	0.375 (9.525)	0.375 (9.525)
6"	150	6.625 (168.28)	0.280 (7.112)	0.280 (7.112)	0.280 (7.112)	--	0.432 (10.973)	0.432 (10.973)
7"	--	7.625 (193.68)	0.301 (7.645)	0.301 (7.645)	0.301 (7.645)	--	0.500 (12.700)	0.500 (12.700)

Figure 7.9: NPS tables for selected pipe sizes (ASME standards B36.10M and B36.19M). [20]

it, ($\simeq 66$ \$/kg), the expected cost is quite significant ($\simeq 62,250$ \$). Moreover, since the fluid is extremely volatile, we should also take into account the effect of unavoidable leakages that will lead to the need for further stocks of fluid.

7.4 Pipes

7.4.1 Nominal pipe size (NPS)

Nominal Pipe Size (NPS) is a North American set of standard sizes for pipes used for high or low pressures and temperatures. "Nominal" refers to pipe in non-specific terms and identifies the diameter of the hole with a non-dimensional number (for example a 2-inch nominal steel pipe consists of many varieties of steel pipe with the only criterion being a 2.375-inch (60.3 mm) outside diameter). The specific pipe is identified by a specifi pipe NPS and another non-dimensional number for wall thickness referred to as the *Schedule* (for example: 2-inch diameter pipe, Schedule 40). The Schedule determines for each pipe a certain wall thickness.

Be careful to the fact that a 2-inch pipe has not exactly an inner bore of 2 *inches*, but its real value depends the schedule. The inner bore is uniquely determined once the schedule is fixed, subtracting two times the wall thickness from the outside diameter (OD). The European and international designation equivalent to NPS is DN, in which sizes are measured in millimetres.

Based on the NPS and the schedule of a pipe, the outside diameter (OD) and wall thickness can be obtained from reference tables such as those of fig. 7.9, which are based on ASME standards B36.10M and B36.19M [22]. The highlighted dimensions are the ones used in the calorimeter cooling system. For example, NPS 14 Sch. 40 has an OD of 14 *inches* (360 *mm*) and a wall thickness of 0.437 *inches* (11.1 *mm*). However the NPS and OD values are not always equal (especially in the smaller sizes), which can create confusion.

Figure 7.10: Typical stainless steel concentric reducer. The ends can be butt-welded to the pipes in order to be tight-leak proof.

7.4.2 Cooling system pipes sizing

The pipes used in the calorimeter cooling system (except for ad-hoc exchangers of front-end and DAQ crates, whose characteristics have already been described) are the following:

- **NPS 1-1/2"**: this dimension is used inside the mechanical room where the flow is splitted in the DAQ line (2 kg/s) and FEE line (2.5 kg/s);
- **NPS 2"**: this pipe size is used inside the mechanical room when the line is only one (from the room inlet port to the separation point, 4.5 kg/s). It is also used for the routing inlet system of DAQ line (2kg/s) and FEE line (2.5 kg/s);
- **NPS 2-1/2"**: this is used in the routing outlet system, where the flow is completely conveyed into one line (4.5 kg/s).

The dimension used for the mechanical alcove are smaller than the ones used in the routing system because the available space in the room is not arbitrarily big. For the routing system is important to reduce as long as possible the head losses using larger diameters. The passage between diameters is done using flow reducers/increasers like the ones shown in fig. 7.10.

Once we have the NPS dimensions we have to choose the proper schedule numbers in order to determine the inner diameter. The standard schedule is the STD class (equal to Sch. 40 for diameters smaller than NPS 10"). A Sch. number indicates approximate value of:

$$Sch = 1000\frac{P}{S}$$

Where P and S are the service pressure and the allowable stress evaluated in psi. The pipes used in the system must be rated for a pressure at least equal to the maximum expected pump discharge pressure, i.e. 12.5 bar (equivalent to $\simeq 181.3\ psi$). A Sch. 40 is normally rated for working pressures around 800 psi, well above our requirements. Nonetheless we can select this Sch. number because it is the more common, reliable, cheap and easy to be found.

Table 7.3: Summary of the pipes used in the system. The outer and inner diameters (OD and ID), and the thickness t are reported in inches due to higher coherence with ASME standards. [29]

NPS	**Sch.**	**OD** [in]	**t** [in]	**ID** [in]	**Working pressure** [bar]
1-1/2	STD	1.9	0.145	1.61	52.4
2	STD	2.375	0.154	2.07	44.8
2-1/2	STD	2.875	0.203	2.47	49.0

Table 7.3 reports all the characteristics of the selected pipes. The rated working pressures are approximatively 4 times the maximum expected pressure, so there are no problem from the standpoint of internal pressure. Obviously the pipeline will need to be properly designed with the right constraints in order to avoid internal stresses due to the mounting and subsequent thermal expansions.

7.5 Valves

The objective of valves, inserted in cooling systems, is to adjust the flow regulation in the various branches of the circuit in order to regulate the heat absorption. To do so, the valves can be divided in big families depending on their function:

- **Control valves**: is a valve used to control the fluid flow by varying the size of the flow passage, as directed by a signal from a controller or a person. This enables the direct control of flow rate and the consequential control of process quantities such as pressure and temperature. The opening or closing of automatic control valves is usually done by electrical, hydraulic or pneumatic actuators. Normally with a modulating valve, which can be set to any position between fully open and fully closed, valve positioners[6] are used to ensure the valve attains the desired degree of opening.

  An automatic control valve consists of three main parts in which each part exist in several types and designs:

  - a valve actuator, which moves the valve's modulating element, such as ball or butterfly;
  - a valve positioner, which ensures the valve has reached the desired degree of opening. This overcomes the problems of friction and wear;
  - a valve body, in which the modulating element, a plug, globe, ball or butterfly, is contained.

- **On-Off valves**: operating positions for 2-port valves can be either shut (closed) so that no flow at all goes through, fully open for maximum flow,

[6]Valve positioners are devices used to increase or decrease the air pressure load driving the actuator of a control valve until the valve's stem reaches a position balanced to the output signal.

or sometimes partially open to any degree in between. Many valves are not designed to precisely control intermediate degree of flow; such valves are considered to be either open or shut, and are called on-off valves. The opening or closing of on-off valves can either be manual or automatic. They have the same structure of control valves, but what really changes is the shape of the valve's stem, that does not allow for fine regulations, but is optimized for an optimal closed or fully open passage.

- **Check valves**: also called non-return valve, reflux valve, retention valve or one-way valve, is a valve that normally allows fluid (liquid or gas) to flow through it in only one direction. There are various types of check valves used in a wide variety of applications. Although they are available in a wide range of sizes and costs, check valves generally are very small, simple, or inexpensive. Check valves work automatically and most are not controlled by a person or any external control; accordingly, most do not have any valve handle or stem. In every check valve there is a closing element that automatically closes the passage once the flow try to go in the wrong direction. An important concept in check valves is the *cracking pressure*, which is the minimum differential upstream pressure between inlet and outlet at which the valve will operate. Typically the check valve is designed for a specific cracking pressure;

- **Relief valves**: is a type of safety valve used to control or limit the pressure in a system. The pressure is relieved by allowing the pressurised fluid to flow from an auxiliary passage out of the system. The relief valve is designed or set to open at a predetermined set pressure to protect pressure vessels and other equipment from being subjected to pressures that exceed their design limits. When the set pressure is exceeded, the valve is forced open and a portion of the fluid is diverted through the auxiliary route;

An important matter is the sizing of control valves. Their choice is not so easy as it can seem, and we'll report some instructions on how to do it efficiently, along with indications on how to select also the other types of valves.

7.5.1 Control valves sizing

Each throttling valve has a *flow characteristic* which describes the relationship between the valve coefficient (k_v) and the valve stroke (%). In other words, as a valve opens, the flow characteristic, which is an inherence to the design of the selected valve, allows a certain amount of flow through the valve at a particular percentage of the stroke.

When selecting a valve for a particular application, the valve coefficient is used to determine the valve size that will best allow the valve to pass the required flow rate, while providing stable control of the process fluid. Valve manufacturers commonly publish k_vs (k_{vs} is the value specified on the catalogue, while k_v is the value calculated for a certain valve in the circuit) data for various valve styles, which are approximate in nature and can vary, up to 10%, according to the

piping configuration. If it is not calculated correctly, the valve usually experiences diminished performance in one of two ways:

- If the k_v is too small for the required process, the valve itself or the trim inside the valve will be undersized, and the process system can be starved for fluid. In addition, because the restriction in the valve can cause a raise in upstream pressure, higher back pressures created before the valve can lead to damage in upstream pumps or other upstream equipment. Undersized k_v can also create a higher pressure drop across the valve, which can lead to cavitation or flashing of the fluid;

- If the k_v is calculated too high for the system requirements, a larger, oversized valve is usually selected. Obviously, the cost, size, and weight of a larger valve size are the major disadvantage. Besides that consideration, if the valve is in a throttling service, significant control problems can occur. Usually the closure element, such as a plug or a disk, is located just off the seat, which leads to the possibility of creating a high pressure drop. In addition, if the closure element is close to the seat and the operator is not strong enough to hold that position, it may be sucked into the seat. This problem is appropriately called the *bathtub stopper effect*.

The k_v is defined as the amount of flow rate (in m^3) of 16 $°C$ water that flows through the fully open valve during 1 hour, with a 1 *bar* pressure differential. In SI units the simplified equation for it is [27]:

$$k_v = \frac{\dot{V}}{\sqrt{\Delta p}}$$

Where k_v is the required flow coefficient for the valve, $\dot{V}$ is the flow rate in m^3/h and Δp is the pressure drop across the valve in *bar*. When calculated properly, k_v determines the correct trim size (or area of the valve's restriction) that will allow the valve to pass the required flow while allowing stable control of the process throughout the stroke of the valve.

The flow rate through a throttling valve is not only affected by the k_v of the valve, but also by the pressure drop across the valve. A valve's flow characteristic acting within a system that allows a varying pressure drop can be much different from the same flow characteristic in an application with a constant pressure drop. When a valve is operating with a constant pressure drop without taking into account the effects of piping, the flow characteristic is known as *inherent flow characteristic*. However, if both the valve and piping effects are taken into account, the flow characteristic changes from the ideal curve, and is known as the *installed flow characteristic*.

Some rotary valves[7], such as butterfly and ball valves have an inherent characteristic that cannot be changed because the closure element shape cannot be modified easily. On the other hand, linear valves[8] usually have a flow characteristic designed into the trim (fig. 7.11).

[7]Valves in which the closing element rotates to open or close the passage.

[8]Valves in which the closure elements have a linear motion.

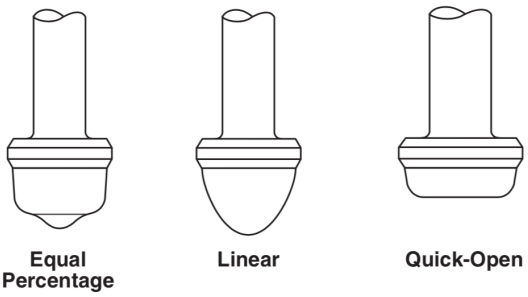

Figure 7.11: Characterizable linear plugs. (Courtesy of Valtek International)

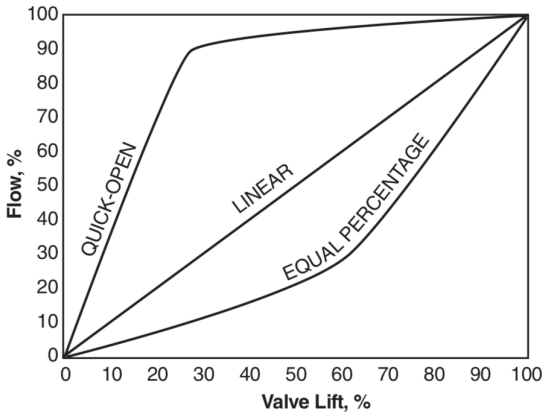

Figure 7.12: Typical inherent flow characteristics. (Courtesy of Valtek International)

The three most common types of flow characteristics are equal percentage, linear, and quick-open. The ideal curves for these three flow characteristics are shown in fig. 7.12. However, the inherent characteristic of these curves can be affected by the body style and design, and piping factors.

The choice of the best flow characteristic valve depends on the application. The problem is that the inherent flow characteristic of a valve is valid only when measured in laboratory, with a certain circuit configuration. The behaviour of the valve can slightly change depending on the real circuit layout. A parameter useful to calculate the behaviour of the valve is the *authority*, defined as the ratio between the valve pressure drop and the head loss of the branch in which the valve is located:

$$A = \frac{\Delta p_{v100}}{\Delta p_b}$$

Where Δp_{v100} is the pressure drop across the fully open valve, and Δp_b the drop between the branches of the circuit containing the valve. The maximum flow rate passing through the valve is called k_{vs}, and is the quantity reported on catalogues. In the ideal case of laboratory the authority is equal to 1, and as a rule of thumb, if it doesn't go below 0.5 the real characteristic remains quite similar to the ideal one [3]. In order to select a valve is then important to evaluate with good accuracy the following values:

- Δp_{v100} as a function of the circuit type;

- $\dot{V}$ passing through the valve.

These two parameters are not considered separately, but joined into the k_v of the valve. This value must be compared with the k_{vs} reported on valves data sheets. Whenever we don't find a k_{vs} coincident with the requested k_v, we must select the valve with the closest possible value. If the requested k_v is exactly in the middle between two proposed valves k_{vs}, is better to use the lower value for two-port valves, and the highest value for three-port valves [3]

7.5.2 On-Off valves sizing

With manually operated on-off valves, the valve is often expected to pass full flow. If the valve's internal flow passage or closure element is sized smaller than the upstream piping, flow will be restricted from that point forward. This will cause the valve to take a pressure drop and pass less flow, defeating the major purpose of the valve. On the contrary, if the valve is sized larger than the upstream piping, installation costs are more expensive (since increasers are required). The larger valve is also more expensive. Therefore, the valve size can sometimes be simply determined by the size of the piping. Manual valves manufacturers often provide sizing charts that indicate the relationship between the flow rate requirement $\dot{V}$ and the minimum and maximum valve size that can pass the given flow rate. The service conditions generally required for correct manual valves sizing are maximum and minimum temperatures, pressures, flow rates and density of the fluid.

7.5.3 Check valves sizing

The most critical element of check valve sizing is that a sufficient pressure drop and minimum flow exist for the check valve to open. Without a pressure drop, the closure element will not open and the valve will remain closed, which is what happens when a pump fails to maintain a proper flow or flow reverses. The minimum pressure drop required for check valves to open is specified on valves catalogue ($\simeq$ 0.1 *bar*), and is called *cracking pressure*. This minimum pressure drop is needed to maintain the open position of the closure element without failing. If the pressure drop is not sufficient, the closure element will float back and forth, which is commonly called *flutter*. As the disk moves toward the seat, the opening narrows and pressure rebuilds, which causes the disk to open higher. This low pressure drop situation will cause this cycle to repeat until the pressure drop is increased, causing wear of the moving parts and shortening the life of the valve. On the other hand, excessive pressure drops lead to severe erosion of the check valves closure elements.

Unless the flow experiences a wide range of variation during the service, check valves are sized for minimum flow, which in turn determines the valve size. This is done using manufacturers sizing charts. If the size provided for the minimum flow is equivalent to or greater than the pipeline size, the pipeline size should be used for the valve size [27].

7.5.4 Relief valves sizing

The relief valves are simply sized choosing the port diameters equal to the pipeline size, and selecting a reasonable value for the maximum pressure allowed in that part of the circuit. They can be of several types, and are fully characterized on manufacturers catalogues.

7.6 Nitrogen purging system

7.6.1 Introduction to purging

Nitrogen has many applications and depending on the industry, it can be used for a wide variety of tasks and objectives. A colorless and odorless gas, this element makes up around 78% of our atmosphere. Although commonly associated with our atmosphere, industrially produced nitrogen is used in several applications. From the beer brewing industry to the petrochemical industry, nitrogen purging allows for a more productive and safe environment.

The nitrogen purging is the act of displacing any undesirable or hazardous atmosphere or contaminant with an inert nitrogen atmosphere. In our cooling system the undesirable atmosphere could be for example external air sucked into the system, that would produce damage to the cooling function, reducing the convection effectiveness.

When it comes to nitrogen purging, there are several systems and methods involved, all of which require different equipment. Easily adapted, the method of nitrogen purging depends on the equipment used (i.e., the shape and type), as well as the location of the purging outlets and inlets. The outlet of our system is considered to be the air separator. The four core methods of nitrogen purging include:

- **Pressure transfer of liquids**: In certain cases, you may want to transfer liquids without using a pump. To complete this task, nitrogen will allow you to pressurize the headspace within a vessel. This is the method most often used when there are space constraints or if there are certain materials that impact pump efficiency. By utilizing this method of purging, you will be able to significantly reduce the risk of oxidation, which often occurs while transferring liquid from one tank to another;

- **The pressure-hold vacuum method**: When conditions do not allow a "sweeping action" of nitrogen, a vessel can be pressurized using nitrogen. Once the contents of the vessel are combined with nitrogen, dilution occurs. Being diluted the contaminants are more easily vented (thanks to separator openings of the vessels), and the process is repeated.

  This method is ideal when a vessel only has one opening. The amount of nitrogen required in this case will depend on the number of pressurized purges required to reduce the contaminant until it reaches an acceptable level. This method is commonly used for vessels purging;

- **Displacement purging**: When equipment has straightforward cross-sections, such as those found in pipelines, this method is ideal. In most cases, a scraping piston, known as a "pig", is propelled by the pressure of nitrogen. As the pig pushes through the line, it effectively purges the contents.

  In this case, the amount of nitrogen required is based on the volume of the pipe. Unlike the other methods, such as dilution purging, you can purge a system without appreciable mixing. Although mechanical pig launchers and receivers are most often used, you can also separate nitrogen and another substance with an inert fluid;

- **Dilution purging**: This option is ideal for complex systems and equipment cross sections which include kilns, columns, reactors, etc. . . .
  By mixing nitrogen with the gas you need to purge, contents can then be effectively purged through an outlet point, which should be as far away from the inlet point as possible. When considering this method, the most important consideration is the location of both the entry and exit points. By diluting and displacing the contents in question, this method results in a more inert environment.

The goal of any nitrogen purging system is to cleanse pipes and other parts that contain contaminants. In doing so, you will significantly reduce any risk associated with hazardous elements, including oxygen. Depending on the method used, nitrogen may circulate at either high or low pressures. Of course, the specific nitrogen displacement procedure used will depend on many factors, including some of the points we discussed above. Regardless of the method used, you will need access to a steady flow of nitrogen.

7.6.2 Purging system sizing

For the calorimeter cooling system the best option is the "Dilution purging method". The pressure transfer of liquids is not needed since we already have a pumping system. The pressure-hold vacuum method can't be used because we have a pipeline to be purged, not only a vessel. And the displacement purging method is not suitable for our system because we have different diameters along the pipeline and the scraping piston would produce damage to the pipes.

Nitrogen is contained into a pressurized vessel, and connected to the pipeline with a 3-way valve. Whenever purging is requested, the 3-way valves connects the high pressure nitrogen to the system, diluting the contaminants and cleaning the system thanks to the air separator located along the circuit.

The only thing to do now is to properly size and then choose on the market a right nitrogen vessel for the system. Is not necessary to select a huge vessel, because nitrogen can always be refilled once it is finished. In order to get into the system, the minimum nitrogen pressure will be the pressure at inlet location. Considering the most probable system, and that the nitrogen bottle is located just downstream of the pump, its absolute minimum pressure will be:

$$p_{min} = 13.5\ bar$$

There are a large number of available tanks of different sizes and maximum pressures (up to 300 *bar*). Being nitrogen quite cheap, it is sufficient choose one tank that fits inside the mechanical room without creating any problem to other equipment, and changing it once the internal pressure lowers to P_{min} range.

In appendix B is reported one example of nitrogen bottles data sheet.

7.7 Conclusion

This Thesis represents a summary and an extension of former works, which employed 35% glycol at higher temperature. They were mainly focused on detailed study at the component level, while the whole system was only drafted. In this text I tried to give a global view of the whole architecture, emphasizing the correlations between the various components, and trying to solve technical problems encountered during the design process. In particular, some previous technical proposals have been rejected because they were inefficient and required too much electric power.

Considering that the fluid has changed, all the previous assumptions and calculations have been deeply investigated and verified. Several problems have been described, and some solutions proposed in order to face different future scenarios. For the time being is practically impossible to give a final detailed design for the cooling system because the technical requirements are still under modifications. For this reason I thought to give more specific information about the single circuit system, which is by far the more probable, and only some indications to cover the eventuality in which the double circuit will be selected.

We didn't repeat the head loss for the crates channels due to difficulties encountered with the supply of PF-5060. That would have been a really important test because it would have avoided the ambiguity in the crates pressure drop. It is a critical part, since produces around 4.5 *bar* of ambiguity in a total circuit loss of 12.5 *bar*. In other words, the real system could require much lower electric power than expected, saving a lot of money during operation.
The difficulty in the PF-5060 supply is due to the 2005 Kyoto Protocol, which has limited its employ due to the high Global Warming Potential. CERN experiments are still running with the PF-5060, but if it will be impossible to find the fluid, we'll have to change it. 3M Novec currently suggests to use new produced fluids, called Novec 649 and 7100, which have thermo-physical properties very close to PF-5060 and are not harmful for the environment. Several tests are running to understand if they are also radiation-hard at the level requested for the calorimeter.

In appendix B I reported a list of devices on the market suitable to realize the system. If the requirements changed as much as to request a totally different layout they wouldn't fit anymore, but the logic behind their choice should be conserved during the selection process.

The next things to do in order to conclude the design process are:

- Fix the system constraints and technical requirements;
- Select a system layout according to the new determined system requirements;

- Choose a new fluid between the Novec 649 and 7100 if the PF-5060 was unavailable;
- Run again the system analysis, as described in Chapter 6;
- Find components available on the market following the indications given in Chapter 7.

I hope that this Thesis will help future engineers and students to conclude rapidly and efficiently the design of the calorimeter cooling system, and to give important suggestions for the design of general hydraulic systems.

Appendix A

Hardy Cross method

A.1 Introduction

This method is a numerical algorithm useful to estimate head loss in a pipe network. It has been used for the calculation of flow distribution in the front-end network represented in fig. 6.5. Hardy Cross originally proposed a method for analysis of flow in networks of conduits in 1936. His method was the first really useful engineering method in the field of pipe network calculation. Only electrical analogs of hydraulic networks were used before. A problem with flow resistance versus electrical resistance makes these electrical analog methods obsolete because flow distribution is not a linear problem.

Networks of pipes are nonlinear systems since the relation between flow and pressure drop is not linear. On the contrary, the relation between current and voltage in electrical networks with regular resistors is governed by the linear Ohm's law. Electrical circuits with diodes as well as hydraulic networks are nonlinear systems where resistance depends on current and voltage, i.e., on flow and pressure. Nonlinear electrical circuits contain nonlinear components. Nonlinear components can be resistive, capacitive, and inductive.

The distribution of flow in a network of pipes depends on the known inputs and consumptions at all nodes, on the given geometry of pipes, and on the network topology. A stable state of flow in a network must satisfy Kirchhoff's laws, which are statements of the conservation of mass and energy in electrical circuits, but can also be applied to hydraulic circuits. Although in theory an indefinite number of flow distributions can satisfy the mass conservation, only one can satisfy also the energy conservation for all the closed path formed by pipes in the network. Since the relation between flow and pressure drop is not linear, Hardy Cross used a relation between an increment of flow and an increment of pressure, as this relation is linear as long as the variations involved are small compared with the absolute values [5]. Today, engineers use the most improved version of the Hardy Cross method (called the ΔQ *method*) which analyzes the whole looped network of pipes simultaneously. For this Thesis the standard method has been used because of the relative network simplicity and as a didactic application.

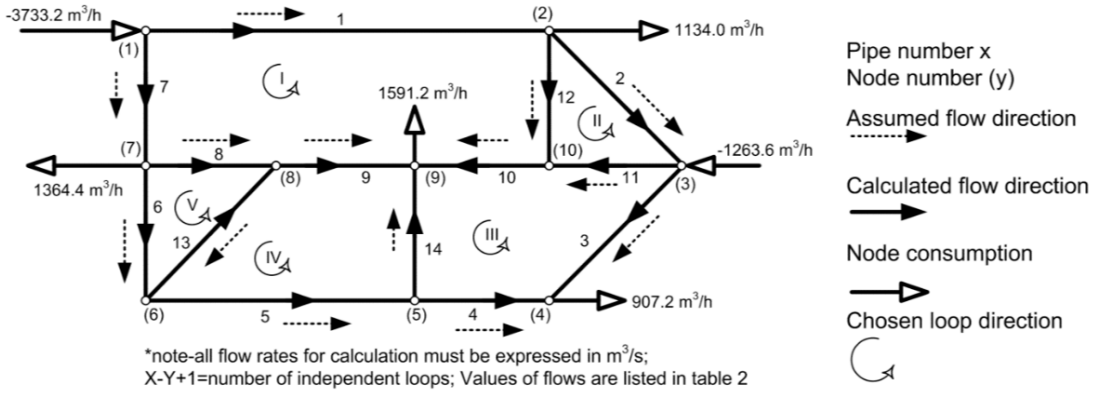

Figure A.1: Example of pipe network used for natural gas distribution for domestic consumption. [5]

A.2 Flow distribution and calculation

A.2.1 Topology of the network

The first step in solving a pipe network problem is to make a network map showing pipe diameters, lengths and connections between pipes (nodes). Sources of fluid supply and consumption rates have to be assigned to nodes. For convenience in locating pipes, code numbers must be assigned to each pipe and closed loop of pipes. Starting from the pipe network of fig. 6.5 the goal is to obtain a network analogue to the scheme of fig. A.1.

The next step is to guess the initial distribution of coolant flow through pipes in the network. Since the front-end network is composed of similar pipes (in length and dimensions), we can simply split the total flow for the number of pipes, obtaining the first estimate of the flow distribution:

$$\dot{m_{i.1}} = \frac{\dot{m_{FEE}}}{38} = 32.9\ g/s$$

Where $\dot{m_{i.1}}$ stands for pipe number i, with $i = 1, 2 \ldots, 38$; relative to the first iteration. The choice of initial flows is not critical, the only important thing is to assume an initial flow distribution satisfying the first Kirchoff's law, i.e. respecting the conservation of mass. Obviously if the assumed flow distribution is very close to the real one, the numerical method will employ less time than in the case in which the initial distribution is very far from the real solution.

A.2.2 Hydraulic model

Now we have to choose a hydraulic model for calculating the head loss through the pipes. The commonly used model for a cooling system employing liquid fluids different from water is based on the well known *Darcy model*, that relates the pressure drops to the second power of the flow rate:

$$\Delta p_i = K_i \dot{m_i}^2$$

Δp_i is the pressure drop across the generic piece of pipe i, in which the mass flow rate is $\dot{m}_i$. K_i is the already seen coefficient that takes into account the length, rugosity, diameter and eventual valves/equipment located along the pipe i. Another model called *Hazen-Williams equation* has an exponent 1.85 in place of 2 and is commonly used in water systems. Since our fluid is PF-5060 and not water, the general Darcy model will be used.

To solve the problem we still have to use the second Kirchoff's law: *around any loop "h" in the grid, the sum of head losses must be equal to zero*:

$$\Delta p_h = \sum_{i}^{i \in h} \Delta p_i = 0$$

where $\sum_i^{i \in h}$ means the sum for every pipe i contained in the loop h.

- conventionally, clockwise flows in a loop are considered positive (+) and produce positive head losses; counterclockwise flows are then negative (-) and produce negative pressure drops;
- This equation is called the head balance of each loop, and this can be valid only if the assumed $\dot{m}_i$ for each pipe within the loop is correct.

A.2.3 Hardy Cross algorithm

Having in mind the introduction to this problem is now possible to illustrate the Hardy Cross algorithm [21]:

1. Assume that the fluid is withdrawn from nodes only; not directly from pipes;
2. The discharge $m\dot{}_{FEE}$ entering the system will have positive value, while the one leaving the system will be considered negative;
3. Assume a first flow distribution. This can be done dividing equally the total mass flow rate among all pipes;
4. Calculate the K_i coefficient for each pipe according to the first assumed flow distribution, because it is a function of the flow rate as well as the geometry. Every iteration needs to update these values;
5. Calculate the head loss Δp_h around any loop h of the network and check if they are all equal to zero. If some of them result (as expected) different from zero we have to find the mass flow rate corrections to apply at any loop;
6. Calculate the correction $\Delta\dot{m}_h$ for each loop. Allowing the mass flow rates to variate, the pressure loss around a generic loop h can be written as:

$$\Delta p_h = \sum_{i=1}^{i \in h} K_i(\dot{m}_i + \Delta\dot{m}_h)^2$$

where Δp_h is the pressure loss around the generic loop h, containing the pipes i. Using the Taylor expansion for $\Delta\dot{m} << \dot{m}$ obtain:

$$\Delta p_h \simeq \sum_{i=1}^{i\in h} K_i(\dot{m_i}^2 + 2\Delta\dot{m}_h)$$

Since that the second Kirchoff's law must always be satisfied we can write:

$$\sum_{i}^{i\in h} \Delta p_i = \sum_{i}^{i\in h} K_i(\dot{m}_i^2 + 2\Delta\dot{m}_h) = 0 \Rightarrow \dot{\Delta m}_h = \frac{-\sum_i^{i\in h} K_i\dot{m}_i}{2\sum_i^{i\in h} K_i}$$

7. Add or subtract the value $\dot{\Delta m}_h$ to each pipe belonging to the loop h. In this step be careful to use the right sign for the network calculations (be coherent with the assumptions previously made on the flow directions). Calculate the new flow distribution and go on to iterate until the errors become smaller than the requested level of accuracy.

A.3 Front-end network results

In this section we report the results of the front-end network results, obtained with the Hardy Cross method. The classification of pipes is described in fig. 6.5, and the results are reported in table A.1.

The large temperature variations among the pipes are due to the different number and type of SiPM encountered. Sometimes shorter pipes have higher head losses (hence lower $\dot{m}$) than longer pipes because they have 180 degree elbows, while the longer ones are simply straight pipes (for example pipe $3ct$ is shorter than $3t$ but has lower $\dot{m}$).

Table A.1: Results of the Hardy Cross method applied to the front-end pipe network. The pipes classification refers to fig. 6.5.

Pipe	**Length** $[mm]$	$\dot{m}$ $[g/s]$	ΔT $[°C]$
1t	511	38.1	0.12
2t	658	35.4	0.34
3t	771	33.7	0.51
4t	863	32.5	0.66
5t	941	31.6	0.78
6t	1009	30.8	0.93
7t	1068	30.2	1.14
8t	1120	29.6	1.15
9t	1165	29.2	0.95
1ct	905	31.4	0.72
2ct	760	33.2	0.58
3ct	734	33.6	0.58
4ct	694	34.1	0.52
5ct	673	34.5	0.53
5cb	673	34.5	0.53
4cb	694	34.2	0.52
3cb	734	33.6	0.58
2cb	760	33.2	0.58
1cb	905	31.4	0.72
9b	1165	29.2	0.95
8b	1120	29.6	1.15
7b	1068	30.2	1.14
6b	1009	30.8	0.93
5b	941	31.5	0.78
4b	863	32.5	0.66
3b	771	33.7	0.51
2b	658	35.4	0.34
1b	511	38.1	0.12
6cb	905	31.4	0.72
7cb	760	33.2	0.58
8cb	734	33.6	0.58
9cb	694	34.1	0.52
10cb	673	34.5	0.53
10ct	673	34.5	0.53
9ct	694	34.2	0.52
8ct	734	33.6	0.58
7ct	760	33.2	0.58
6ct	905	31.4	0.72

Appendix B

Components data sheets

In this appendix we report the data sheets for some circuit components. The items are thought to be used in the single circuit system, due its higher probability. In case the project team chose to operate with the double circuit system these components will not fit anymore, and will need to be changed. The information about the valves data sheets refer to [18].

COOLING TECHNOLOGY INC

Cooling Technology Inc
1800 Orr Industrial Court
Charlotte, NC 28213

+1 (704) 596-4109
+1 (704) 597-8697 Fax
www.coolingtechnology.com

September 19, 2019

Mr. Francesco Neri
FERMI LABORATORIES
Batavia, Illinois

Subject: Low Temperature Chiller System
Reference: **CTI RFQ # 1909105-A-PO**

Dear Mr. Neri:

Thank you for your inquiry about a water-cooled, low temperature chiller that will meet the following specifications...

- Chemically compatible with PF5060 (C6F14) fluid
- Fermi to supply cooling fluid to chiller at a rate of 2.5 kg/sec (22.2 GPM)
- Leaving Fluid temperature: -20C (-4F); Max -10C (+16F)
- Entering Fluid Temperature -16C (+3.2F); Max. -6C (+21.2F)
- Maximum thermal load shall be 11 kW
- Available condenser water temperature is 40F
- Evaporator will be UL/CUL rated for 652 psi working pressure
- See attached specifications for the electrical power, COP and unit dimensions and weight
- The fluid can be throttled at the source (at your pump discharge). However, there is a flow switch in the chiller that must be satisfied for a minimum flow rate (5 GPM) to enable chiller to operate.

Based on above, we offer a Model PCW-03LLTX chiller that is rated for an actual cooling capacity of 39,400 BTU/h (11.6kW) when operating at -20C (-4F). The chiller will be designed to operate in a range from -20C to -6C.

* Fluid Specific Gravity: 1.8
* Fluid Specific heat 0.23

Special features of the chiller will include...

- 39,400 BTU/h (11.6 kW) cooling capacity
- -20C (-4F) operating temperature
- Entering Fluid temperature: -16C (+3.2F)
- Fluid: PF5060 (C6F14)
- Fluid Flow Rate: 2.5 kg/s (22.2 GPM)
- Number of incoming water channels: 1
- Number of outgoing water channels: 1
- Operating voltage: 460V-3-60Hz
- Environment Friendly refrigerant R404A
- BITZER SEMI HERMETIC Reciprocating compressor for industrial duty application.
- Water Cooled Coil-in-Coil (Co-axial) condenser

Figure B.1:
(**Page 1/2**): Quote and specifications of Chiller model PCW-03LLTX, referring to chiller option 1, section 7.1.1. (*Courtesy of Cooling Technology Inc*)

COOLING TECHNOLOGY INC
COOLING TECHNOLOGY INC
1800 ORR INDUSTRIAL COURT
CHARLOTTE, NC 28213
+1 (704) 596-4109
+1 (704) 597-8697 FAX
WWW.COOLINGTECHNOLOGY.COM

- Stainless Steel, Insulated, Brazed Plate Evaporator
- Pressure drop at evaporator: 8.01PSI
- Stainless Steel, insulated fluid lines
- Refrigerant High/Low pressure cut-off safeties
- Refrigerant high-pressure relief valve
- Freeze protection thermostat

- Flow switch
- Compressor Crank Case Heater
- Compressor suction, Discharge service valves and internal check valve
- Condenser water regulating valve
- Hot Gas Bypass capacity control.
- Chiller includes suction line accumulator
- NEMA-12 electrical control panel with NEMA rated pilot lights and switches
- CAREL electronic temperature controller
- Thermostatic Expansion valve
- Control panel includes 120-volt control voltage transformer and a two-circuit utility outlet
- Unit built on structural steel base with lifting lugs
- All major components are bolted to the structural members and with easy accessibility for service/repair
- Chiller is fully charged with refrigerant, factory tested and ready to be placed in service once it is connected to water lines and electric power through a field supplied disconnect switch.

Please review the attached specifications and let us know if you need additional information.

PRICE:

Product	Price
One Model PCW-03 LLTX water cooled chiller	**$28,869.00**

Terms & Conditions:

Freight	FOB Charlotte, NC. Freight allowed.
Shipment	Product will ship 6-8 weeks after drawing approval. Submittal drawings will be available no later than 5-7 business days from receipt of purchase order.
Order Confirmation	We will confirm receipt of your order within 48 hours with a more accurate ship date.
Warranty	Please see attached "Standard Product Warranty"
Payment Terms	50% down payment, balance at the time of shipment. This order is effective only upon receipt of confirming purchase order. Quote is valid 30 days from the date of this quotation.

We value this opportunity to provide you with a solution to your needs. We look forward to working with you. Please contact me if you have any questions.

Best Regards,

Pat Oza, P.E., Sales

Figure B.2:
(**Page 2/2**): Quote and specifications of Chiller model PCW-03LLTX, referring to chiller option 1, section 7.1.1. (*Courtesy of Cooling Technology Inc.*)

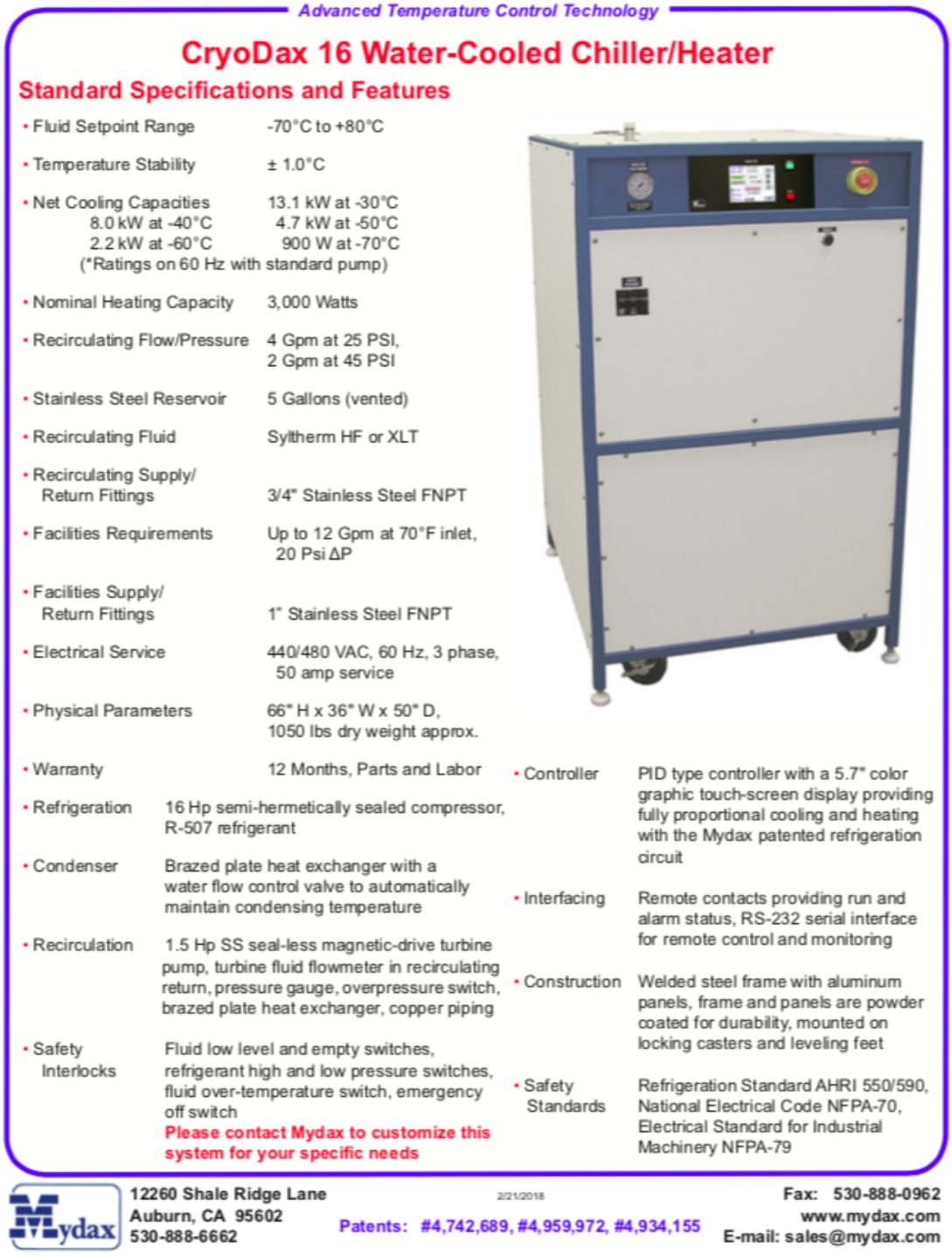

Advanced Temperature Control Technology

CryoDax 16 Water-Cooled Chiller/Heater

Standard Specifications and Features

• Fluid Setpoint Range	-70°C to +80°C
• Temperature Stability	± 1.0°C
• Net Cooling Capacities	13.1 kW at -30°C 8.0 kW at -40°C 4.7 kW at -50°C 2.2 kW at -60°C 900 W at -70°C (*Ratings on 60 Hz with standard pump)
• Nominal Heating Capacity	3,000 Watts
• Recirculating Flow/Pressure	4 Gpm at 25 PSI, 2 Gpm at 45 PSI
• Stainless Steel Reservoir	5 Gallons (vented)
• Recirculating Fluid	Syltherm HF or XLT
• Recirculating Supply/ Return Fittings	3/4" Stainless Steel FNPT
• Facilities Requirements	Up to 12 Gpm at 70°F inlet, 20 Psi ΔP
• Facilities Supply/ Return Fittings	1" Stainless Steel FNPT
• Electrical Service	440/480 VAC, 60 Hz, 3 phase, 50 amp service
• Physical Parameters	66" H x 36" W x 50" D, 1050 lbs dry weight approx.
• Warranty	12 Months, Parts and Labor
• Refrigeration	16 Hp semi-hermetically sealed compressor, R-507 refrigerant
• Condenser	Brazed plate heat exchanger with a water flow control valve to automatically maintain condensing temperature
• Recirculation	1.5 Hp SS seal-less magnetic-drive turbine pump, turbine fluid flowmeter in recirculating return, pressure gauge, overpressure switch, brazed plate heat exchanger, copper piping
• Safety Interlocks	Fluid low level and empty switches, refrigerant high and low pressure switches, fluid over-temperature switch, emergency off switch **Please contact Mydax to customize this system for your specific needs**

• Controller	PID type controller with a 5.7" color graphic touch-screen display providing fully proportional cooling and heating with the Mydax patented refrigeration circuit
• Interfacing	Remote contacts providing run and alarm status, RS-232 serial interface for remote control and monitoring
• Construction	Welded steel frame with aluminum panels, frame and panels are powder coated for durability, mounted on locking casters and leveling feet
• Safety Standards	Refrigeration Standard AHRI 550/590, National Electrical Code NFPA-70, Electrical Standard for Industrial Machinery NFPA-79

Mydax
12260 Shale Ridge Lane
Auburn, CA 95602
530-888-6662

2/21/2018

Patents: #4,742,689, #4,959,972, #4,934,155

Fax: 530-888-0962
www.mydax.com
E-mail: sales@mydax.com

Figure B.3:
(**Page 1/2**): Quote and specifications of Chiller model Cryodax 16-FT, referring to chiller option 2, section 7.1.2. (*Courtesy of Mydax Inc.*)

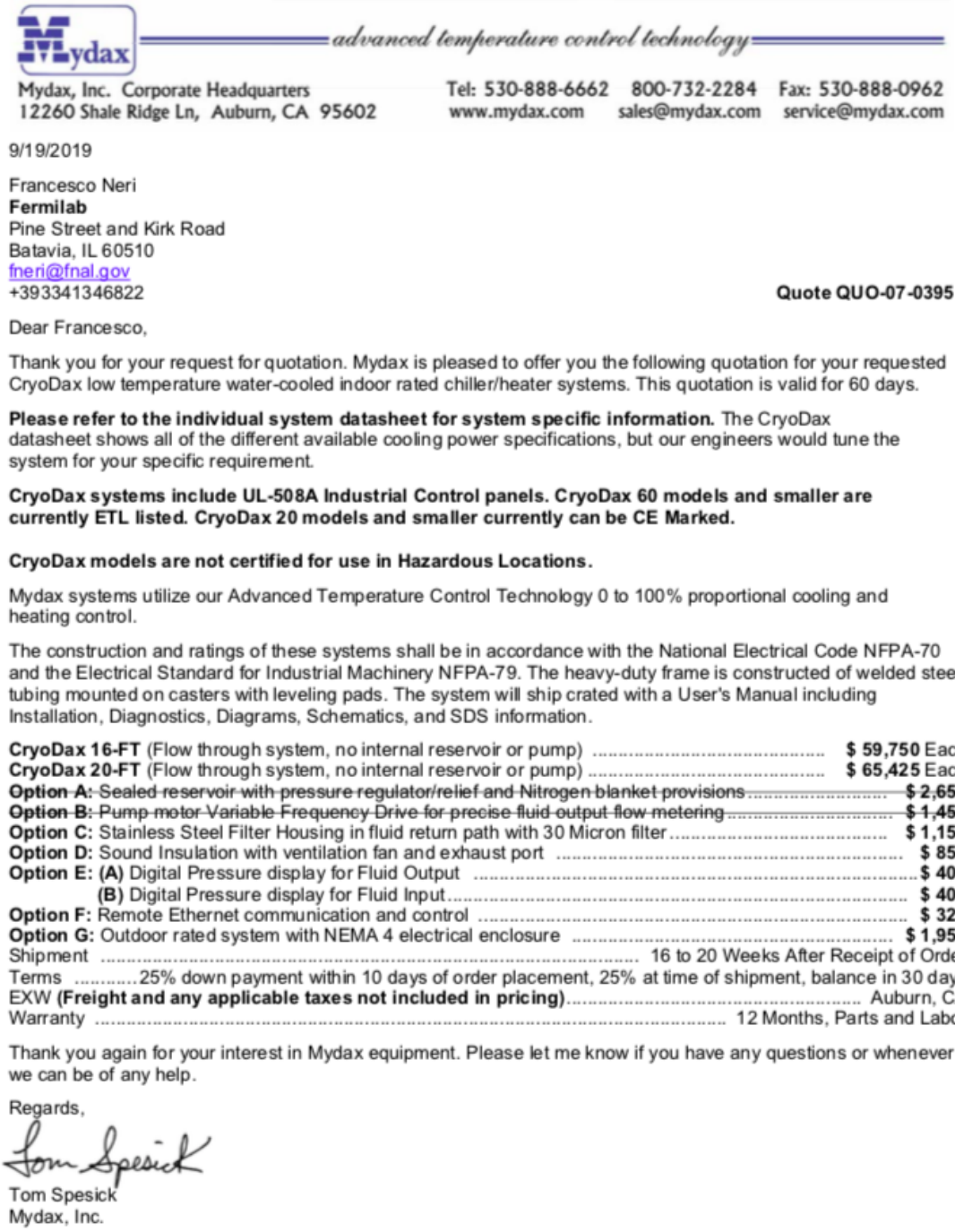

Mydax — advanced temperature control technology

Mydax, Inc. Corporate Headquarters
12260 Shale Ridge Ln, Auburn, CA 95602

Tel: 530-888-6662 800-732-2284 Fax: 530-888-0962
www.mydax.com sales@mydax.com service@mydax.com

9/19/2019

Francesco Neri
Fermilab
Pine Street and Kirk Road
Batavia, IL 60510
fneri@fnal.gov
+393341346822

Quote QUO-07-0395

Dear Francesco,

Thank you for your request for quotation. Mydax is pleased to offer you the following quotation for your requested CryoDax low temperature water-cooled indoor rated chiller/heater systems. This quotation is valid for 60 days.

Please refer to the individual system datasheet for system specific information. The CryoDax datasheet shows all of the different available cooling power specifications, but our engineers would tune the system for your specific requirement.

CryoDax systems include UL-508A Industrial Control panels. CryoDax 60 models and smaller are currently ETL listed. CryoDax 20 models and smaller currently can be CE Marked.

CryoDax models are not certified for use in Hazardous Locations.

Mydax systems utilize our Advanced Temperature Control Technology 0 to 100% proportional cooling and heating control.

The construction and ratings of these systems shall be in accordance with the National Electrical Code NFPA-70 and the Electrical Standard for Industrial Machinery NFPA-79. The heavy-duty frame is constructed of welded steel tubing mounted on casters with leveling pads. The system will ship crated with a User's Manual including Installation, Diagnostics, Diagrams, Schematics, and SDS information.

CryoDax 16-FT (Flow through system, no internal reservoir or pump)	**$ 59,750** Each
CryoDax 20-FT (Flow through system, no internal reservoir or pump)	**$ 65,425** Each
Option A: Sealed reservoir with pressure regulator/relief and Nitrogen blanket provisions	**$ 2,650**
Option B: Pump motor Variable Frequency Drive for precise fluid output flow metering	**$ 1,450**
Option C: Stainless Steel Filter Housing in fluid return path with 30 Micron filter	**$ 1,150**
Option D: Sound Insulation with ventilation fan and exhaust port	**$ 850**
Option E: **(A)** Digital Pressure display for Fluid Output	**$ 400**
(B) Digital Pressure display for Fluid Input	**$ 400**
Option F: Remote Ethernet communication and control	**$ 325**
Option G: Outdoor rated system with NEMA 4 electrical enclosure	**$ 1,950**
Shipment	16 to 20 Weeks After Receipt of Order
Terms	25% down payment within 10 days of order placement, 25% at time of shipment, balance in 30 days
EXW **(Freight and any applicable taxes not included in pricing)**	Auburn, CA
Warranty	12 Months, Parts and Labor

Thank you again for your interest in Mydax equipment. Please let me know if you have any questions or whenever we can be of any help.

Regards,

Tom Spesick
Mydax, Inc.

Figure B.4:
(**Page 2/2**): Quote and specifications of Chiller model Cryodax 16-FT, referring to chiller option 2, section 7.1.2. (*Courtesy of Mydax Inc.*)

DPK350

Max Flow: 100 gpm (379 lpm)

Donaldson. FILTRATION SOLUTIONS

DPK350 In-Line Cartridge Filters

Working Pressures to:
350 psi / 2400 kPa / 24 bar

Rated Static Burst to:
700 psi / 4800 kPa / 48 bar

Flow Range To:
100 gpm / 379 lpm

Applications

- In-plant Systems
- Process Fluids
- Lube Oil Systems

Features

DPK350 duplex filter assemblies allow continuous filtration during filter servicing to avoid machine shutdown. The DPK350 duplex design combines lighter weight aluminum heads with durable steel housings for a high-performance assembly. Choose between optional features such as no by-pass, by-pass valve, visual indicators or combination electrical/visual indicators for a customized assembly that best fits the needs of your specific application. Filter performance ranges from 5µ to 25µ at beta 1000 and high collapse elements are available at 5µ and 27µ, offering additional flexibility to achieve the filtration level your system requires.

- Head Material: Anodized Aluminum Alloy
- Housing Material: Steel
- Optional visual and visual / electric indicators
- Self locking transfer valve
- Automatic bleed-over valve

Beta Rating

- Performance to $\beta_{x(c)}=1000$

Porting Size Options

- 1-½" SAE 4-Bolt Flange Code 61

Replacement Filter Lengths

- 14.62" / 371mm

Standard Bypass Ratings

- 50 psi / 345 kPa / 3.5 bar
- No bypass

Assembly Weight

- 44 lbs / 20 kg

Operating Temperatures

- -40° to 250°F (-40° to 121°C)

Filter Collapse Ratings

- 300 psid / 207 kPa / 21 bar (standard)
- 3045 psid / 2100 kPa / 210 bar (high collapse)

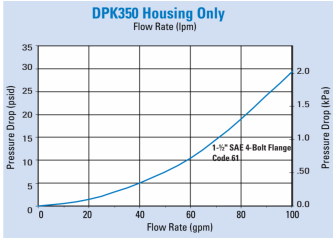

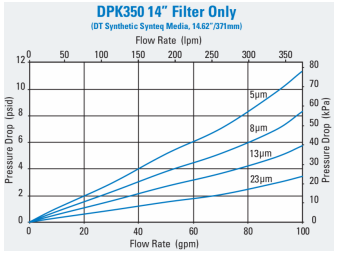

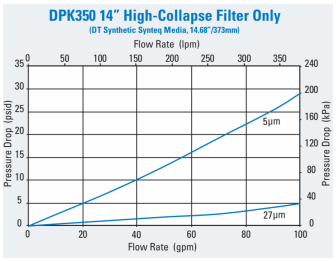

Figure B.5:
(**Page 1/2**): Datasheet of the Donaldson filter model DPK350. (*Courtesy of Donaldson inc.*)

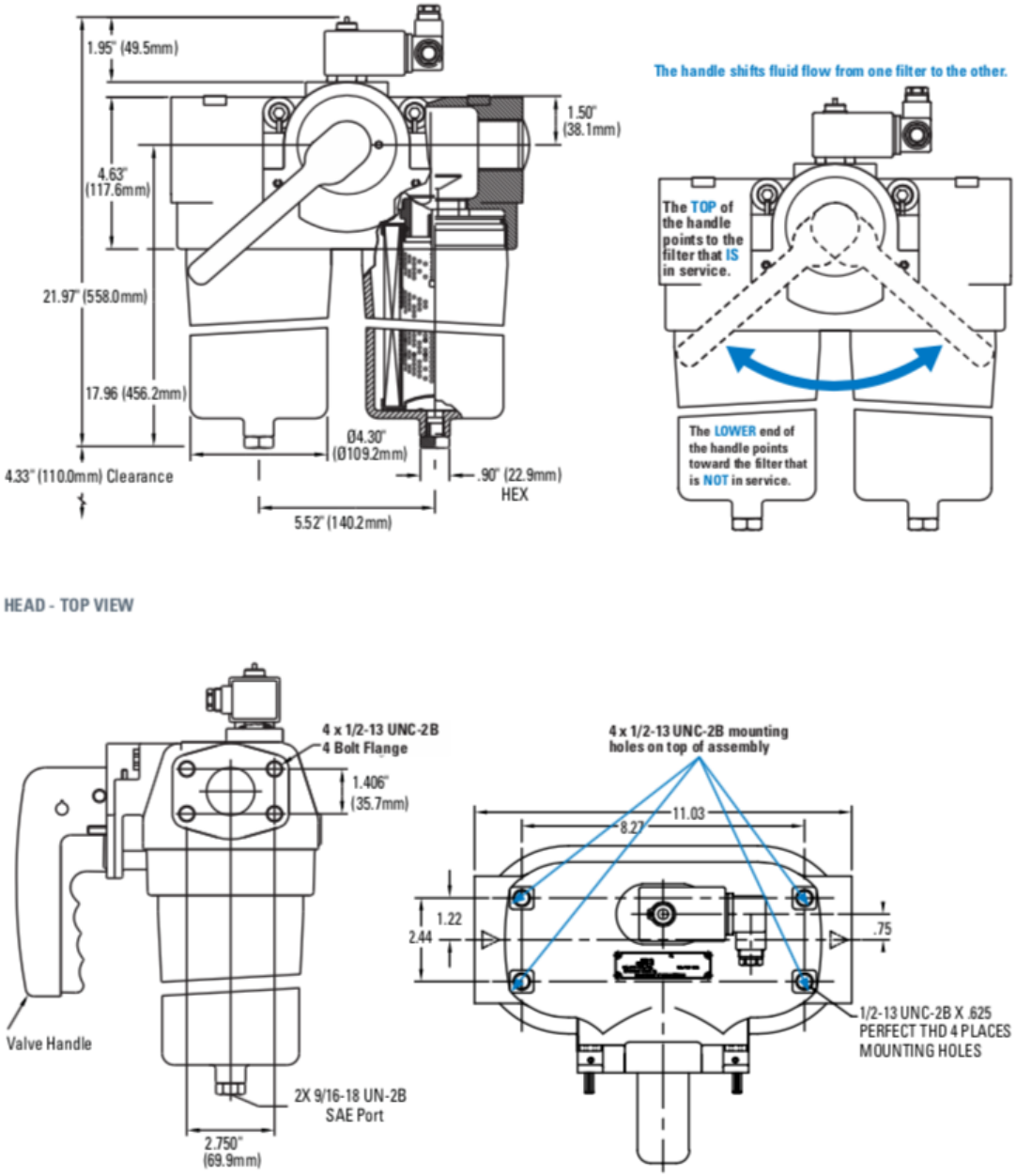

Figure B.6:
(**Page 1/2**): Datasheet of the Donaldson filter model DPK350. (*Courtesy of Donaldson inc.*)

Technical Sheet

Nitrogen

SUPAGAS
YES WE CAN!

Description

Nitrogen is a non-flammable gas which does not support combustion. It is colourless, odourless and non-toxic; it is almost a totally inert gas (containing approx 79% volume of air).

Signal Word:	Warning
UN No.:	1066
Hazard No.:	2(T)
Chem Symbol:	N_2
Pictograms:	

Applications

- Purging and pipeline testing
- Tyre inflation
- Inert atmospheres
- Food packaging and wine making
- Gauge calibration
- Metal degassing
- Aerosol propellant
- Hydraulic systems and air tools
- Photo processing
- Plastic forming
- Fire fighting

Hazard statement(s)

- Contains gas under pressure; may explode if heated.

Prevention statement(s)

- None allocated.

Response statement(s)

- None allocated.

Storage statement(s)

- Protect from sunlight. Store in a well-ventilated place.

Other hazards

- Asphyxiant. Effects are proportional to oxygen displacement.

Figure B.7: (**Page 1/2**): technical sheet of nitrogen bottles. (*Courtesy of Supagas Inc.*)

Technical Sheet

Nitrogen

SUPAGAS
YES WE CAN!

General Specifications

Specifications	D Cylinder	E Cylinder	G Cylinder	GX Cylinder	12 Pack	16 Pack Offshore
Cylinder/Pack (101.325kPa @15°C) - L	1.5	3.5	9.1	12.8	153.0	208.0
Water capacity per cylinder - L	10	23	50	50	600	800
Cylinder Colour	Pewter					
Outlet Connection	Type 50			Type 51	Type 50/51	
Package Dimensions (H x W x D) - mm	645 x 180	780 x 230	1,580 x 230	1,630 x 230	1,900 x 1,020 x 780	2155 x 1065 x 1065

Cylinder dimensions are approximate – variations may occur due to manufacturing tolerances. Height includes the valve. Container sizes may vary from state to state.

Package Sizes Available

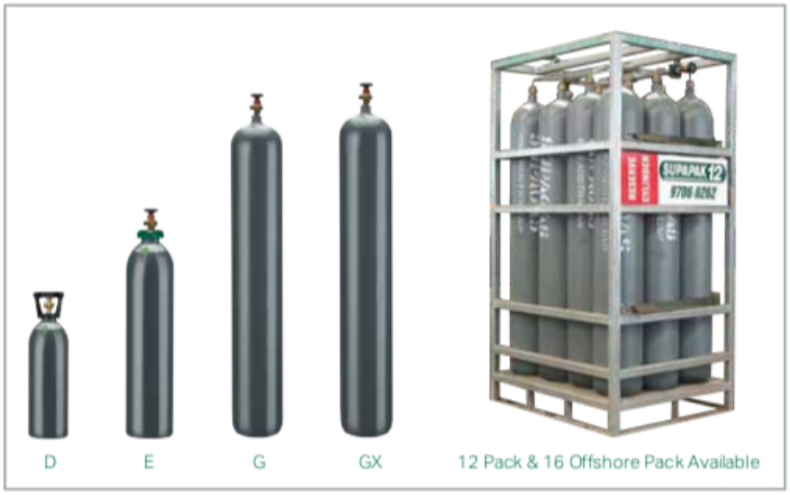

Typical Analysis

Product Type	N_2	O_2	Moisture	CxHy
UHP Grade	>99.999%	<2ppm	<3ppm	<0.5ppm
HP Grade	>99.995%	<10ppm	<10ppm	-
Food Grade	>99.995%	<10ppm	<10ppm	-
Industrial Grade	>99.9%	<750ppm	-	-

Quality Assurance

Supagas Pty Ltd is committed to comply with the requirements of ISO 9001-2015 and to continually improve the effectiveness of our Quality Management System.

Everyone at Supagas understands we must provide a safe environment for both our employees and the wider community. We are therefore committed to implement and maintain a continual improvement approach throughout the organisation whilst also meeting all applicable statutory and regulatory requirements.

NATA Accreditation

The Supagas Laboratory located in Ingleburn, NSW has a NATA Accreditation (No. 18955). Accredited for compliance with ISO/IEC 17025 and ISO Guide 34, Reference Gas Mixtures prepared to ISO 6142.

For Further Information

On how we can help you with all your gas and welding needs, drop in to your local Supagas branch or call Customer Service on 13 78 72.

Nitrogen_v3 10092018

FREE DELIVERY *TO MOST AREAS

13 SUPA
13 78 72
supagas.com.au

Figure B.8: (**Page 2/2**): technical sheet of nitrogen bottles. (*Courtesy of Supagas Inc.*)

Pipe Size	Model Number		A Dia.	B Max.	C	D	E	F	G Dia.	H Inch	Max. Flow	Strainer Free Area	C_v Factor	Approx. Wt. (LBS.)	C_v Factor	Approx. Wt. (LBS.)
Inch	Less Strainer	With Strainer	Inch	Inch	Inch	Inch	Inch	Inch	Base Ring		GPM	Inch²	Less Strainer		With Strainer	
2	AC02	AC02F	12	22-1/8	13	7-9/16	7	14	-	-	80	31	86	40	72	45
2-1/2	AC025	AC025F	12	22-1/8	13	7-9/16	7	14	-	-	130	38	122	40	102	45
3	AC03	AC03F	14	27-1/4	22	8	11-1/4	24	12	6-1/2	190	51	190	90	162	110
4	AC04	AC04F	16	31-3/8	24	9-5/16	12-3/4	26	12	7	330	80	325	115	272	145
5	AC05	AC05F	16	32-1/2	24	9-3/8	13-3/4	26	12	7	550	112	510	130	422	165
6	AC06	AC06F	20	36-7/8	27	11-1/16	14-3/4	30	16	6-3/4	900	180	750	170	618	215
8	AC08	AC08F	20	45-1/2	27	14-1/16	17-3/8	30	16	6-3/4	1500	246	1260	270	1060	345
10	AC10	AC10F	24	47-3/4	32	14-15/16	17-7/8	36	20	6-3/4	2600	392	2000	350	1670	465
12	AC12	AC12F	30	59-3/4	37	17-5/8	24-1/2	42	24	7-3/4	3400	548	2900	600	2400	775
14	AC14	AC14F	36	68-1/2	44	20-3/4	27	48	30	7-3/4	4700	732	3500	805	2850	1035
16	AC16	AC16F	36	75-1/2	43	22-1/4	31	48	30	7-3/4	6000	845	4600	875	3800	1150
18	AC18	AC18F	48	84-1/4	56	24-5/8	35	64	40	7-3/4	8000	1290	5900	1550	4900	1900
20	AC20	AC20F	48	91	56	26	39	64	40	8 5/8	10000	1435	7400	1700	6200	2150

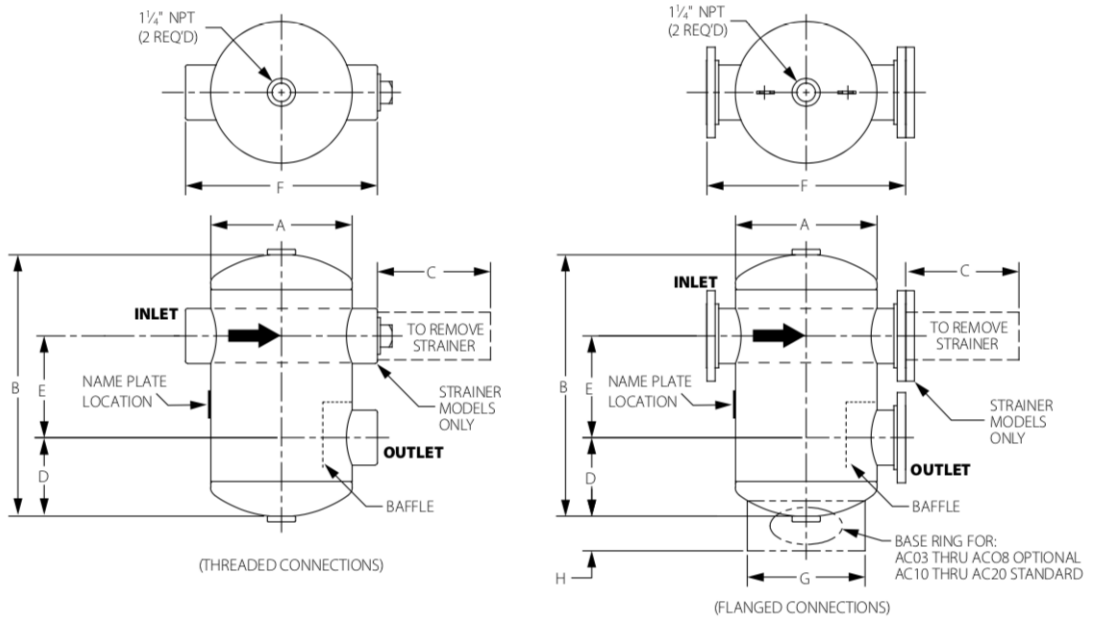

Figure B.9: Datasheet of the Taco air separator model AC02. (*Courtesy of Taco Comfort Solutions inc.)*

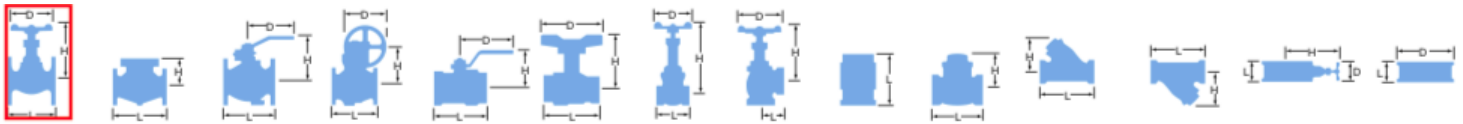

TYPE			A-SERIES GATE			A-SERIES GATE			A-SERIES GATE			A-SERIES GATE			A-SERIES GATE		
Stainless Steel																	
FIG			20UMAM / 20UMAMT			150UMA / 150UMAT			150UMAM / 150UMAMT			300UMA			300UMAM		
PRESSURE			20K			Class 150			Class 150			Class 300			Class 300		
END CONNECTION			JIS B2220			ASME B16.5			ASME B16.5			ASME B16.5			ASME B16.5		
DIMENSIONS	inch	mm	L	H	D	L	H	D	L	H	D	L	H	D	L	H	D
	½	15	140	209	100	108	201	90	108	201	90	140	209	100	140	209	100
	¾	20	152	220	100	117	211	90	117	211	90	152	220	100	152	220	100
	1	25	165	239	100	127	224	100	127	224	100	165	239	100	165	239	100
	1½	40	190	294	140	165	284	140	165	284	140	190	294	140	190	294	140
	2	50	216	355	180	178	336	160	178	336	160	216	355	180	216	355	180
	2½	65	241	404	180	190	374	180	190	374	180	241	404	180	241	404	180
	3	80	283	472	225	203	444	200	203	444	200	283	472	225	283	472	225
	4	100	305	560	250	229	523	225	229	523	225	305	560	250	305	560	250
	5	125	381	626	300	254	606	250	254	606	250	381	626	300	381	626	300
	6	150	403	753	350	267	711	250	267	711	250	403	753	350	403	753	350
	8	200	419	968	400	292	924	300	292	924	300	419	968	400	419	968	400
	10	250	457	1177	450	330	1126	350	330	1126	350	457	1177	450	457	1177	450
	12	300	502	1378	500	356	1336	400	356	1336	400	502	1378	500	502	1378	500
	14	350	762	1590	600	381	1486	450	381	1486	450	762	1590	600	762	1590	600
	16	400	838	1810	600	406	1690	600	406	1690	600	838	1810	600	838	1810	600
	18	450	914	1980	680	432	1890	600	432	1890	600	914	1980	680	914	1980	680
	20	500	991	2190	760	457	2100	680	457	2100	680	991	2190	760	991	2190	760
	24	600	1143	2580	910	508	2460	760	508	2460	760	1143	2580	910	1143	2580	910
BODY			SCS14A			A351 Gr.CF8			A351 Gr.CF8M			A351 Gr.CF8			A351 Gr.CF8M		
BONNET			SCS14A			A351 Gr.CF8			–			A351 Gr.CF8			A351 Gr.CF8M		
COVER			–			–			A351 Gr.CF8M			–			–		
STEM			SUS316			TYPE 304			TYPE 316			A276 TYPE 304			A276 TYPE 316		
DISC			SCS14A			A351 Gr.CF8			A351 Gr.CF8M			A351 Gr.CF8			A351 Gr.CF8M		
			Fig. 20UMAMT : Gland Packing / PTFE			Fig. 150UMAT : Gland Packing / PTFE			Fig. 150UMAMT : Gland Packing / PTFE								

Figure B.10: Datasheet of the Kitz gate valve models 300UMA. (*Courtesy of Kitz inc.*)

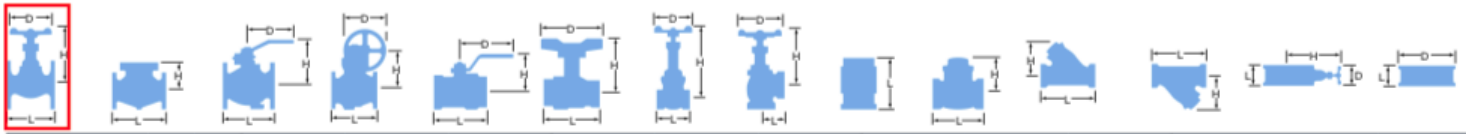

TYPE			A-SERIES SWING CHECK			A-SERIES SWING CHECK			A-SERIES SWING CHECK			A-SERIES SWING CHECK			A-SERIES SWING CHECK		
Stainless Steel																	
FIG			150UOAM / 150UOAMT			300UOA			300UOAM			600UOA			600UOAM		
PRESSURE			Class 150			Class 300			Class 300			600LB			600LB		
END CONNECTION			ASME B16.5			ASME B16.5			ASME B16.5			ASME B16.5			ASME B16.5		
DIMENSIONS	inch	mm	L	H	D	L	H	D	L	H	D	L	H	D	L	H	D
	½	15	–	–	–	–	–	–	–	–	–	165	90	95	165	90	95
	¾	20	–	–	–	–	–	–	–	–	–	190	96	117	190	96	117
	1	25	–	–	–	–	–	–	–	–	–	216	109	124	216	109	124
	1½	32	–	–	–	–	–	–	–	–	–	–	–	–	–	–	–
	1½	40	165	111	127	241	121	156	241	121	156	241	126	156	241	126	156
	2	50	203	121	152	267	143	165	267	143	165	292	189	165	292	189	165
	2½	65	216	134	178	292	163	190	292	163	190	330	213	190	330	213	190
	3	80	241	148	190	318	178	210	318	178	210	356	239	210	356	239	210
	4	100	292	162	229	356	201	254	356	201	254	432	279	273	432	279	273
	5	125	330	192	254	400	231	279	400	231	279	–	–	–	–	–	–
	6	150	356	217	279	444	259	318	444	259	318	559	339	356	559	339	356
	8	200	495	264	343	533	292	381	533	292	381	660	414	419	660	414	419
	10	250	622	287	406	622	356	444	622	356	444	–	430	–	–	430	–
	12	300	698	315	483	711	373	521	711	373	521	838	477	508	838	477	508
	14	350	787	363	533	–	–	–	–	–	–	–	–	–	–	–	–
	16	400	864	407	597	–	–	–	–	–	–	–	–	–	–	–	–
BODY			A351 Gr.CF8M			A351 Gr.CF8			A351 Gr.CF8M			A351 Gr.CF8			A351 Gr.CF8M		
COVER			A351 Gr.CF8M			A351 Gr.CF8			A351 Gr.CF8M			A351 Gr.CF8			A351 Gr.CF8M		
STEM			–			–			–			–			–		
DISC			A351 Gr.CF8M			A351 Gr.CF8			A351 Gr.CF8M			A351 Gr.CF8			A351 Gr.CF8M		
HINGE PIN			TYPE316			A276 TYPE304			A276 TYPE316			TYPE304			TYPE316		
			Fig. 150UOAMT : Gasket / PTFE														

Figure B.11: Datasheet of the Kitz swing check valve models 300UOA. (*Courtesy of Kitz inc.)*

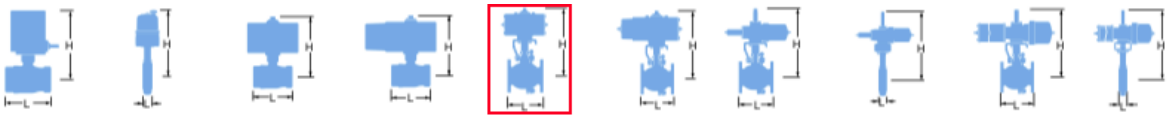

TYPE			FLOATING BALL			FLOATING BALL			FLOATING BALL			FLOATING BALL			FLOATING BALL		
Actuators Valves																	
FIG			FA-150SCTDZ			FA-150UTDZ			FA-20SCTDZ			FA-20UTDZ			FA-300SCTDZ		
PRESSURE			Class 150			Class 150			20K			20K			Class 300		
END CONNECTION			ASME B16.5			ASME B16.18			JIS B2220			JIS B2220			ASME B16.5		
DIMENSIONS	inch	mm	L	H	D	L	H	D	L	H	D	L	H	D	L	H	D
	½	15	108	215	–	108	215	–	108	215	–	140	215	–	140	215	–
	¾	20	117	218	–	117	218	–	117	218	–	152	218	–	152	218	–
	1	25	127	240	–	127	240	–	127	240	–	165	240	–	165	240	–
	1¼	32			–	140	244	–	–	–	–	178	244	–	–	–	–
	1½	40	165	297	–	165	297	–	165	297	–	190	297	–	190	297	–
	2	50	178	306	–	178	306	–	178	306	–	216	306	–	216	306	–
	2½	65	190	363	–	190	363	–	190	363	–	241	363	–	241	363	–
	3	80	203	419	–	203	419	–	203	419	–	283	419	–	283	419	–
	4	100	229	447	–	229	447	–	229	447	–	305	447	–	305	447	–
	5	125	356	519	–	356	519	–	356	519	–	381	419	–	–	–	–
	6	150	394	552	–	394	552	–	394	552	–	403	552	–	403	552	–
	8	200	457	656	–	457	656	–	457	656	–	502	656	–	502	656	–
BODY			A216 Gr.WCB			A351 Gr.CF8			SCPH2 (WCB)			SCS13A			A216 Gr.WCB		
BONNET			A216 Gr.WCB			A351 Gr.CF8			SCPH2			SCS13A			A216 Gr.WCB		
STEM			A276 TYPE304			A276 TYPE304			SUS304			SUS304			A276 TYPE304		
DISC			A276 TYPE304 / A351 Gr.CF8			A276 TYPE304 / A351 Gr.CF8			SUS304 / SCS13A			SUS304 / SCS13A			A276 TYPE304 / A351 Gr.CF8		
SEAT			HYPATITE® PTFE			HYPATITE® PTFE			HYPATITE® PTFE			HYPATITE® PTFE			HYPATITE® PTFE		
			Full Port			Full Port			Full Port			Full Port			Full Port		

Figure B.12: Datasheet of the Kitz actuated floating ball valve models FA-300SCTDZ. (*Courtesy of Kitz inc.*)

Ball Valves
ANSI Flanges, 3-way
Steel & Stainless Steel

Industrial Controls

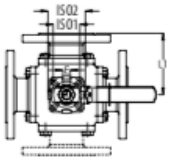

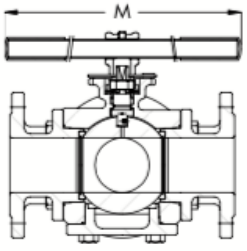

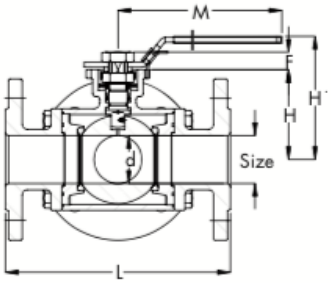

Dimensions

Size (in)	d	L	L1	M	F	H	H1	E	ISO1	ISO2	Weight (lbs)	Operation
	Inches											
½	0.59	5.91	2.95	5.71	0.35	2.09	3.27	0.35	F03	F04	9.92	Lever
¾	0.79	6.50	3.25	5.71	0.35	2.30	3.48	0.35	F03	F04	13.01	Lever
1	0.98	7.13	3.56	6.89	0.43	2.76	4.09	0.43	F04	F05	19.18	Lever
1¼	1.26	7.48	3.74	6.89	0.43	3.05	4.39	0.43	F04	F07	24.25	Lever
1½	1.5	8.35	4.17	7.87	0.55	3.41	4.74	0.55	F05	F07	31.75	Lever
2	1.93	9.02	4.51	7.87	0.55	3.62	4.96	0.55	F05	F07	42.33	Lever
2½	2.48	11.42	5.71	10.43	0.67	4.21	6.10	0.67	F07	F10	69.89	T-bar
3	2.95	12.20	6.10	10.43	0.67	4.69	6.57	0.67	F07	F10	95.90	T-bar
4	3.90	14.45	7.22	15.75	0.87	5.91	8.43	0.87	F10	F10	141.98	T-bar

Switching Possibilities

Model	Ball position			
	Standard		Optional	
	A	B	C	D
7282L, 7292L				
7282T, 7292T				

Standard: Flow can be switched from A to B.
Option: Handlever can be changed for switching from C to D.

Torque Tables

Size \ ΔP	75 psig	150 psig	285 psig
	in-lbs		
½	71	71	71
¾	106	106	106
1	159	159	168
1 - 1¼	204	204	239
1 - 1½	283	283	336
2	389	443	495
2 - 2½	620	699	761
3	974	1,080	1,221
4	1,682	1,850	2.053

www.industrialcontrolsonline.com

Figure B.13: Datasheet of the Indutrial Controls 3-way valve, model 7292T. (*Courtesy of Industrial Controls inc.*)

500 Series
Multi-Purpose Safety Relief Valves

Section VIII
Pressure Vessels

Versatile safety relief valve available in bronze, carbon steel or all stainless steel construction, suitable for a wide range of steam, air, gas and liquid applications. High capacity full nozzle design is available with metal to metal, PCTFE or elastomer O-ring seating. Short tuned blowdown and backpressure tight body minimizes fugitive emissions and product losses in the event of valve operation.

ASME Section VIII Air, Steam, and Liquid service
Sizes 1/2" through 2" NPT
Set pressure range 5-900 psig @ 800°F max.
(See press. / temp. limit chart below for specific ratings for each model).

Applications:
- Pressure Vessels and Pressure Piping Systems
- Pumps, Tanks and Hydraulic Systems
- Thermal Relief of Liquid Filled Vessels
- Chemical, Process and other Industrial Plants.
- Power Plant Auxiliary Systems
- Cryogenic and Industrial Gases
- Air and Gas Compressors and Dryers
- Vacuum Relief

Features
- Wide Range of Materials and Options
- One Trim Design is Suitable for Steam, Air / Gas and Liquid Service
- High Capacity Full Nozzle Design
- Stainless Steel Springs
- Integral Lift Stop
- Self - Aligning Pivoting Disc
- API 527 Seat Tightness, standard for all models
- Tuned Blowdown - Short and Adjustable, reduces product losses.
- Backpressure Tight Design Minimizes Fugitive Emissions
- CSA B51 CRN OG8547.5C

Options
- Screwed Cap (standard), Packed Lift Lever
- Test gags
- Elastomer or PCTFE Soft Seat for Exceptional Seat Tightness
- High Temperature Alloy Springs for 422°F - 800°F Service
- Special Cleaning Available
- Cryogenic Preparation (Consult factory)

500 Series Model Numbering System

52	3	J	H	B	K	M	AA	0425
Series Body/Trim Mat'l	**Cap**	**Orifice Letter**	**Inlet Size**	**Connection**	**Service**	**Seat**	**Special Options**	**Set Pressure**
51=Bronze/Brass 52=Bronze/ Stainless 53=Carbon/ Stainless 54=All Stainless	1=Screwed Cap 2=Screwed + Gag 3=Packed Lever 4=Packed + Gag	D E F G H J	C=1/2 D=3/4 E=1 F=1-1/4 G=1-1/2 H=2	B=MNPT X FNPT D=3/4 Outlet (Model 510 & 520 D Orifice Only)	J=Sec VIII Liquid K=Sec VIII Air/Gas L=SEC VIII Steam M=Non Code Liquid N=Non Code Air / Gas P=NON CODE Steam Q=Vacuum	M=Metal B=BUNA-N E=EPR K=PCTFE N=Neoprene S=Silicone V=Viton	Factory Issued Letters / Numbers For Special Options Or Features "AA"=Default Standard "HT" High Temp Spring "OX"=Cleaned For Oxygen	Set pressure psig (4 Digits) Vacuum "HG" Prefix + 2 Digits

Figure B.14:
(**Page 1/3**): Datasheet of the Apollo/Conbraco safety relief valves. (*Courtesy of Apollo/Conbraco inc.)*

500 Series
Multi-Purpose Safety Relief Valves

Soft Seat Pressure & Temperature Limits* - 500 Series

Seat Material	Set Pressure Min.	Set Pressure Max.	Temperature Min.	Temperature Max.	Service Recommendations**
VITON	15	900	-15°F	400°F	AIR, BENZENE, BUTANE, CARBON DISULPHIDE, CARBON TETRACHLORIDE, DOWTHERM A, ETHYL CHLORIDE, ETHYLENE, ETHYLENE GLYCOL, FUEL OIL, GASOLINE, HYDRAULIC FLUID, JP-4 AND -5 FUEL, KEROSENE, LUBE OIL, NATURAL GAS, NAPTHA, NITROGEN, PROPANE, PROPYL ALCOHOL, PROPYLENE, SULPHUR DIOXIDE, TOLUENE, TRICHLORETHYLENE, TURPENTINE, VINYL CHLORIDE, WATER
EPDM	15	900	-70°F	250°F	STEAM, WATER, HOT WATER, ACETONE, BEER, BRAKE FLUID, HYDROGEN SULPHIDE, SULPHUR DIOXIDE, ACIDS, ALKALIS, KETONES
SILICONE	15	900	-60°F	450°F	AIR, HELIUM, NITROGEN, OXYGEN (GASEOUS)
NEOPRENE	15	900	-35°F	225°F	ANHYDROUS AMMONIA, BUTANE, BUTYL ALCOHOL, CASTOR OIL, DENATURED ALCOHOL, ETHANOL, ETHYL ALCOHOL, FREON 12, 13, 14 & 22, GLYCOLS, NATURAL GAS, OXYGEN (GASEOUS), SILICATE ESTERS
NITRILE / BUNA-N	15	900	-30°F	250°F	AIR, BUTANE, CARBON DIOXIDE, DIESEL OIL, FUEL OIL, GASOLINE, HELIUM, HYDRAULIC FLUID (PETROLEUM BASED), KEROSENE, LUBE OIL, NATURAL GAS, NITROGEN, PROPANE
PCTFE	15	500	-320°F	250°F	CRYOGENIC SERVICE INCLUDING ARGON, CARBON DIOXIDE, HELIUM, HYDROGEN, NITROGEN, OXYGEN

Notes:

** Subject to valve body material pressure / temperature limitations. See chart below.*

*** Service recommendations are provided as a guide only. Material suitability and selection should be determined by the end user.*

Pressure and Temperature Ratings

Series	510	520	530	540
Body	Bronze	Bronze	Carbon Steel	Stainless Steel
Trim	Brass	Stainless	Stainless	Stainless
Max. Set-Steam	250 PSI	300 PSI	900 PSI (D/E) 600 PSI (F/G) 500 PSI (H/J)	900 PSI (D/E) 600 PSI (F/G) 500 PSI (H/J)
Max. Set-Air/Gas/Liquid	300 PSI	900 PSI (D/E) 600 PSI (F/G) 500 PSI (H/J)	900 PSI (D/E) 600 PSI (F/G) 500 PSI (H/J)	900 PSI (D/E) 600 PSI (F/G) 500 PSI (H/J)
Temp. Limits*	-60/406°F	-60/422°F	-20/800°F	-60/800°F

Notes:

- *Limits based upon materials of construction and use of metal to metal seating. Refer to 500 series soft seat chart for limitations based upon elastomer.*
- *Specify "HT" high temperature Inconel springs for service temperature beyond 422°F.*

** Models 510, 520 and 540 are suitable for cryogenic service to -320°F, subject to special preparation and use of "K" option PCTFE seat. Consult factory for details.*

Selection/Dimensions and Weights

Model Number	Orifice Letter	Size Inlet x Outlet	A (in./mm.)	B (in./mm.)	C (in./mm.)	Weight (Lb../kg.)
5xxDC	D	1/2 X 1	2.38 60	7.5 191	1.63 41	2 0.9
5xxDCD*	D	1/2 X 3/4	2.38 60	7.5 191	1.63 41	2 0.9
5xxDD	D	3/4 X 1	2.38 60	7.5 191	1.63 41	2 0.9
5xxDDD*	D	3/4 X 3/4	2.38 60	7.5 191	1.63 41	2 0.9
5xxED	E	3/4 X 1-1/4	2.63 67	9 229	2 51	3 1.4
5xxEE	E	1 X 1-1/4	2.63 67	9 229	2 51	3 1.4
5xxFE	F	1 X 1-1/2	2.83 73	10.25 260	2.38 60	5 2.3
5xxFF	F	1-1/4 X 1-1/2	2.83 73	10.25 260	2.38 60	5 2.3
5xxGF	G	1-1/4 X 2	3.25 83	13.25 337	2.63 67	9 4.1
5xxGG	G	1-1/2 X 2	3.25 83	13.25 337	2.68 67	9.5 4.31
5xxHG	H	1-1/2 X 2-1/2	3.5 89	15 381	2.75 70	15.5 7.0
5xxHH	H	2 X 2-1/2	3.5 89	15 381	2.75 70	16 7.3
5xxJH	J	2 X 3	4 102	17 432	3.25 83	24 10.9

** 3/4" Outlet option available with 510 and 520 bronze bodied models only.*

Figure B.15:
(**Page 2/3**): Datasheet of the Apollo/Conbraco safety relief valves. (*Courtesy of Apollo/Conbraco inc.)*

500 Series

Multi-Purpose Safety Relief Valves

ASME Section VIII Water

U.S. GALLONS PER MINUTE (CUBIC METERS PER HOUR) OF WATER AT 10% OVER PRESSURE.
NATIONAL BOARD CERTIFIED. RATINGS ARE 90% OF ACTUAL.

U.S. Customary Units GPM

Orifice Letter	D	E	F	G	H	J
Area (In.²)	0.1295	0.2282	0.3589	0.5890	0.9195	1.5044
Set Pressure psig						
5*	13	24	37	61	95	156
10*	14	24	38	63	98	161
15	14	25	40	65	102	167
20	16	29	45	74	115	189
25	18	32	50	82	127	208
30	19	34	54	89	138	226
35	21	37	58	96	149	244
40	22	40	62	102	160	261
45	24	42	66	108	169	277
50	25	44	70	114	178	292
55	26	46	73	120	187	306
60	28	48	76	125	195	320
65	29	50	79	130	203	333
70	30	52	82	135	211	345
75	31	54	85	140	218	357
80	32	56	88	145	226	369
85	33	58	91	149	233	381
90	34	59	93	153	239	392
95	35	61	96	158	246	402
100	36	63	98	162	252	413
125	40	70	110	181	282	462
150	44	77	121	198	309	506
175	47	83	130	214	334	546
200	50	89	139	229	357	584
225	53	94	148	242	378	619
250	56	99	156	256	399	653
275	59	104	163	268	418	685
300	62	108	171	280	437	715
325	64	113	178	291	455	744
350	66	117	184	302	472	772
375	69	121	191	313	489	799
400	71	125	197	323	505	826
425	73	129	203	333	520	851
450	75	133	209	343	535	876
475	77	136	215	352	550	900
500	79	140	220	361	564	923
525	81	143	226	370	-	-
550	83	147	231	379	-	-
575	85	150	236	388	-	-
600	87	153	241	396	-	-
625	89	157	-	-	-	-
650	91	160	-	-	-	-
675	92	163	-	-	-	-
700	94	166	-	-	-	-
725	96	169	-	-	-	-
750	97	171	-	-	-	-
775	99	174	-	-	-	-
800	100	177	-	-	-	-
825	102	180	-	-	-	-
850	104	183	-	-	-	-
875	105	185	-	-	-	-
900	107	188	-	-	-	-

Metric Units m³/hr.

Orifice Letter	D	E	F	G	H	J
Area (Cm.²)	0.8352	1.4721	2.3155	3.8001	5.9321	9.7058
Set Pressure barg						
0.4*	2.0	3.6	5.6	9.2	14.4	23.6
0.8*	2.9	5.1	8.0	13.1	20.4	33.3
1.1	3.3	5.9	9.3	15.2	23.8	38.9
2	4.4	7.7	12.1	19.8	30.9	50.6
3	5.3	9.4	14.8	24.2	37.8	61.8
4	6.1	10.8	17.0	28.0	43.6	71.4
5	6.9	12.1	19.0	31.3	48.8	79.8
6	7.5	13.3	20.9	34.2	53.4	87.4
7	8.1	14.3	22.5	37.0	57.7	94.5
8	8.7	15.3	24.1	39.5	61.7	101.0
9	9.2	16.2	25.6	41.9	65.5	107.1
10	9.7	17.1	26.9	44.2	69.0	112.9
12	10.6	18.8	29.5	48.4	75.6	123.7
14	11.5	20.3	31.9	52.3	81.6	133.6
16	12.3	21.7	34.1	55.9	87.3	142.8
18	13.0	23.0	36.1	59.3	92.6	151.5
20	13.7	24.2	38.1	62.5	97.6	159.7
22	14.4	25.4	39.9	65.6	102.3	167.5
24	15.1	26.5	41.7	68.5	106.9	174.9
26	15.7	27.6	43.4	71.3	111.3	182.0
28	16.3	28.7	45.1	74.0	115.5	188.9
30	16.8	29.7	46.7	76.6	119.5	195.5
32	17.4	30.6	48.2	79.1	123.4	202.0
34	17.9	31.6	49.7	81.5	127.2	208.2
36	18.4	32.5	51.1	83.9	-	-
38	18.9	33.4	52.5	86.2	-	-
40	19.4	34.2	53.9	88.4	-	-
42	19.9	35.1	-	-	-	-
44	20.4	35.9	-	-	-	-
46	20.8	36.7	-	-	-	-
48	21.3	37.5	-	-	-	-
50	21.7	38.3	-	-	-	-
52	22.2	39.0	-	-	-	-
54	22.6	39.8	-	-	-	-
58	23.4	41.2	-	-	-	-
62	24.2	42.6	-	-	-	-

Set Pressure Limits
510 Series - 300 psig/20.7 barg
520 Series - 900 psig/62.1 barg
530 Series - 900 psig/62.1 barg
540 Series - 900 psig/62.1 barg

Note: To determine water capacity at 25% overpressure, multiply the capacity at 10% by 1.066.

**Pressure settings below 15 psig/1.03 barg are non-ASME code.*

Figure B.16:
(**Page 3/3**): Datasheet of the Apollo/Conbraco safety relief valves. (*Courtesy of Apollo/Conbraco inc.)*

Bibliography

[1] 3M. Pf-5060 safety data sheet 1100286. https://multimedia.3m.com/mws/mediawebserver?mwsId=SSSSSuUn_zu8l00x4xtZmxmUNv70k17zHvu9lxtD7SSSSSS--, 08/20/2019. pages

[2] L Bartoszek, E Barnes, JP Miller, J Mott, A Palladino, J Quirk, BL Roberts, J Crnkovic, V Polychronakos, V Tishchenko, et al. Mu2e technical design report. *arXiv preprint arXiv:1501.05241*, 2015. pages

[3] Belimo. *Water Book, documentazione tecnica*. 2014. pages

[4] Eugenio Benedetti. Design and thermal analysis of the cooling system of the electromagnetic calorimeter of the mu2e experiment at fermilab. *Università di Pisa*, 2017-2018. pages

[5] Dejan Brki? and Pavel Praks. Hardy cross method for pipe networks. https://www.researchgate.net/publication/331095044_Hardy_Cross_Method_for_Pipe_Networks, 2019. pages

[6] Enrico Ciulli. Dispense di progetto di supporti e dispositivi di lubrificazione. *Università di Pisa*, 2006. pages

[7] Federico Crisci. Design of the cooling system of the mu2e electromagnetic calorimeter at fermilab. *Università di Pisa*, 2016-2017. pages

[8] Luca D'Agostino. Heat conduction notes. *Università di Pisa*, 2015. pages

[9] Luca D'Agostino. Heat convection notes. *Università di Pisa*, 2015. pages

[10] Luca D'Agostino. Heat radiations notes. *Università di Pisa*, 2015. pages

[11] Luca D'Agostino. Laminar viscous flows notes. *Università di Pisa*, 2015. pages

[12] Luca D'Agostino. Turbomachines notes. *Università di Pisa*, 2015. pages

[13] Luca D'Agostino. Turbulence and flow stability notes. *Università di Pisa*, 2015. pages

[14] Paolo Di Marco. Appunti ed esercizi di fisica tecnica e macchine. *Università di Pisa*, 2009. pages

[15] Gianmarco Ducci. Design and preliminary tests of the cooling system of the mu2e electromagnetic calorimeter at fermilab. *Università di Pisa*, 2015-2016. pages

[16] Isaak E Idelchik. Handbook of hydraulic resistance. *Washington, DC, Hemisphere Publishing Corp., 1986, 662 p. Translation.*, 1986. pages

[17] Leonardo Lucchesi. Design, thermal analysis and validation test of the mu2e electromagnetic calorimeter cooling system at fermilab. *Università di Pisa*, 2016-2017. pages

[18] Leonardo Lucchesi. The mu2e calorimeter cooling system. *Università di Pisa*, 2018. pages

[19] Leonardo Lucchesi. Performance of the mu2e electromagnetic calorimeter cooling system as a function of the coolant temperature and concentration. *Università di Pisa*, 2018. pages

[20] Mohinder L Nayyar et al. *Piping handbook*, volume 1. Mcgraw-hill, 1992. pages

[21] University of Gaza. Water distribution systems. `http://site.iugaza.edu.ps/sghabayen/files/2012/02/ch4-part-2.pdf`, 2015. pages

[22] American Society of Mechanical Engineers (ASME). Asme/ansi b36.10/19. `http://www-eng.lbl.gov/~shuman/NEXT/CURRENT_DESIGN/PV/movesa/PipeSize(B36.10_19).pdf`, 2019. pages

[23] Daniele Pasciuto. Design of the cooling system of the mu2e electromagnetic calorimeter at fermi national accelerator laboratory. *Università di Pisa*, 2014-2015. pages

[24] Fabrizio Raffaelli. Calorimeter construction readiness review of mechanical system. *INFN,Fermilab*, 2019. pages

[25] R.Ray. Mu2e technical design report. `https://mu2e-docdb.fnal.gov/cgi-bin/private/ShowDocument?docid=4299`, 2014. pages

[26] Francesco Ruiu. Design and thermal analysis of the mu2e electromagnetic calorimeter cooling system at fermilab. *Università di Pisa*, 2017-2018. pages

[27] Skousen. *Valve handbook*. Mc Graw Hill, 2004. pages

[28] Gabriele Taddei. Risk analysis of the mu2e calorimeter cooling system. *Università di Pisa*, 2019. pages

[29] The Engineering Toolbox. Wrought steel pipes: Bursting pressures. `https://www.engineeringtoolbox.com/wrought-steel-pipe-bursting-pressure-d_1123.html`, 2019. pages